1971

Analysis of streamer propagation in atmospheric air

Manfred Heiszler
Iowa State University

Analysis of streamer propagation in atmospheric air

by

Manfred Heiszler

A Dissertation Submitted to the

Graduate Faculty in Partial Fulfillment of

The Requirements for the Degree of

DOCTOR OF PHILOSOPHY

Major Subject: Electrical Engineering

Approved:

Signature was redacted for privacy.

In Charge of Major Work

Signature was redacted for privacy.

For the Major Department

Signature was redacted for privacy.

For the Graduate College

Iowa State University
Of Science and Technology
Ames, Iowa

1971

TABLE OF CONTENTS

		Page
I.	INTRODUCTION	1
II.	REVIEW OF LITERATURE	4
	A. The General Streamer Model	4
	B. The Critical Avalanche	6
	C. The Burst Pulse and Streamer Onset	9
	D. Streamer Propagation	13
	E. Streamer Length	18
	F. Streamer Impact on the Cathode	20
III.	DEFINITION OF THE PROBLEM	21
IV.	EXPERIMENTAL TECHNIQUES	22
	A. Electrodes	24
	B. The Impulse Generator	24
	C. Oscilloscope	25
	D. Measuring Techniques	25
	1. The Lichtenberg figure technique	26
	2. The photomultiplier technique	27
	E. Statistical Evaluation of the Results	27
	F. Error Estimation	28
	1. Lichtenberg figure technique	28
	2. The photomultiplier technique	29
	3. Effect of the film on streamer processes	32
	4. Computation of the field distribution	32
	5. Measurement of time interval on the oscilloscope	33

		Page
V.	RESULTS	35
	A. Measurements Using Lichtenberg Technique	35
	1. General Observations	35
	2. Streamer propagation studies	37
	3. Streamer onset studies	39
	B. Measurements With the Photomultiplier Technique	40
	1. General Observations	40
	a. Observation of burst pulses	40
	b. Observations of leaders	43
	c. Effect of light pipe	44
	2. Streamer onset studies	44
	3. Streamer propagation studies	46
	a. Pulse width measurements	47
	b. Measurements of propagation time	47
	c. Measurements of the streamer intensity	50
VI.	THEORETICAL STUDY OF STREAMER PROCESS	52
	A. Computation technique	52
	B. Comparison of Computed Data With Experimental Results	54
	C. Avalanche and Streamer Onset Conditions	55
VII.	DISCUSSION	63
	A. The Onset of Streamers	63
	B. The Propagation of Streamers	66
VIII.	CONCLUSIONS	76
IX.	LITERATURE CITED	78
X.	ACKNOWLEDGMENTS	89
XI.	APPENDIX A	90
XII.	APPENDIX B	95
XIII.	APPENDIX C	97

Page

XIV. APPENDIX D 103

XV. APPENDIX E 105

XVI. APPENDIX F 110

XVII. APPENDIX G 133

I. INTRODUCTION

Since the discovery of the three basic modes of gas discharges in air at positive electrodes, the streamer, the glow, and the leader, or pre-breakdown streamer, by Faraday and Gauguin (Wesendonk 1890), great effort was directed toward the investigation of these phenomena by various researchers. However, understanding of the ionization processes developed only slowly, as the measuring techniques improved, and as fast electroscopes became available, still today none of the various phenomena is completely understood.

A streamer occurs in a gas exposed to a high electric anode field. It emerges from an electron avalanche as it reaches a high degree of amplification. At that moment, the light radiation due to deexcitation in the avalanche head becomes intensive enough to produce photoelectrons in sufficient number, in order to preserve the ionization processes by electron avalanches initiated by photoelectrons.

It was recognized early, that the space charge accumulated in the streamer discharge has considerable influence on its propagation characteristics (Rogowski 1936), and the essential stages of streamer development still were later discovered by different techniques (Kip, 1939; Raether, 1939; Trichel, 1939). In the nonuniform field the existence of the burst pulses and streamer was established, as was the relationship between streamer onset and anode surface field, which remains constant for increasing gap length, and decreases with increasing radius of the anode in a point-to-plane gap. It was also found that the streamer increases in length with the point radius, and that it is replaced by a

steady glow, when the anode potential is raised. The availability of oscilloscopes with shorter resolution helped in obtaining more properties of the streamer and differentiate between burst pulses and streamers. The former is an ionization pulse that spreads laterally along the anode surface and is used in Geiger-counters. Streamers have an onset voltage only a few hundred volts above the onset voltage level of the burst pulses (English and Loeb, 1949). The streamer velocity was measured to be in the order of 10^7 to 10^8 cm/sec (Nasser, 1971 and Loeb, 1965). The regions of existence of the various corona modes of the gas discharges were firmly established and are shown in Figure 1 (Hermstein, 1960a, Schwab and Zentner, 1968).

The research in gas discharges concentrates now on studying the details of the various modes, again taking advantage of greatly improved measuring devices. Among other things, attention is focused on the propagation characteristics of the streamer process, which are known to advance into very low field regions of a nonuniform field in anode vicinity. Theoretical studies on the laws of streamer formation were made by Rather, Meek, Loeb, Wijsmann and Nasser. By 1965 two theories were developed as to how the streamer is able to propagate in a low field. One theory assumes, that the streamer is a plasma channel, which represents an extension of the anode, thus carrying the high anode field into the low field region (Wright, 1964), the other one suggests, that a streamer head is formed by a strong isolated space charge of ions, which generates a local high intensity field, sufficient to sustain ionization and streamer propagation (Dawson and Winn, 1965). Considerable

effort was made since then to clarify these aspects of the streamer propagation theory and this thesis attempts to contribute to the solution of the problem.

II. REVIEW OF LITERATURE

A. The General Streamer Model

In the vast literature on streamers, there is an inherent inconsistency in the nomenclature. It seems, therefore, appropriate to begin with a presentation of a general description of a streamer process, and to introduce the terminology, as it will be used in the sequel.

Any streamer event is known to be preceded by an electron avalanche process. Under the influence of a strong positive electric field at least one free electron, the "trigger electron", in the gas will be accelerated toward the anode. Upon collision with other molecules the electron may ionize or excite the molecule depending on the amount of kinetic energy it acquires from the external field between two successive collisions along its path. The effectiveness of the ionization by collision is described by "Townsend's first ionization coefficient", α, which specifies the number of electrons produced through ionization by collision per unit length in field direction. The value of α was determined experimentally by many researchers for a great variety of gases at a wide spectrum of pressures and fields (Brown, 1966 and Nasser, 1971). The general relationship between α, the external field, and the pressure can be expressed by the empirical Equation (1)

$$\alpha = p*A*e^{-B*p/E} \quad ; \tag{1}$$

where: p = Pressure

E = External electric field

A,B = Constants, which may assume different magnitudes for various regions of E/p.

An avalanche can occur in the gap region where α is larger than 1. For air, this is the case when E/p is larger than about 30 [V/cm-Torr]. The first avalanche will be called "initial avalanche" and any avalanche succeeded by a streamer process will be referred to as a "critical avalanche".

The transition from an avalanche process to a streamer has been assumed to occur when the number of electrons in the avalanche head exceeds about 10^5 in an inhomogeneous field or 10^8 in a homogeneous field. At these points the avalanche is said to have reached its "critical amplification". Although there is still considerable doubt as to the magnitude of the critical amplification, a general description of the transition processes may be given. With the increase of the avalanche space charge due to that processes the number of excited states, and consequently the light radiation increases as well. Therefore, also the probability of photoionization increases. If the avalanche reaches its critical amplification, the numerous photoelectrons generated can lead to another "avalanche generation" which may produce as much space charge as that of the critical avalanche. If this continues, the process is selfsustained due to the photoionization processes, and because no other trigger electrons are necessary to entertain the discharge other than the ones supplied by the discharge process itself. The streamer propagation mechanism is schematically drawn in Figure 2 assuming the electrons of the critical avalanche have been absorbed by the anode and all of the positive ions are concentrated in an almost spherical volume in front of the anode surface. An effective propagation of the streamer

can take place if the avalanche generation triggered by the photoelectrons produces approximately the same amount of space charge in front of the space charge from the critical avalanche. This is possible, because of the enhancement of the external field by the ion space charge in front of the anode, which means in effect that the streamer propagation process is greatly effected by the field of the space charges involved.

B. The Critical Avalanche

It can be shown that the growth of an avalanche subject to the α process obeys the equation

$$n_x = n_o * e \int_o^x \alpha(x)\, dx \quad ; \qquad (2)$$

n_o is equal to the number of trigger electrons which are mostly generated by the external electric field causing electron detachment from negative ions in the region where an avalanche process is possible (Waters, et al. 1965 and Saint-Arnaud, 1969). Also, n_x is the number of electrons after the avalanche advanced the distance x. In a cloud track chamber Raether found, that in a homogeneous field the critical avalanches is amplified to 10^8 electrons, and for a long time this value was thought to be the same for streamer onset in any gap configuration (Raether, 1939 and 1964). From current measurements English was able to deduce, however, that avalanche sizes in the order of 10^5 to 10^6 exist under extremely inhomogeneous field conditions (English and Loeb, 1949). It was suggested then that several avalanche generations are necessary to increase the space charge from 10^5 to 10^8 before a streamer could propagate into the gap (Loeb, 1965). This assumption was supported by measurements of the formative

time lag of streamer onset which yielded an interval of approximately 10^{-7} sec between the application of the potential pulse and the appearance of a streamer (Menes and Fisher, 1954). These measurements were verified recently by Waters, et al. and Saint-Arnaud. Saint-Arnaud, however, attributes the time lag, not to the formation of tens of avalanche generations, but he estimates that on the average about 10^{-7} sec are necessary alone for the electron detachment from negative ions (Waters, et al., 1968 and Saint-Arnaud, 1969). Since the avalanche speed was determined at 10^{7} cm/sec (Raether, 1964), and the avalanche length in an inhomogeneous field is of the order of 10^{-2} cm (Loeb, 1965), there will be only little time left for avalanche generations to develop so that it might be actually possible for streamer to develop from space charges less than 10^{8} electrons. The question which remains open is "Can a space charge of 10^{5} electrons produce a field strong enough to significantly influence the streamer propagation?" At the densities derived and measured for the homogeneous field it could not (Loeb, 1965). The relationship for the space charge radius as derived for the inhomogeneous field by Dawson and Winn is given in Equation 3

$$r_o = (6 * \int_{r_2}^{r_1} D/v_- \, dr)^{\frac{1}{2}} \; ; \qquad (3)$$

with D = Thermal diffusion coefficient

v_- = Electron drift velocity

r_2, r_1 = Limits of the avalanche path

r_o = Space charge radius

Except for the integral this relationship is essentially the same as the one derived for the homogeneous field and, therefore, it does not consider a possible influence of the radial field components present in the inhomogeneous field. Space charge densities determined with this equation, therefore, can be inaccurate. Actually, Raether measured a space charge density of 1.3×10^{12} ions/cm^3 in the homogeneous field, while 10^{13} ions/cm^3 were measured in Loeb's laboratory for the inhomogeneous field. All mathematical calculations neglected the findings of Tholl, until now on the influence of the ion space charge on α. As the space charge of an avalanche increases to above 10^6 it reduces the ionization efficiency, and a corrected value of α, α', has to be used (Tholl, 1967). At approximately 3×10^8 ions $\alpha' = \frac{1}{2} \alpha$ for the same E/p with no space charge present.

In the last decade, it was also shown that light emission may become an important factor in an avalanche process as the amplification rises to 10^5 and above. Using a highly sensitive image intensifier and a moving film behind it Wagner recorded light emission from an avalanche in N_2 gas at amplifications above 10^5. The light emitting portion of the avalanche had eliptical shape and increased in size as the avalanche advanced (Wagner, 1965). What was probably a similar event was observed by Winkelnkemper, who reported observing "anode directed streamer" before the streamer advanced to the cathode, and Lampe, who used the same terminology (Lampe, 1963 and Winkelnkemper, 1966). Recently a relationship between the ions generated by collision processes and the ones generated by photoionization was developed as (Penney and Hemmert, 1970)

$$N_p = N_d * \varphi(r,p) * \lambda * d * p \; ; \qquad (4)$$

where N_p = Number of photoions

N_d = Number of collision ions

φ = Empirical function of ratio between photoions and collision ions

λ = Fraction of photoions incident on collector

d = Distance at which photoionization occurs

p = Pressure

Unfortunately it is not possible to calculate by hand the amount of photoions generated by an avalanche of 10^5 ions from the given function φ. Still precise conditions for the avalanche space charge at streamer and/or radiation onset remain unresolved.

C. The Burst Pulse and Streamer Onset

In the broadest sense streamer onset for a long time was associated with the appearance of the luminous phase of the gas discharge. In the foregoing chapter we have seen, however, that this is a very vague limit as luminescence may occur in avalanches as well. Not only a distinction must be made between an avalanche and a streamer, but also between a burst pulse and a streamer, any of which may appear under approximately the same field intensity conditions. While very little is known about criteria for light emission in avalanches, the burst and streamer pulses were subject to extensive research after the distinction was made by Kip (Kip, 1938 and Loeb, 1965). Using continuous potential, Amin found that burst pulses appear at a very irregular rate at threshold (Amin,

1954 a and b, and Loeb, 1965). A burst pulse lasts approximately 100 nsec, and the minimum interval between two successive pulses is 2 μsec. The number of pulses increases rapidly as the potential is raised slightly above the threshold level. In a sequence of pulses the first one has a considerably large amplitude than the successors. The duration of such a string of bursts grows with both the potential and the point radius and may well exceed 500 μsec. If it is interrupted, however, it may take 10 m sec or longer before a new burst pulse appears. This interval is termed the "clearing time" and refers to the time necessary for the positive ion space charge to diffuse out of the region in front of the anode. Most recent measurements of the burst pulse current yielded magnitudes in the order of 10^{-7} A (Krätzig, 1967, Plinke, 1967, and Miyoshi and Hosokawa, 1970).

Streamers were investigated at both continuous and impulse potential, and, although the threshold potential is approximately the same for burst and streamer current pulses, the streamer current exceeds the burst currents by an order of magnitude (Krätzig, 1967). The space charge associated with both types of discharges was measured by English at 2.7×10^{4} ions for a burst pulse and at 3.0×10^{5} ions for a streamer, and thus they differ by a factor of ten (English and Loeb, 1949). Measurements of the streamer pulse duration differ greatly from 10^{-7} sec (Perelman, 1969), and 10^{-6} (Amin, 1954b) to 10^{-4} sec (Miyoshi and Hosokawa, 1970). In addition to the current measurements, it was observed that burst pulses spread over the anode surface while streamer propagate in a narrow channel into the gap space.

Based on this knowledge Loeb and Wijsman suggested the following models for streamer and burst pulse onset (Loeb, 1965).

At the burst pulse threshold several avalanche generations accumulate ion space charge in front of the anode and cause a drop in the field intensity very near to the anode surface. According to Equation 2, however, most of the avalanche amplification would take place in this area, so that the later avalanche generations are choked off in this low intensity field region unless they pursue a path which circumvents the ion space charge. Thus, the discharge spreads over the whole anode surface and is finally choked off completely when a sheath of positive ion space charge surrounds completely the highly stressed point of the anode. The burst pulse can recur only after the ions have drifted away by diffusion processes and the anode region has become reasonably space-charge free. This will take several msec. It should be emphasized that these avalanche generations are triggered mainly by photoelectrons resulting from the radiation in the avalanche head.

Unlike burst pulse, for the streamer to propagate the density of the avalanche space charges must be sufficient, to significantly raise the field intensity for the succeeding avalanche generations. Thus, ionization can advance into the gap space by adding up the space charges of the avalanche generations. Loeb points out that the essential differences between burst and streamer pulse lie in the length of the photoionizing free path $1/\mu$ of the photons, and the density of the ion space charges. If the mean ionizing free path of the photons--the distance after which a photon is most likely to ionize a molecule--is

longer than the ionizing zone of the space charge, then avalanches can be triggered which are able to bypass the ion space charge and spread the discharge over the anode surface. The ionizing zone of the space charge is the region in which the combined field intensity of ion space charge and anode is larger than about 30 V/cm-Torr in atmospheric air. However, if $1/\mu$ is of the order, or smaller than the ionizing zone, then all the avalanche generations will feed into the same space charge until it is strong enough to allow a critical avalanche process to develop before it enters the low field region between ion space charge and anode. Careful studies were made which yielded a slightly higher onset potential for streamer discharges than for burst pulses. For a 1 mm point diameter and 8 cm gap distance burst pulses started at 7.5 kV, and streamers at 7.9 kV, which is believed to be sufficient to effect the changes described above, if $1/\mu$ in air is equal to .16 cm at normal temperature and pressure (NTP).

In order to show that this model is realistic, Loeb and Wijsman formulated mathematically the onset condition for burst and streamer pulses for the homogeneous field conditions (Loeb, 1965). Nasser modified this model to fit the point-to-place geometry (Nasser, 1971). Abou-Seada transcribed this criterion for the inhomogeneous field configuration of a line conductor and used the criterion to compute digitally the corona onset potential of various conductor configurations with good results (Abou-Seada, 1970). In particular he was able to verify a well known fact that the field intensity at the anode does

not vary with the gap distance at corona onset except for very short gap distances. The onset criterion of Loeb and Wijsman is derived in Appendix A.

D. Streamer Propagation

Once a streamer is initiated it rises to its peak intensity extremely rapidly. The estimation of the rise time of the streamer tended towards shorter values as the measuring equipment improved. Latest estimates suggest that the luminosity rises to this peak in less than 1 nsec (Zentner, ca., 1970). Most of the light radiation of the streamer lies in the spectrum between 2976 Å and 4667 Å, although, peaks were also observed at 1000 Å (Loeb, 1965). The propagation velocity of a streamer is highest near the anode and decreases gradually as the streamer head advances into the low field region (Nasser, 1971). Using two photomultipliers Hudson recorded streamer propagation velocities of 10^8 cm/sec (Hudson and Loeb, 1961) as did other authors, using also photomultipliers (Gallimberti and Rea, 1970) or Lichtenberg figure technique (Nasser, 1971). Also, lower values were measured by several authors. Hamouda deduced speeds of up to 6×10^7 cm/sec from electrostatic probe measurements (Hamouda and Meek, 1967) from Marodes streak camera observations a speed of 4.5×10^8 cm/sec can be inferred (Marode, 1970) and Amin, using photomultipliers, as did Lemke, also arrived at 10^7 cm/sec (Amin, 1954b and Lemke, 1968). Amin could show that the velocity increased not only with the applied potential, but also with the radius of the anode (Amin, 1954b). He also showed that streamer velocity and streamer

intensity are proportional. These findings were confirmed by Hudson, who also investigated the streamer intensity profile along the propagation path in a 6.4 cm gap at various point diameters (Hudson and Loeb, 1961). The intensity rose during the first 1.5 to 2.0 mm of advance for a 1.0 and 2.5 mm point diameter respectively, and remained constant for the next 2.0 or 8.0 mm before it gradually decayed. This characteristic was more pronounced when the observation slit of the photomultiplier was narrowed. Loeb and Hudson, therefore, assumed that this plateau is due to later arriving streamer branches which are generated in a large number as shown by Nasser (Nasser, 1971). Nasser used the Lichtenberg figure technique to investigate streamer branching which until then was almost neglected, although, Lichtenberg figure studies of this kind were undertaken already in the early thirties by Marx, Hippel, and Merrill (Merrill and Hippel, 1939). Nasser derived general equation for streamer branching (Nasser and Schah, 1969)

$$n = n_o * e^{(x/L_i - x/L_d)} \qquad (5)$$

where n = Number of branches

x = Distance from the anode

L_i, L_d = Constants for gap configuration and potential.

Nasser and Shah could show that the streamer branching increases as long as the streamer propagate in the high anode field. The branching decreases when the streamers advance into the field region where the intensity is lower than approximately 600 V/cm. The rate of decrease of streamer

branching is then proportional to the decrease of the volume enclosed by the 600 V/cm equigradient surface.

A much disputed aspect of the streamer propagation process concerns the space charge distribution along the streamer path. As mentioned above, the space charge is known to play a vital role in the streamer propagation process and different models have been derived to describe the streamer propagation process based on opposing assumptions on the streamer space charge distribution along its path. Differences of opinion range from viewing the streamer path as a highly conductive channel (Wright, 1964 and Alexandrov, 1969) to assuming that there is no conductivity at all in the streamer path behind the advancing streamer head (Dawson and Winn, 1965, and Acker and Penney, 1968). It seems, however, most likely that there is some electron conduction current present behind the streamer head although there is no luminosity. In the presence of a small potential gradient the electron drift towards the anode, hereby many of them will be absorbed by attachment processes and relatively few will arrive at the anode. Thus, the streamer head can be considered as approximately spherical in shape and containing the space charge which can be regarded as practically isolated from the anode (Lemke, 1968).

Since the state of the streamer path is most important to its propagation characteristics, experiments were undertaken to investigate the relationship between external field and streamer propagation. Lichtenberg figures showed that streamer, in general, follow the field lines and never cross (Nasser, 1971). Marode conducting simultaneous

current measurements and streak camera photographs could show that there is always a conduction current present at the anode while the streamer crosses the gap; however, only in the first quarter of its path the electron conduction current increases and remains constant for the rest. The displacement current due to the ion space charge was seen to increase with the electron current and then to decrease as the space charge moved away from the anode, while the displacement current at the cathode increased continuously as the ion space charge in the streamer head approaches (Marode, 1967 and 1970). Acker and Penney generated repetitive streamers by overlaying a 1 kV pulse to a 20 kV continuous potential at the anode and observed that the streamer velocity is slightly higher if a streamer follows the path of a preceding one (Acker and Penney, 1968 and 1969). They suggest that a streamer path consists mainly of metastable molecules formed by the electron attachment behind the streamer head. Evidence of low conductivity in the streamer channel was found earlier already by Park and Cones (Park and Cones, 1956) and at the same time also by Lemke (Lemke, 1968). Many of these findings lend support to a propagation model suggested by Dawson and Winn. Investigating the streamer propagation with a voltage pulse of very short duration--40 nsec--they observed that streamers kept propagating up to 35 nsec after the pulse fell back to zero. They concluded then that a streamer propagates solely by using up the potential energy which is stored in the ion space charge according to Equation 6

$$W_s = (n * e)^2 / (2 \times r_o) \qquad (6)$$

with W_s = Energy

n = Number of ions

e = Electron charge

r_o = Space charge radius

The streamer acquires this energy in the high field region close to the anode, where the external field alone is sufficient to entertain the streamer process, and it gradually releases it in the low field region to balance the deficit which occurs when the external field is too weak to sustain the streamer process. The ionization processes, therefore, can take place only in the vicinity of the ion space charge as it was also suggested by Acker and Penney since the high field region of the space charge extends only within the order of the space charge radius.

In general terms, the streamer can be thought of as a wave of ions which travels through the gap without any actual ion motion. The phase velocity of the wave is equivalent to the streamer velocity. The maximum of the wave comes about through the ionization processes in front of the streamer tip and the recombination processes behind, so that there is practically no net charge loss. There are indications, as reported by Goldmans research group, that the streamer actually progresses stepwise in intervals of less than one nsec as would be expected from the model described above. The interval corresponds to the time which is necessary for an avalanche generation in front of the space charge to develop (Laboratoire de Synthese Atomique et d'Optique Protonique, 1971).

E. Streamer Length

The validity of any streamer propagation model can be tested in two different ways. First tests can be made of the onset voltage of streamers as described above. Another test can be made by determining how accurately the model is able to predict the length of a streamer. Hence, the propagation model should be able to give some information regarding the length of streamers. Before the streamer length or range was measured, it was generally known that streamers advance further at a constant anode potential if the point radius is increased; and that in the uniform field a streamer initiates a complete voltage breakdown as soon as it arrives at the cathode. With the Lichtenberg figure studies Nasser was able to show that in a nonhomogeneous field a streamer can reach the cathode well below breakdown voltage (Nasser, 1963). Winn showed that the streamer length is proportional to the anode potential (Loeb, 1965) and inversely proportional to the pressure (Dawson and Winn, 1965). Applying again the Lichtenberg figure technique, Nasser, et al. showed that a streamer would advance under any given anode potential and any gap configuration to the region where the external field is approximately 600 V/cm (Nasser, et al., 1968). If the field throughout the gap was above that level, a streamer was able to cross the gap. These values were confirmed by Lemke, who also used Lichtenberg figures, and also calculated the average field over the whole streamer path to be 4.5 kV/cm (Lemke, 1968). In longer point-to-plane gaps over 100 cm, Bazelyan found an average field along the streamer path between 3.0 and 5.0 kV/cm (Bazelyan, et al., 1961). These values were arrived at by varying the gap distance only.

The question was raised whether this low field value at which the streamers stopped was the limit of continuous streamer propagation or represents a more or less accidental limit where, according to Winn and Dawson's theory, the streamer happens to have used up its energy. In order to find an answer to this question Acker and Penney set up an experiment where they allowed a streamer, which was generated at a point anode to enter a controlled homogeneous field region, and found that streamers are able to cross the homogeneous field region if its field is higher than 4.6 kV/cm (Acker and Penney, 1969). A same idea was pursued by Phelps and Vonnegut who mounted the point electrode through a whole in the plate of a homogeneous field gap so that it would not protude. By applying a voltage pulse to the point and a continuous voltage to the plate they could generate a streamer which then advanced into the homogeneous field region. They determined a field of 7 kV/cm to be necessary for the streamer to cross a 60 cm gap, and observed that most of the growth occurred within 10% of this field limit (Phelps and Vonnegut, 1970). They point out that there is a difference between the field where a streamer comes to a halt as measured by Nasser, and the continuous propagation field measured by them. With reference to Dawson propagation theory they explain that a field of 7 kV/cm just can balance out the energy deficit which occurs in the reproduction process of the streamer space charge, therefore, a streamer is theoretically able to travel in such a field to infinity. Since, however, nothing is known about the influence of the electrodes of the homogeneous field as they might collect considerable space charge (Waters, et al., 1968 and 1970), the problem remains far from being resolved.

F. Streamer Impact on the Cathode

In nonhomogeneous fields streamers arrive at the cathode well below breakdown voltage (Nasser, 1971). It was observed that as the streamer hits the cathode there is a general increase in the light intensity in the whole gap and instantaneously a leader discharge develops from the anode (Dawson, 1965b). The event observed also by many other authors is believed to be a potential wave travelling from the cathode back to anode at approximately 10^9 cm/sec causing intensive ionization along its path, which is believed to be the preceding streamer path (Loeb, 1965 and Nasser, 1971). A great deal of understanding of this phenomenon was brought about by the recent studies of Marode (Marode, 1970 and Laboratoire de Synthese Atomique et d'Optique Protonique, 1971). At streamer impact at the cathode Marode recorded a conduction current increase at the cathode by a factor of 10 while the anode conduction current remained constant. Simultaneous streak camera photographs also showed the initiation of the leader discharge at the time of streamer impact. Marode concluded from his measurements that the burst of electrons which is liberated from the cathode by field emission--he also could show that all the conduction current was generated in the narrow region of streamer impact--contributes exclusively to the leader discharge and practically none of them arrived at the anode. The leader, therefore, develops only because of the presence of the cathode electrons in the gap.

III. DEFINITION OF THE PROBLEM

This thesis is intended to contribute to the understanding of the streamer propagation problem. In particular it shall be attempted to resolve the contradictions between Nasser's 'Minimum Propagation Field' theory, and Dawson's 'Zero Field' theory. The dependence of streamer characteristics such as streamer formation, streamer intensity, and streamer velocity on the high field region around the anode shall be investigated. All these parameters reflect in part the energy content of the space charge according to Equation 6, as it was accumulated in the high field region which may be the determining factor for the streamer length. Loeb's criterion shall be programmed to be solved with a digital computer and its results be compared with test results to check its validity. As it describes all the basic processes involved in streamer formation it shall be used to study the variation of space charge size and energy consumed by the initial avalanche, while some of the physical parameters are changed since these variables are very difficult to determine in experiments. The results of the computer study shall be compared with the experiments to find out whether the trend of their variation reflects the variation of the propagation parameters. By correlating the various results it is hoped that a clarification of the streamer propagation criterias will be achieved and an explanation for the minimum propagation field as determined by Nasser can be found.

IV. EXPERIMENTAL TECHNIQUES

A great variety of experimental methods are applied in research work on gaseous ionization. There are two categories of measuring techniques: (1) the optical mode, recording light emission which occurs during the ionization processes, and (2) the electrical mode, observing the electric current due to the charge development in the discharge. The optical mode allows deductions regarding streamer velocity, time resolution of the streamer development, spacial propagation characteristics, and space charge size. The electrical mode yields results on the space charge magnitudes, time resolution of the streamer development, as well as other types of discharges. Most often the sensitivity of both modes is limited by the capabilities of the oscilloscope used to display the measured signals, and until now, no oscilloscope has been available which could resolve in real time the rise of light emission while a streamer is generated. Most knowledge of the streamer process, therfore, remains speculative.

The choice of the potential--continuous or impulse--and the electrode configuration--generating a homogeneous or nonhomogeneous field distribution--allows one to isolate the different types of gas discharges, but also renders certain measuring techniques invaluable at times. In general, larger gap distances do not allow the use of the electric mode if impulse potentials are applied since conduction and displacement currents cannot be separated easily. Image intensifiers cannot be used either because of their small dimensions, while streak camera loose sensitivity because of the large distances at which they have to be mounted from the electrodes.

Small gap distances reduce the time resolution of velocity measurements, and also very often the effect of the second electrode becomes considerable, when investigations in the nonhomogeneous field are made. While a nonhomogeneous field offers the advantage of limiting the ionization process to a small area around one electrode, the evaluation of the results is complicated by the fact that the field distribution of most technical gaps is difficult to determine. In homogeneous fields both electrodes usually influence the ionization process and it is most difficult to keep the gap from arcing over once a discharge is initiated, so that pre-breakdown events alone hardly can be observed. The use of impulse voltage allows the observation of ionization events without the buildup of space charge prior to the event, however, due to the slow rise of the impulse compared to the speed at which the ionization processes occur, and due to the decline of the potential while the processes last, the potential is not very well defined throughout the period of observation. The buildup of space charge at continuous potential, however, leads to very particular types of discharges as can be seen from Figure 1. For this investigation of streamer processes the use of the Lichtenberg figure technique and the photomultiplier technique were chosen. The streamer processes were generated in a nonhomogeneous field of a hemispherically capped cylinder to plane gap by applying a positive impulse potential to the cylinder. The details of the setup are described in the sequel. All experiments were performed in room air, at a temperature of approximately 75^{o}F. controlled by an air conditioner. The humidity was not controlled.

A. Electrodes

The hemispherically capped cylinder-to-plane configuration was chosen since a computer program was available, allowing accurate calculation of the field distribution throughout the gap space (Abou-Seada and Nasser, 1968). By generating a high field intensity only around the anode, i.e., the cylinder, it is possible to investigate streamer processes without any possible disturbance by the cathode. Field computations show that the distribution of the field intensity around the cylinder varies the most if the radius of the cylinder is changed, while it varies hardly at all with the gap distance. Therefore, three different point radii of 0.5 mm, 3.0 mm, and 5.0 mm were used while the gap distance was adjustable between 0.0 cm and 50.0 cm. The maximum gap length was chosen so that the maximum output voltage of the impulse generator allowed breakdown between the gap. Gap distances shorter than 50 cm are sufficient to observe streamer propagation on a real time basis. A detailed description of the construction of the gap is given in Appendix B.

B. The Impulse Generator

Since streamer onset and propagation characteristics are best observed if no space charge from preceding ionization events are present, the use of impulse potential was appropriate. In order to avoid ionization while the potential rises, a steep front of the pulse is desirable and a long tail half time must be provided to ensure an approximately constant potential during the first tens of microseconds when the discharge develops. The impulse generator used developed a potential wave on the cylinder electrode with a rise time of approximately 75.0×10^{-9} sec and a tail

half time of 900.0 x 10^{-6} sec as shown in Figures 53 and 54. The maximum output voltage of the generator is 120 kV and can be adjusted from 1 kV to its maximum in steps of 0.9 kV. Only single pulses can be generated. A detailed description of the impulse generator is given in Appendix C.

C. Oscilloscope

A Tektronix 585 A with dual trace plug-in amplifier, type 82, was used to record the photomultiplier signals. The smallest measurable voltage signal is 0.002 V, the fastest rise time is 3.7 ns, sufficient to resolve most of ionization processes. The fastest sweep speed is 10 ns/cm. The photographs of the oscillograms were made with high speed polaroid film, polascope type 410 (ASA 10000). Figure 4 shows the attenuation of voltage pulses with durations less than 10 ns as measured on the oscilloscope. Figure 3 gives a sample of oscilloscope response to the nanosecond pulses. As was expected, pulses with less than 3 ns duration cannot be recorded with the oscilloscope.

D. Measuring Techniques

Since it was impossible to perform conduction current measurements at the given gap sizes without considerably distorting the external field distribution, only techniques of the optical mode were applied. Photomultiplier and Lichtenberg figure technique again were the most suitable and economic ones for the given gap configurations.

1. The Lichtenberg figure technique

The Lichtenberg figure technique records the light radiation of the ionization process directly on a photographic film as shown in Figure 59a and b. It offers the advantage of noise-free recordings and high sensitivity regardless of the speed at which the processes occur. The autographs provide a permanent record of the spatial distribution of the discharges which developed on or very near the surface of the film. It was possible to show that the traces of the Lichtenberg figures actually were caused by streamers or leaders, but it is not possible to infer directly from the width of the traces the width of a streamer channel (Nasser, 1963). However, streamer length, streamer patterns, and streamer branching can be measured accurately with the Lichtenberg figure technique.

The main drawback of this technique lies in the fact that the insertion of a photographic film into the gap space very likely may cause a distortion of the streamer development. Nasser (1963) could show that streamers are somewhat attracted by the film surface, but they do not build up any space charge on the film surface itself. Comparing results from streamer onset studies made with current measurements and Lichtenberg figures, Schroder (1970) found that Lichtenberg figures tend to reduce slightly the onset potential of streamers, especially if the film touches the anode. Still, a model of the streamer propagation the technique provides very useful information on the streamer process, although its results have to be checked with another method. The setup for the Lichtenberg figure measurements is described in Appendix D.

2. The photomultiplier technique

Photomultipliers (PM) are widely used in gaseous ionization research, since they are very sensitive, have a fast time response and allow the display of the signal to be measured on the oscilloscope. In order to achieve spacial selectivity, however, special precautions have to be taken to restrict the viewing area of the PM tube, like installing slits in front of the tube (Lemke, 1968 and Acker and Penney, 1969), lenses (Hudson and Loeb, 1961), or light pipes (Zentner, ca., 1970). The most efficient recent method is the application of light pipes (LP). Both spatial selectivity and light sensitivity can be varied easily by varying the cross section of the LP. On the other hand, the dimensions of the LP can be kept small enough so that there is no significant distortion of the streamer process. Light pipes of 1.0 mm, 3.0 mm, 4.0 mm, and 6.0 mm were used in connection with a RCA 1P28A PM tube. The LP consisted of fused quartz glass rods, utilizing atmospheric air as a reflecting medium. Two PM systems were used to allow velocity measurements. One unit triggered the oscilloscope and the other observed the ionization event. A detailed description of the PM systems is given in Appendix E.

E. Statistical Evaluation of the Results

Ionization processes in gases are characterized by a large spread of the experimental results. Every data point presented in the sequel represents the average of at least 20 measurements. In high voltage breakdown measurements, the 50% value is often used to represent the breakdown value of an electrode system; it is equivalent to the value

of a parameter which causes a reaction to occur in 50% of all investigated cases. This procedure was adopted for measurements of streamer onset when carried out with the PM's. The values obtained from the Lichtenberg figures represent an average of the lengths observed for a certain voltage, unless the absolute maximum is given.

F. Error Estimation

1. Lichtenberg figure technique

Aside from the distortions which a film introduces to the ionization processes, leading to a reduction of the onset potential of approximately 10% (Schroder, 1970), most of the errors inherent in the Lichtenberg figure technique stem from the fact that it is difficult to suspend the film accurately in the gap. The variation of the gap distances make the use of stiff plates very unpractical Rolled film, therefore, was used and cut to adequate length prior to its application. The film pieces then had a strong tendency to roll up, and it was virtually impossible to stretch the film completely unless a large amount of hardward was put into the gap space. This, of course, was undesirable as well because of the effects the hardware can exert on the streamer processes. Also, it turned out to be quite difficult to execute rectangular cuts of the film, since the film had a tendency to warp on the cutting table on impact of the blade. If the point radius of the cylinder electrode is small the film cannot be placed immediately in front of the tip of the point, but has to be leaned against the cylinder as shown in Figure 59. This leads to other sources of error; the streamer process does not

start on the film surface, so that the exact origin of the streamer has to be estimated on the film and there is probably a shift of the discharge area from the streamer tip to the wedge area between the film and the point. This position of the film, however, is not expected to have any influence on the streamer propagation occurring away from the point.

For large cylinder electrodes and long gap distances the maximum error in the measurements is estimated to be 3%. Due to the high sensitivity of the film, no significant error is expected as far as the determination of the streamer tip is concerned.

2. The photomultiplier technique

As mentioned before, valid estimations of the rise time of the streamer light emission cannot be made with the measuring devices used. For spacial measurements, a major source of error is caused by the large aperture angle of the LP, although it is slightly reduced by the shield. All light originating from within a cone with a full angle of 100 degrees will be recorded by the photomultiplier. Streamers travelling farther away from the LP tip generate a wider pulse and a lower peak, if the light intensity is the same. However, it is not possible to calibrate the system adequately enough so that differences could be recognized from the oscillograms. In order to get at least some estimate on the region of reception of the LP for low-intensity streamers onset streamers were observed with the 1 mm LP from various positions, and the limit was determined from where streamers could be detected. The test was performed in a 10 cm gap with 1 mm cylinder diameter at 9.8 kV. Using the small point radius insured that the streamer is generated at a fairly fixed

location, the onset conditions were chosen to avoid branching of the streamers so that all together the location of the light source was reasonably well defined.

Results of the tests are given in Table 1. The notation used in Table 1 to describe the position of the tip of the LP is illustrated in Figure 5. The gap space is described by a rectangular coordinate system, with the x-axis pointing to the right seen from the photomultiplier, the y-axis pointing away from the photomultiplier being parallel to the light pipe, and the z-axis pointing down to the ground plate. In the sequel, all positions in the gap space will be referred to by their (x,y,z) coordinates.

Table 1. Reception region of the 1mm light pipe.

Position (x,y,z)(cm)	Intensity (V)	Pulse Width (nsec)	Rise Time (nsec)	% of Occurrence (%)
0, -.6, 0	.44	103	30.5	100
0, -1.1, 0	.26	123	43.0	70
0, -1.3, 0	0	0	0	0
-.5, -.6, 0	0	0	0	0
-.4, -.6, 0	.09	106	40.0	45
0, -.5, .5	.26	123	45.0	18

From the results of Table 1, we can estimate that low intensity pulses can be detected from within a cone with 50^{o} half angle and 1.2 cm length. Considering that the intensity of streamers at the location

where they extinguish is less than onset intensity, we can estimate the error in determining the location of streamer termination to be less than $\pm$ .25 cm, well within the statistical spread of the results.

Other source of error in the PM technique consist of nonlinearities in the components and in the inaccuracies made when evaluating the oscillograms. The latter is estimated to be 10%. From Figure 67 it can be seen that the anode current of the PM-tube is quite linear at an operation voltage of 100 V for values less than 2 mA, which corresponds to a voltage drop of 2 V across the load resistance. Since the FET saturates above 2 V, all nonlinearities can be taken into account by evaluating Figure 75, which relates anode voltage to the output voltages of the measuring circuit. This characteristic curve was determined with an accuracy of 10%.

When measurements close to the ground plate are taken, reflection may enter the LP and lead to erroneous results since, like all the other hardware, the cathode cannot be painted black. The reflections cannot be avoided when the large diameter LP's are used. Only with the 1 mm LP, by shielding the tip properly and positioning the tip on the positive y-axis, could the reflections be eliminated. Figures 6, 7, and 8 allow a comparison of measurements in a 10 cm gap, 5 mm point radius at 58 kV, with the tip of the LP in the positions (0,0,9.5), (0,0,9.5), and (0,1.8,9.5), respectively. Figure 6 was obtained with an unshielded LP, Figure 7 with an unshielded LP; however, the cathode being covered with a black rayon cloth, Figure 8 with the LP shielded as shown in Figure 66.

3. Effect of the film on streamer processes

To investigate the influence of the film on the streamer processes, a comparison was made between PM measurements with and without a piece of film inserted into the gap, under otherwise identical conditions. The film was suspended in the gap in the axial mode perpendicular to the light pipe which was in position (0,0,.5). The oscilloscope was triggered with the second PM unit, and 13.5 kV were applied to a 1 mm diameter cylinder of a 10 cm gap. Figure 9 shows the measurements without film; Figure 10 with the film inserted. Without film a constant signal was received with an average peak of .69 V; with film in only two out of eleven tests was a signal observed at approximately half the average peak. Pulse rise time and pulse width, however, remained unchanged. This result suggests that the film influences the streamer process; however, the PM technique does not allow the determination of any correction factors since it cannot be calibrated sufficiently itself. The fact that the basic shape of the light signals remains unchanged suggests, furthermore, that the process itself remains unchanged.

4. Computation of the field distribution

The field values of the hemispherically capped cylinder to plane gap were determined with a digital computer program based on the method of images (Abou-Seada and Nasser, 1968). The error of the program is less than 2%. All field values, given in the sequel, are the axial components of the field. Radial components or absolute field values off the symmetric axis will be referred to specifically.

5. Measurement of time interval on the oscilloscope

By controlling the trigger signal of the oscilloscope, either with the voltage from the potential divider or with the signal of one of the PM, formative time lag of ionization processes or propagation velocity measurements can be made using the calibrated horizontal deflection of the oscilloscope. However, corrections must be made since several components of the measuring circuit introduce a delay of the measured signals. A block diagram in Figure 11 illustrates the path of the signal and the delays caused by the various circuit elements.

If formative time lag measurements are made and the oscilloscope is triggered with the voltage pulse while the streamer signal is measured with PM set II an error of 85 nsec enters the oscillograms resulting from the delay in the photomultiplier tube (17 nsec), the field effect transistor (8 nsec) and the delay line built into the oscilloscope (60 nsec). To measure the elapsed time while a streamer advances from PM set I to PM set II, only the oscilloscope delay line has to be considered since the effects of the other components cancel each other. The travel time on the coaxial cables is neglected, since they all have approximately the same length.

No corrections will be made with respect to the applied potential to account for the formative time lag of streamer processes. Since the tail half time of the pulse is 1000 μs, and the average formative time lag is at the most 10 μs, the error should not exceed 2%. The error of time interval measurements becomes large for short distances between

PM I and II and high voltages because the electric noise on the oscillograms does not allow determination of the point of pulse rise more accurately than $\pm$ 10 μs which is already the order of the travel time.

V. RESULTS

A. Measurements Using Lichtenberg Technique

1. General Observations

It is quite fascinating to look at a typical streamer pattern as shown in Figure 60 and 61 and to observe some general characteristics, which are revealed from the Lichtenberg figures. Figure 60 is taken in a 15 cm gap with a 5 mm cylinder radius at 26.6 kV corresponding to streamer onset conditions with anode on top and cathode on bottom. The actual length of the axial streamer is 3.5 cm. Figure 61 is taken in a 2.5 cm gap with 5 mm point radius at 26.2 kV, with the film placed 1 cm from the point. The actual width of the figure is 10 cm.

At first glance it seems that the streamer advance reflects in general the field pattern. An area of continuous luminosity can be recognized around the point and the angle between the streamer branches is fairly constant. If the autographs are examined with more scrutiny however, one notices that the streamers are bent away from the longitudinal axis, whereas the field is bent towards the axis. This is especially true for streamers which emerge from the point at a large angle to the axis. These streamers are bent backwards and even move away from the cathode. Also the length and the path pattern of the many short streamers branches does not seem to be quite arbitrary. Instead, the vicinity of other streamers is very influential. One can observe branches to bend into or against the general field direction to evade other branches. Immediately after two main branches split, there is not any branch development

at all on the sides of the streamers facing each other, until a minimum distance of approximately 1 mm is established between the two main branches. In this small region the streamer channel is very smooth, whereas usually it shows many small tips emerging from the flanks of the channels. These tips reappear as soon as the distance to other branches is sufficient. Streamers only split into two new branches at one single point. Very rarely three branches can be observed to develop together whereby usually the third branch in the middle is immediately, i.e., after less than 1/2 mm, suppressed. If two branches approach each other, then a significant change of direction occurs if they are at a distance of approximately 2 mm, which tends to maximize the distances between themselves and all the other streamer branches. The small branches in between the main branches very often seem to travel at a lower speed than the main branches especially at higher voltage levels. If their tips advance close to the trunk of the faster branches (at least to 1.5 mm) then a brush like pattern between tip and branch occurs. This discharge always leads to the extinction of the respective smaller branch. The angle at which streamers branch vary from only between 20^{o} and 40^{o}. If the potential is increased the angles get smaller, the channel width in the neighborhood of the points, however, gets larger and also the number of branches increases. The general tendency of the streamer branches to seek maximum distance from each other remains the same, but more often they approach closer than 1.5 mm and the brush like discharges occur. All these characteristics are apparent from Lichtenberg figures taken both in the axial and coplanar mode, although the change

of streamer direction in the vicinity of other branches is more clearly visible in the coplanar mode.

2. Streamer propagation studies

Extensive studies with Lichtenberg figures showed that streamers tend to stop advancing in a very low field region of approximately 500 to 600 V/cm (Nasser et al., 1968). These findings were briefly examined with the available experimental setup. In Figure 12 a comparison of data is given between the studies of Nasser et al.(1968) and the ones obtained in this study. The agreement at lower voltages is good. At higher voltages the better sensitivity of the TRI-X-Pan film compared to the Lino-Write-3B photographic paper used previously resulted in longer streamers, and a linear relationship between applied potential and streamer length. Some characteristic data and minimum field values are given in Table 2. Table 3 lists the minimum field strength at the streamer tip according to the data of Figure 12. Rz, hereby, represents the absolute maximum at which streamers could be observed. The results from both tables show that as the rod radius is increased from .5 to 5 mm the minimum field strength increases from approximately 850 V/cm to 1300 V/cm, i.e., by more than 60%. On the other hand, the streamers are able to penetrate further into the low field region if the anode potential is increased, however, an absolute minimum is measured around 600 V/cm, which agrees very well with the earlier findings of Nasser et al. (1968). The field intensity at the streamer tip decreases by approximately 50% when compared with the values obtained at or near onset conditions.

Table 2. Field strength of the streamer tip for various gap configurations.

Anode Voltage V[kV]	Gap Distance d[cm]	Rod Radius R[mm]	Streamer Length R_z[cm]	Anode Field E_A[kV/cm]	Streamer End Field E_z[V/cm]
8.85	10	.5	1.25	102.3	831.8
8.85	15	.5	1.1	100.5	902.7
8.85	25	.5	1.1	97.3	867.3
22.5	10	3.0	3.65	53.0	1072.5
22.5	15	3.0	3.4	50.5	1074.7
22.5	25	3.0	2.75	47.8	1158.0
28.2	10	5.0	4.5	42.5	1208.3
28.2	15	5.0	3.75	40.4	1318.0
28.2	25	5.0	3.4	38.0	1323.0

Table 3. Minimum propagation field for d = 15 cm, R = .5 mm.

Anode Voltage V[kV]	Streamer Length R_z[cm]	Anode Field E_A[kV/cm]	Streamer End Field E_z[V/cm]
7.25	.8	82.78	1186.1
8.05	.9	91.95	1085.14
8.85	1.1	100.5	902.7
20.0	3.15	228.36	644.0
25.5	5.1	291.16	510.0
38.5	6.9	439.59	623.0
43.3	8.0	494.4	605.0
52.9	10.75	604.01	688.0
62.5	12.6	713.62	625.0

3. Streamer onset studies

For the same gap configurations the minimum anode potential was determined for which streamer could be recorded on the autogram. The results of the experiments are listed in Table 4 which also lists the maximum length of onset streamers and the field intensity at both the anode and the streamer tip. Figures 13, 14, and 15 illustrate the streamer onset potential, field intensity at anode, and streamer length, respectively. These conditions hardly change with an increase in gap length, but change considerably with increasing point radius. For instance, streamer length increases from .75 to 4.0 cm with an increase of the point radius from .5 to 5 mm. The field at the onset streamer tips, however, remains approximately constant at 1200 V/cm. Onset potential increases as well from 7.25 KV to 27.4 kV respectively. However, the field intensity at the anode decreases from 88.33 to 36.9 kV/cm. At an increase in gap distance there is a slight increase of the onset potential whereas the results of streamer length and onset field give no clear indication of a significant change in any direction.

The trend of the variation of anode field intensity seems to indicate that the intensity level gradually decreases to the uniform field level, which is around 26 kV/cm for gap lengths equivalent to the ones used in the experiments, as the point radius increases. However, investigations with a relatively large sphere (1.6 cm radius) at distances around 8 cm do not quite substantiate this assumption since the onset value for this gap configuration is 5% above the value of the 5 mm point electrode at comparable distances. Lichtenberg figures are obtained at an anode field

Table 4. Streamer onset measurements.

Anode Potential [kV] V	Gap Distance [cm] d	Point Radius R[mm]	Streamer Length R_z[cm]	Field intensity at Streamer tip E_z[V/cm]	Anode Field E_A[kV/cm]
7.25	10	.5	0.75	1334.0	85.55
7.25	15	.5	0.8	1186.1	82.78
8.05	25	.5	0.8	1265.46	88.37
20.9	10	3.0	3.35	1038.03	49.13
21.7	15	3.0	3.30	1036.54	48.7
22.5	25	3.0	2.75	1158.00	47.9
25.8	10	5.0	4.0	1235.05	38.87
26.6	15	5.0	4.0	1173.60	38.0
27.4	25	5.0	3.5	1238.48	36.9

intensity of approximately 41 kV/cm. The equivalent anode potential is 68.5 kV, and the onset streamer length 8 cm.

B. Measurements With the Photomultiplier Technique

1. General Observations

a. Observation of burst pulses Streamer can be very easily distinguished from other types of discharges, like glow or leader, on Lichtenberg figures autographs because of their typical pattern. Distinction with a good degree of certainty is not as simple with the photomultiplier technique where the types of discharges have to be

identified from the pulse shape. Preliminary studies were made therefore to recognize the various types of corona discharges from the current oscillograms.

Burst pulses which appear to have not been observed in connection with impulse potentials before, could be observed using the 6 mm light pipe. As it is the case under continuous potentials, burst pulses appear at around the streamer onset voltage level within approximately 2 kV. They have a comparatively slow rise time in the order of 100 nsec, and a short pulse width of a few hundred nanoseconds. Contrary to burst pulses, streamers have an extremely fast rise time, a larger pulse width, and also much higher intensity. Therefore, burst pulses could not be observed with 3 or 1 mm light pipes.

Figure 16 a and b shows the oscillograms of the light emission of a burst pulse and a streamer pulse. The pulses were recorded in a gap of 10 cm distance with a cylinder electrode radius of 5 mm. The actual difference in intensity can not be deduced from Figure 16 since the FET of the measuring circuit becomes saturated by the radiation from the streamer pulse. However, the difference in rise time and pulse width is quite apparent.

A further difference between burst pulses and streamer pulses was found to exist when the time lag between potential pulse and the light pulse was investigated. Figure 17 shows a series of streamer and burst pulses taken under identical conditions at 28.5 kV (d = 10 cm, R = 5 mm) with the 6 mm light pipe. The difference in the pulse width is apparent, but one notes also that the time lag of burst pulses is considerably longer. The average time lag of burst pulses is 50 μsec whereas it is

8.5 μsec for streamers. Frequently burst pulses are preceeded by smaller pulses of the same kind at an interval of .7 μsec. A double pulse of this kind is shown in Figure 18. These first pulses have very low intensity since even with the 6 mm light pipe the FET does not become saturated and the distance of the light pipe to the point electrode is less than 1 mm. From Figure 17 we can also observe that streamers are followed by extremely low intensity light emission which lasts for approximately 50 μsec. It manifests itself in a noisy tail of the streamer pulse which does not follow at all the burst pulses. One has to note, however, that the burst pulses as observed in Figures 16 through 18 are generated under somewhat artificial conditions, since the tip of the light pipe had to be placed extremely close to the point electrodes which results in a lower onset potential. In that, the light pipe produces the same effect as the photographic paper used in the Lichtenberg figure techniques. However, it is not expected that this changes the basic characteristics and properties of the phenomena.

If the light pipe is moved further away to about 2 mm, burst pulses can be hardly observed because of their extremely low intensity. Figure 19 shows on the upper trace one burst pulse, measured for d = 15 cm, R = 5 mm at 33 kV. Generally burst pulses are more readily observed in a more uniform field. They increase in number considerably as the point radius increases. Figure 20 shows two traces of burst pulses obtained with a point radius of 16.0 mm at 67 and 61 kV, respectively, for d = 20 cm. From Figures 19 and 20, then it is apparent that unless the light pipe tip is placed very close to the point surface, burst pulses are not likely to develop and appear in the current oscillograms.

b. Observations of leaders Leaders are known to develop in nonuniform electric fields at potential levels near breakdown. Therefore, a misidentification of the streamer onset light pulses made with the 6 mm light pipe is not likely. To confirm this, the voltage level is raised to near the breakdown level and the light intensity around the point surface can be observed (Figure 21). An initially low intensity radiation develops around the point and persists over several hundreds of microseconds. Raising the voltage increases both duration and intensity of this steady radiation which will finally last for more than 2 microseconds when breakdown occurs. This confirms the findings from Lichtenberg figures in which a diffuse glow near the point can be clearly seen (Figure 60). This "glow" stem from the stray light falling on the film or the light pipe and originating from the streamers themselves.

Figure 22 shows the oscillograms from three flashovers (d = 10 cm, R = 5 mm, V = 76, 77, and 78 kV) observed with a 1 mm light pipe at (0, 0, 7.5). All three oscillograms show the streamer developing immediately after the voltage pulse is applied. After a dark period which lasts up to 80 microsecond a series of fast pulses cross the gap over an interval of approximately 4 μsec before flashover occurs. In one instance a single low intensity pulse can be observed approximately 25 μsec after the initial streamer pulse. Clearly no continuous light emission resulting from any steady radiation around the anode is recorded in the gap space, and the events possibly relating to the leader occur after a long interval which means that no overlapping with streamer events can occur.

c. Effect of light pipe The use of the 6 mm light pipe always leads to saturated signals except when burst pulses are observed as shown in Figure 16. The reduction of the light pipe diameter lowers pulse peaks and reduces the pulse width. Figure 23 shows a series of streamer pulses observed with the 1 mm light pipe, at the point electrode in a gap with d = 10 cm, R = 5 mm. The pulse height is reduced to less than the saturation level, and the width to .160 μsec compared to 1.6 μsec in Figure 16. On the other hand, neither burst pulses nor the glow at the point can be observed with the 1 mm light pipe and, therefore, the 6 mm pipe was used for onset studies only while the 1 mm light pipe, which also provides sufficient selectivity (see Sec. IV.D.2), was used for the propagation measurement. To investigate the maximum streamer length, however, the Lichtenberg figure technique had to be relied upon completely since the light pipes proved to be unsatisfactory for this purpose. While the 1 mm pipe is lacking sensitivity, the 3 and 6 mm pipes are lacking spacial selectivity, so that the results from photomultiplier measurements will always have a larger error than the Lichtenberg figures. In order to employ photomultipliers in this kind of study and decrease the error magnitude it would be necessary to obtain coated light pipes with a controlled aperture angle.

2. Streamer onset studies

As to be expected from the error estimation, the streamer onset potential observed with the photomultiplier is 5% to 23% higher than the results obtained with the Lichtenberg figures (Table 5.). Again the minimum potentials and field intensities at which streamers could

Table 5. Streamer onset potential photomultiplier technique.

Onset Anode Potential V[kV]	50% Onset Anode Potent. V[kV] 50%	Gap Distance d[cm]	Cyl. Radius R[mm]	Onset Anode Field E[kV/cm] Photomul-tiplier	Onset Anode Field E[kV/cm] Lichtenberg Figure
9	9	10	.5	106.24	85.55
10	10	15	.5	114.18	82.78
9	9	20	.5	100.47	-
10	10	25	.5	109.48	88.37
23	25	10	3.0	54.06	49.13
23	24	15	3.0	51.62	48.70
28	29.5	20	3.0	60.85	-
28	29.5	25	3.0	59.62	47.90
30	33	10	5.0	45.20	38.87
31	34	15	5.0	44.29	38.00
33	35	20	5.0	45.55	-
33	35	25	5.0	44.43	36.90

be observed vary only slightly with the gap distance. The field intensity increases considerably as the point radius is decreased while the potential increases with the point radius. The spread of the values is larger, especially for the small point radii where the measurements might be more sensitive to the minimum distance of the light pipe from the electrode. Possibly, also 25 measurements per test point might not have been suf-

ficient to obtain the actual minimum value.

The 50% onset value coincides with the minimum value for the .5 mm point radius, but becomes progressively larger as the point radius increases. An increased variance in the statistical behavior of the streamer process with an increasing point radius manifests inself also in several other aspects.

The time lag increases with the point radius, and also the variation around the average value becomes larger as can be seen from Figure 24a, b, and c. The average time lag at onset lies between 5 and 10 μsec. The variation of the time lag with the potential and the point radius for d = 10 cm is given in Figure 25. At twice the onset potential the time lag of streamers is of the order of 10^{-7} sec which agrees well with the findings of Menes and Fisher (1954). With an increasing point radius also the region of existence for burst pulses increases, and extends over several kV's around the onset potential level (Figure 20), indicating that streamer onset conditions are not as well defined in more uniform fields.

3. Streamer propagation studies

These studies were made at four different gap configurations. At a distance d = 10 cm with cylinder electrodes of radius R = .5 mm, 3.0 mm, and 5.0 mm. At R = 5.0 mm a gap distance d = 15 cm was also included. Streamer intensity, time of propagation, and pulse width were measured at various distances s from the point tip for a variety of potentials.

a. Pulse width measurements The pulse width was determined by measuring the elapsed time from the initiation of the pulse to the point of the tail where the pulse decayed to 50% of its peak value. Results are given in Figure 26 a to d, and show that the pulse width stays within 100 to 200 μsec for most of the potentials and gap configurations. Near the point, however, there is a rise in pulse width which varies slightly with the point radius (Figure 27). It increases with the point radius when the potential remains constant, but it decreases when the gap distance is increased and the point radius is kept constant.

b. Measurements of propagation time The travel time of the streamer over the distance s at various potential levels is plotted in Figure 28 a through d. The curves are dashed in the region near the anode where an exact evaluation of the travel time is not possible because of electric noise (see Sec. IV.F.5). For any given gap configuration the travel time decreases with an increase of the applied potential. A comparison of the variation of travel time with the potential is made for the three different point radii in Figure 29. There is only a slight variation for the different radii at short distances from the point (estimated values) but at large distances above 5 cm the differences are quite pronounced. At $s = 6$ cm for example, the travel time increases 5 times as fast for $R = 3.0$ mm as the voltage decreases. At 9.5 cm the rate of change also for $R = .5$ mm increases considerably while for $R = 5.0$ mm it varies only slightly.

From the above results, it is not possible to deduce a consistently higher or lower traveling time or speed of propagation through the gap

for any rod radius. This is also illustrated in Figure 30 for d = 10 cm at 44 kV anode potential. The streamers originating from a point radius of .5 mm are the fastest far away from the point, whereas at v = 61 kV streamers coming from a point with 3.0 mm radius are faster (dashed curves). Streamers in the gap with d = 15 cm are the slowest in both cases. The variation of the travel time does not completely agree with Amin's results (Amin, 1954b), who obtained his results for d = 5 cm and R = .5, 1.0, 1.25 mm and found that point radius and travel time are proportional.

From the curves of Figure 28 the velocity distribution can be determined by computing the slope of the time versus distance curves. The results are shown in Figure 31 a through d. The curves of Figure 31 again illustrate the fact that there is no simple relationship between streamer velocity, the electrode radius, and the applied potential. In any gap configuration the magnitude of the streamer velocity lies between 10^7 and 10^8 cm/sec which is in good agreement with other results from the literature (see Sec. II.D). For R = 5 mm it appears that streamers increase their velocity in front of the cathode.

Figure 31 a through c includes also equigradients lines for E = 4.4, 2.7, 1.9, 1.6, and 1.12 kV/cm. Until now no intensity or velocity measurements were investigated in this manner, so that no comparison to other results can be given. However, no direct relationship between field intensity and streamer velocity can be derived from these plots. The magnitudes of the streamer velocity, occurring at certain field intensities, varies considerably both with the potential and the gap

configuration as shown in Table 6 for a potential range from 36 to 61 kV.

In general, within the potential interval the variation of the velocity over the field gradient decreases in the low field region, and the mean velocity throughout the propagation region decreases as the point radius is increased.

Table 6. Relationship of streamer velocities and field intensities.

d [cm]	R [mm]	ΔV [kV]	E [kV/cm]	V_{max} [cm/sec]x10^7 x 10^7	V_{min} [cm/sec]x10^7 x 10^7	V_{med} [cm/s]x10^7
10	.5	25	4.4	8.0	3.25	5.62
			2.7	7.45	3.05	5.25
			1.9	6.75	2.9	4.82
			1.6	6.1	2.7	4.4
			1.12	3.4	2.4	2.9
10	3.0	25	4.4	7.1	4.2	5.66
			2.7	6.3	3.5	4.9
			1.9	4.7	2.75	3.72
			1.6	4.0	1.6	2.8
10	5.0	25	4.4	7.2	3.05	5.13
			2.7	4.7	2.0	3.35
			1.9	2.5	1.5	2.0
			1.6	1.25	1.15	1.20

c. Measurements of the streamer intensity Streamers at the same gap configurations were investigated at the same potentials as for the velocity measurements. The variation of the light intensity along the streamer path is plotted in Figures 32 a through d. All intensity values are given in percent of the maximum value observable with the photomultiplier.

Equigradients lines for E = 4.4, 2.7, 1.6, 1.12, and 1.0 kV/cm are added to the plots. The characteristics of the intensity distribution is similar to the one found for the velocity distribution. The intensity decreases gradually as the streamer progresses into the low field region. However, there is no direct relationship between field intensity and light intensity nor is there any simple relationship between potential or point radius and streamer intensity (Table 7 and Figure 33). Again the variation of the intensity around a mean value decreases with the field intensity.

Investigations in the vicinity of the anode did not yield any peak in streamer intensity within 1 cm of the anode which would be similar to the one observed by Amin (Loeb, 1965). The amount of data that could be collected for Figure 34, however, was limited by the saturation of the photomultiplier or by the spacial selectivity of the light pipe, so that no final conclusions can be made from these results.

Table 7. Relationship of streamer intensity and field intensity.

d [cm]	R [mm]	V_{med} [kV]	E [kV/cm]	$Int._{max}$ [%]	$Int._{min}$ [%]	$Int._{med}$ [%]
10	.5	35.5 ± 8.5	4.4	96	51	73.5
			2.7	66	44	55.0
			1.9	47	33	40.0
			1.6	34	26	30.0
			1.12	18	15	16.5
			1.0	13	8	10.5
10	3.0	44.5 ± 8.5	4.4	58	11	34.5
			2.7	38	8	23.0
			1.9	17	5.5	11.25
			1.6	9	3.5	6.25
10	5.0	44.5 ± 8.5	4.4	83	19	51
			2.7	53	10	31.5
			1.9	30	6	18.0
			1.6	19	1	10.0

VI. THEORETICAL STUDY OF STREAMER PROCESS

A. Computation technique

Many years ago, Wigsman and Loeb proposed a streamer theory based on the physical mechanism of the streamer. The theoretical condition for a streamer to materialize is known as Loeb's criterion for streamer onset and is derived in Appendix A. It can be solved only with the aid of a digital computer because of its complexity. The computer solution allows to study some of the parameters involved in streamer processes in nonuniform fields such as point-to-plane gaps. Before solving this equation, however, the exact values of the electric field intensity near the anode must be known. For this purpose parts of programs written by Abou-Seada for the field computation of point-to-plane gaps were used. The solution of Loeb's criterion is based on the previous corona onset computations on bundle conductors because the computation techniques are essentially identical (Abou-Seada, 1970 and Abou-Seada and Nasser, 1968).

The computation of electric field intensity and direction are based on the method of images and the charge simulation technique. The hemispherically capped cylinder and the ground plane are simulated by a system of point and line charges as shown in Figure 35. For these finite numbers of charges a system of simultaneous equations as well as boundary conditions on the rod surface can be found which allow for the solution of the charge magnitudes. Once the charges are known the potential throughout the gap space can be found by superposition. Field intensity can be computed using finite difference method (Abou-Seada and Nasser, 1968).

Equation 18 is computed iteratively. All parameters in the equation which depend on the field can be determined in subroutines for any location in the gap space. The iteration cycle is terminated if Equation 18 is fulfilled within the limit of 20%.

Several modifications were introduced in the program to allow for a more detailed study of streamer processes. The energy which is drawn from the external electric field by the electrons while they are moving towards the anode was computed by solving Equation 7

$$W = e^* \int_{x_1}^{d} n(x) * E(x) * dx \qquad (7)$$

where

e = Electron charge

n = Number of electrons at x

E = External field at x

The electron current of the initial avalanche was computed for the case where the electron cloud arrives at the anode using Equation 8

$$i = e * n_d * A_d * V_d \qquad (8)$$

with

e = Electron charge

n_d = Electron density

A_d = Cross section of the electron cloud

V_d = Electron velocity at the anode

The computational program was also made to allow the variation of the position of the trigger electron and the variation of the region of

effective photo ionization. A printout of the program which is written in Fortran IV and a sample of the results is given in Appendix F.

B. Comparison of Computed Data With Experimental Results

To examine the correctness and accuracy of Loeb's model for streamer onset in a hemispherically capped cylinder-to-plane gap, several cases were computed and compared with the results published by various authors. Figures 36 and 37 show the computed and measured results for rods with 1.0 cm and 1.0 mm diameters. The results from reference 6 were obtained with the Lichtenberg figure technique which tend to produce slightly lower onset values (see Sec. V.B.2). The agreement between measured and computed results is very good, even at very short gap distances where the onset potential varies considerably. It is apparent from the experimental results in Section V that the field strength at the anode remains practically constant over a wide range of gap distances. The computed values for the anode field strength shown in Figure 38 not only produce the same characteristic, but also accurately furnish field magnitudes in close agreement with those obtained by measurements.

Other facts, established in earlier experiments by various authors which could be verified by the computation of the theoretically derived streamer model. These are:

1. The number of electrons in the initial avalanche at streamer onset is in the order of 10^5 in nonuniform fields (Loeb, 1965, p. 55).
2. The travel time of the initial avalanche is in the order of nanoseconds (Raether, 1964).

3. The current of the initial avalanche is of the order of less than 10^{-4} A (Loeb, 1965, p. 131).

Regarding the last statements, it may be pointed out that Amin recorded a streamer current of .021 mA for a gap distance of 4 cm and a rod radius of 0.05 cm, and he estimated the streamer channel diameter to be 0.02 cm. The computed values for the initial avalanche in a gap with d = 10 cm, R = .05 cm are 0.5 mA and 0.003 cm, respectively (see Appendix F). Loeb estimates the number of avalanche ions for 0.1 - 0.5 mm rods to be 10^4 - 10^5 (Loeb, 1965, p. 108).

From the comparison of computed and experimental data, the conclusion must be made that Loeb's criterion provides a good computation model of the streamer onset process, and consequently the program may be used for a study of parameters involved in these processes.

C. Avalanche and Streamer Onset Conditions

The results of the computer study, shown in Table 8, suggest that the number of electrons generated in an initial avalanche is neither proportional to the point radius, R, nor to gap distance to radius ratio. The number of electrons actually may decrease as the radius of the anode increases, although the optimal length of the initial avalanche, L_{min}, increases continuously. We also can see, however, as calculated from

$$E_{av} = \frac{1}{L_{min}} \int_{x}^{L_{min}} \frac{\Delta E}{\Delta x} \, (x)dx$$

that the average field gradient in the region of avalanche propagation decreases rapidly at a faster rate than the length of the avalanches

Table 8. Computed number of particles in initial avalanche.

1 Point Radius R, cm	2 Gap Distance d, cm	d/R	3 Number of Electrons x 10^5	4 Length of Avalanche L, cm	5 Average Field Gradii E_{AV} kV/cm^2	6 Energy x 10^{-10} W, kJ	7 Anode Field E_n kV/cm
.003	11.0	2,730	3.578	.0144	31067.9	.208	471.21
.05	10.0	200	4.558	.065	1342.6	.769	110.813
.3	10.0	27.3	.484	.21	186.35	.206	61.38
.5	10.0	20	.24	.25	115.38	.101	53.08
1.0	10.0	10	.20	.40	54.43	.124	45.39
1.58	9.0	5.7	.255	.632	31.27	.278	41.33

Table 9. Corona onset study of a hemispherically capped cylinder to plane gap with R = 1.0 cm.

Cylinder Radius cm	Gap Distance cm	Onset Voltage kV	Anode Field kV/cm	Cathode Field kV/cm	Expon. Alpha x 10^5	Transit Time μ_{sec}	Avalanche Length cm (preset)	Space Ch. Radius cm	Average Field Grad. kV/cm^2	Energy in Avalanche kJ x 10^{-12}
1.0	1.0	25.67	44.9	18.89	.277	.03369	.5	.009322	43.84	22.7
1.0	2.0	35.53	45.25	10.5	.213	.02593	.4	.00818	52.89	12.7
1.0	3.0	41.00	45.48	6.965	.242	.02592	.4	.00818	53.88	14.5
1.0	4.0	44.44	45.44	5.083	.223	.02597	.4	.00819	54.11	13.5
1.0	5.0	47.00	45.45	3.96	.221	.02598	.4	.00819	54.28	13.5
1.0	10.0	54.06	45.39	1.788	.200	.02604	.4	.008197	54.43	12.4
1.0	15.0	57.82	45.422	1.122	.205	.02603	.4	.008195	54.53	12.7
1.0	20.0	60.39	45.495	.809	.219	.02601	.4	.008191	54.64	13.5
1.0	25.0	62.42	45.64	.629	.252	.025948	.4	.001812	54.82	15.4
1.0	50.0	67.65	45.55	.288	.231	.025987	.4	.008188	54.74	14.2
1.0	75.0	70.38	45.42	.183	.204	.026041	.4	.008197	54.60	12.6
1.0	100.0	72.72	45.645	.134	.253	.025948	.4	.008182	54.87	15.4
1.0	125.0	74.25	45.654	.105	.255	.025945	.4	.008182	54.88	15.6
1.0	150.0	75.29	45.548	.086	.230	.025989	.4	.008189	54.75	14.1

increases leading to a disproportionate variation of the energy which the avalanches can draw from the external electric field. A comparison of columns three and six in Table 8 actually shows the same tendency of variation and suggests that the number of electrons in the initial avalanche is proportional to the energy which the avalanche can gain from the external electric field. A comparison of the computed onset field intensity with the experimental results of Table 5 shows good agreement again, especially with the results obtained from photomultiplier studies.

If the length of the avalanche and the average field gradient along the path of the avalanche are related to each other, one finds a unique dependence shown in Figure 39. The data for Figure 39 is obtained from streamer onset computations not only for point-to-plane gaps but also for single unipolar conductors, and bipolar twin bundle conductor. A sample of computations leading to Figure 39 is given in Table 9. It shows that as the gap distance is increased, the onset potential rises steadily, whereas the onset field remains reasonably constant except for distances smaller than 2 cm. Like the onset field at the anode, the optimal avalanche length, the average field slope along the path of the avalanche, the number of charged particles in the avalanche, transit time of the avalanche, and space charge radius remain constant as well. The field distribution throughout the gap space, however, changes considerably as can be seen from the decrease of the cathode field.

In these computations it was tacitly assumed so far that the trigger electron originates from an area of the gap where the external field is

approximately 30 V/cm-Torr. If the origin of the avalanche is allowed to change around this value then higher onset potentials must be expected in any case as shown in Table 10 where E/p, the ratio of field intensity and atmospheric pressure, is varied from 50 to 5 V/cm-Torr. Clearly there is a minimum for the onset potential if E/p is equal to the optimal case. But also the number of space charges is at a minimum, whereas space charge radius avalanche energy and avalanche length increase inversely proportional to E/p. The variation of the minimum avalanche field actually simulates the case of a free electron which is available at positions other than the one where E/p = 30 V/cm-Torr. These results, therefore, can be interpreted as indicated that streamers will be initiated at minimum onset potential only if a free electron is available in the 30 V/cm-Torr region. A variation of this minimum field by $\pm$ 60% leads to an onset potential variation of only 4% as shown by the values V_o at E/p = 50 and 11 V/cm-Torr in Table 10, respectively.

Another aspect of streamer propagation was studied using the mathematical model discussed previously. It has been observed, as mentioned in the introduction, that streamers are capable of advancing into regions of very low fields. A minimum field value for the sustained streamer propagation in the order of 500 V/cm was suggested by Nasser et al. This is far below the values necessary to initiate a streamer process, and it is therefore assumed that streamers propagate mainly under the influence of their own space charge. Although the program does not provide for the simulation of the streamer propagation process, it can be used to obtain some insight into the effect of the space charge since

Table 10. Variation of the minimum avalanche field for a rod-to-plane gap.

r=1.50 cm V_o (kV)	d=10 cm E_{Ao} (kV/cm)	E_{ca} (kV/cm)	$\int_e \alpha(x)dx$ x 10^5	E/p_{min} V/cm-Torr	W_{Ava} (kJ)x10^{-10}	Avalanche length (cm)	Space Ch. Radius (cm)	Transit Time (μsec)
36.63	55.1	.981	.461	50	.0795	.15	.004637	.00833
35.23[a]	53.084	.944	.24	30	.101	.25	.00644	.0161
35.7	53.789	.956	.451	20	.524	.5	.0105	.0428
36.778	55.414	.985	1.770	11	3.45	.95	.0175	.1181
39.029	58.805	1.045	43.933	5	123.0	2.05	.03292	.4218

[a]Optimal case.

the model illustrated in Figures 45 and 46 can be thought of as an instantaneous picture of a streamer tip, provided the rod radius is chosen small enough. In Table 11, onset data is given for the field conditions around the anode for decreasing anode diameters, down to values corresponding to radii on streamer channels. External field and space charge field are listed separately for a distance 2 x R from the anode surface. A comparison shows that the space charge field increases rapidly as the anode radius decreases. It is of the same magnitude of the external field for an anode radius smaller than approximately 0.02 cm. For the anode radius equal to 0.003 cm the space charge field is twice the external field in the vicinity of the space charge, and clearly should dominate the ionization processes in this region. The predominance of the space charge field over the external field is only preserved within a short range. In this particular case at a distance of 0.004 cm, approximately equal to three times the space charge radius, the external field will be equal to the space charge field, and at a distance beyond 0.007 cm, the ionization factor due to the space charge field will be less than 1.0. The external field decays to that value at a distance of 0.016 cm from the electrode tip.

At large point radii, the space charge is completely insufficient to make any contributions to the streamer process.

Table 11. Effect of the space charge on the field intensity.

Rod Radius cm	Gap Distance cm	Anode Field E_A kV/cm	Space Charge Field $E_{sp.ch}$ kV/cm	Field at 2r From Anode E_{2R} kV/cm	Space Charge Radius r, cm
.003	11.0	471.2	357.52	143.15	.001314
.038	1.0	130.65	49.44	100.44	.00269
.05	10.0	110.813	39.08	88.169	.003054
.3	10.0	61.38	.2855	56.807	.0059
.5	10.0	35.23	.0931	50.4536	.0064
1.58	9.0	41.334	.02194	40.213	.01093

VII. DISCUSSION

A. The Onset of Streamers

Prior to analyzing any of the above results it is important to know the effect of the variation of the gap parameters on the distribution of the electrostatic field. Figure 40 a and b show the field distribution in per unit Volts/cm for the various gap configurations used in the experiments. The plots demonstrate that the slope of the field intensity decreases as the point radius increases. For a given potential there is also a drop of the anode surface field intensity in the order of 10 if the point radius is increased by a factor of 10. In different gap regions, different point radii will produce a maximum field intensity. Within 1.5 mm from the anode tip the field of the .5 mm point is the highest. Then, between 1.5 and 4.0 mm the field of 3.0 mm point, and from 4.0 mm on throughout the gap space the 5.0 mm point produces maximum field intensity. An increase of the gap length does not produce any drastic change on the field distribution. The field for d = 15 cm and R = 5 mm is only approximately 17% lower than for d = 10 cm and R = 5.0 mm throughout the comparable gap range for the same potential.

In view of the variation of the field intensity the relationship between optimum avalanche length and the field slope from Figure 39 finds a simple qualitative explanation. Since the avalanche length is determined by the location of the field value equal to 30 V/cm-Torr, there must be a minimum distance L_{min} for a given field distribution where an avalanche can reach its critical amplification to fulfill Loeb's criterion. The

avalanche has to be amplified sufficiently before the light radiation can generate enough photoelectrons to reproduce the space charge of the initial avalanche.

Two parameters are important in this process; the ionization coefficient α which depends on the field, and the absorption coefficient μ which is independent of the external field. If the anode potential is too low and the avalanche starts too close to the anode there will be comparatively little photon radiation from the avalanche head and the probability that the photoelectrons are generated within the field region above 30 V/cm-Torr is small. Therefore, there is little chance that successive avalanches reproduce the space charge of the primary avalanche.

At the onset limit the potential has to be raised only slightly to add a few ionizing free paths to the avalanche length to fulfill the the onset conditions. Due to the double exponential amplification of the avalanches the photon radiation rises drastically, and the probability that photoelectrons are generated within the region of E larger than 30 V/cm-Torr increases exponentially with the increase of photon absorption. Therefore, the streamer onset limit is extremely sharply defined. If we assume that the field distribution is approximately linear, then we can relate a unique boundary L_{min} to any field gradient above 30 V/cm-Torr beyond which the onset condition can be fulfilled. This is illustrated in Figure 41 for the point-to-plane gaps used in the experiments. If the slope is steep the initial avalanche is amplified quickly, therefore, L_{min} is short. If the slope is flat, L_{min} has to be longer. The relationship is not linear because a larger proportion of the light

radiation is absorbed within the field region above 30 V/cm-Torr, and also because of the nonlinear avalanche amplification. Since the slope of the field hardly changes around the anode if the gap distance is increased (Figure 40b) the onset field stays constant as found in the experiments (Figure 14) and the computations (Figures 36 through 38). The relationship between field slope and initial avalanche length is shown in Figure 39. It was found to be true not only for point-to-plane gaps but also for other gap configurations like unipolar and bipolar cylindrical conductors parallel to ground. Since it is actually determined for E/p it should also be true for different pressures. A least square fit through the data points of Figure 39 yielded the empirical relationship

$$Y = 12.8 * L_{min}^{-1.76} \qquad (9)$$

with

Y = Average rate of decrease of the field intensity

L_{min} = Distance from the anode to the point where the field is equal to 30 V/cm-Torr.

This relationship also explains the minimum onset voltage if the initial avalanche starts at a field of 30 V/cm-Torr as suggested by the results of the computer study in Table 10. An increase of the minimum E/p corresponds to a reduction of the avalanche length, and the decrease of E/p leads to a physically unrealistic situation of avalanche sizes smaller than 1 electron which can be accounted for by electron attachment on gas molecules. Although the mathematical model in the latter case

does not truly reflect the physical conditions in all details it produces the right tendencies. For example, if an electron should start in a region below the 30 V/cm-Torr limit it must drift into that region before an avalanche process can start and the longer it must drift in a low field region the smaller the probability that it actually will initiate an avalanche. The long time lag at onset may be in part a consequence of this effect. Table 10 lists the transit time for electron avalanches and shows that the time to develop only the initial avalanches is already of the order of a μsec if much of its path goes through the low field region. As to the varying scatter of the time lag at onset potential described in Figure 24 one may conclude that due to the steep field drop at large d/R, there is only a small region from where electrons may drift to the high field region, while for smaller field gradients this region becomes progressively larger.

The probability that free electrons are produced by detachment processes from negative ions in the region of fields around 30 V/cm-Torr is enhanced because of the increase in volume in which this field intensity prevails. Since the detachment processes of this field intensity may require up to 10^{-6} sec (Saint-Arnaud, 1969), streamers with long time lags of that order of magnitude will occur as observed and described in Figure 24.

B. The Propagation of Streamers

Having determined and explained the influence of the various parameters that govern streamer onset, it is important now to explain which parameters

govern the process of the continued propagation of streamers. The relationship between streamer radiation intensity and/or propagation velocity and the external field shall be evaluated and the results shall be investigated for possible consistencies in the intensity decline. According to Equation 9 the radiation intensity of streamers is proportional to the number of ions in the streamer space charge. The number of ions in the space charge on the other hand is directly related to the energy content of the streamer according to Equation 6. If the external field is the dominant parameter in the streamer propagation process, some relationship between field intensity and streamer intensity should be found.

The results from the propagation measurements shown in Figure 31 and 32, however, do not suggest any such relationship between streamer intensity or streamer velocity on one hand and the field intensity on the other hand. On the contrary, for the same field intensities there are considerable differences in the streamer intensities and velocities throughout the gap space. Table 12 through 14 list the results from streamer velocity and intensity measurements for d = 10 cm and R = .5, 3.0, 5.0 mm. The values of intensity decline are given in percent per cm. The relative decrease of streamer intensities as they propagate was calculated using the initial intensity at any x as a base. The mean field intensity E_m was also determined at these locations. According to the calculations summarized in Tables 12 through 14 neither "absolute" nor relative decline of streamer intensity seems directly related to the prevailing mean field intensities over the observed intervals. The same

Table 12. Streamer propagation intensity and velocity d = 10 cm, R = .5 mm.

V [kV]	E [kV/cm]	E_M [kV/cm]	S [cm]	Int. [%]	Abs. Decr. [%/cm]	Rel. Decr. [$\%^2$/cm]	Vel. [cm/sec]x10^7
36	4.25		0.0	100			
	4.1		1.0	71			
	1.94	3.02	2.0	113	28	39	3.33
	1.3	1.62	3.0	22	21	49	2.18
	1.23	1.28	3.18	19	16	75	2.63
	1.15	1.19	3.3	17	16.6	88	2.5
	1.15	1.13	3.5	14	15.0	89	2.44
	1.04	1.07	3.7	11	15.0	102	2.38
	1.0	1.02	3.4	8	15.0	136	2.27
	.936	.97	4.2	5	10.0	125	2.17
44	5.02		1.0	100			
	2.38	3.7	2.0	58	42	42	1.17
	1.58	1.98	3.0	33	25	43	3.57
	1.36	1.47	3.5	25	16	48.5	3.13
	1.27	1.31	3.75	22	12	48	3.03
	1.19	1.23	4.05	19	10	45.6	2.14
	1.1	1.14	4.45	16	7.5	40	2.76
	.9	1.0	5.6	10	5.3	34	2.63
	.83	.77	6.25	8	3.0	31	2.33
53	1.63		3.5	68			
	1.43	1.53	4.0	53	30	44	4.17
	1.165	1.29	5.0	30	23	43.4	3.71
	1.16	1.162	5.25	25	20	66	3.57
	1.12	1.14	5.5	22	12	48	3.33
	1.06	1.09	5.75	19	12	54.5	3.13
	1.0	1.03	6.25	15	8	42	2.78
	.9	.95	7.25	10	5	33	2.21
	.85	.87	8.0	8	2.66	26.6	1.5
	.82	.835	9.5	5	2	25	1.34
61	1.22		6.0	37			
	1.1	1.16	7.0	27	10	27	3.13
	1.07	1.09	7.25	25	8	29.6	2.63
	1.0	1.035	8.15	20	5.06	25.2	2.56
	.975	.985	8.4	19	4.0	21.0	2.5
	.964	.97	9.35	16	3.1	19.3	2.17
	.945	.954	10.0	14	2.1	15.0	2.15

Table 13. Streamer propagation intensity and velocity d = 10 cm, R = 3.0 mm.

V [kV]	E [kV/cm]	E_M [kV/cm]	S [cm]	Int. [%]	Abs. Decr. [%/cm]	Rel. Decr. [$\%^2$/cm]	Vel. [cm/sec]x10^7
36	89.6		0.0	85			
	6.85		1.0	16			
	2.85	4.35	2.0	8	8	50	3.72
	1.8	2.3	3.0	5	3	37	2.33
	1.53	1.66	3.5	3.5	3	60	2.05
44	103.5		0.0	100			
	8.36		1.0	41			
	3.08	5.73	2.0	19	22	54	4.72
	2.9	2.95	2.3	16	10	53	3.03
	2.2	2.55	3.0	11	7.15	44.7	2.43
	1.8	2.03	3.5	9	4	52	2.78
	1.67	1.73	4.0	7.5	3	33	2.21
	1.36	1.5	5.0	5	2.5	33	1.19
	1.21	1.28	6.0	3.5	1.5	33	.47
53	10		1.0	100			
	4.2	7.1	2.0	63	37	37	5.0
	2.62	3.4	3.0	37	26	41.4	3.85
	2.26	2.4	3.5	26	22	59.5	3.33
	1.96	2.11	4.0	19	14	54	3.13
	1.88	1.92	4.25	16	12	63	3.13
	1.53	1.7	5.5	8	6.4	40	2.21
	1.32	1.42	7.0	5	2.0	25	2.03
	1.22	1.27	9.5	3.5	.6	12	1.64
61	2.6		3.5	42			
	2.0	2.3	4.5	32	10	24	5.0
	1.89	1.95	5.0	28	8	25	5.0
	1.68	1.78	6.0	22	6	21.5	5.0
	1.52	1.6	7.0	19	3	13.6	4.116
	1.4	1.46	8.5	16	2	10.5	4.16
	1.38	1.39	10.0	12.5	2.3	14.4	3.57

Table 14. Streamer propagation intensity and velocity d = 10 cm, R = 5.0 cm.

V [kV]	E [kV/cm]	E_M [kV/cm]	S [cm]	Int. [%]	Abs. Decr. [%/cm]	Rel. Decr. [$\%^2$/cm]	Vel. [cm/sec]x10^7
36	54.		0.0	90			
	7.55		1.0	34			
	4.4	5.95	1.7	19	21.4	63	2.8
	4.0	4.2	1.85	16	20.0	105	2.78
	3.6	3.8	2.0	13	20.0	125	2.5
	3.02	3.33	2.3	8	16	128	2.14
	2.7	2.86	2.55	5	12	150	2.08
	2.48	2.6	2.65	3.5	15	300	2.0
44	5.72		1.5	90			
	4.4		2.0	73			
	2.78	3.6	3.0	47	26	35	4.17
	2.11	2.45	4.0	28	19	40.5	3.23
	1.8	1.45	4.75	19	10.7	38	2.5
	1.7	1.75	5.1	16	6.6	45	2.05
	1.6	1.65	5.5	13	7.5	47	1.54
53	5.3		2.0	97			
	3.34	4.3	3.0	71	26	26.1	5.0
	2.55	2.45	4.0	50	21	29	4.17
	2.07	2.3	5.0	34	16	32	2.86
	1.93	2.0	5.5	28	12	35	2.08
	1.7	1.815	6.65	19	7.8	28	1.54
	1.59	1.64	7.3	16	4.6	32	1.18
	1.44	1.51	9.5	13	1.35	8.5	1.13
61	4.7		2.5	98			
	3.3	4.0	3.5	73	25	25	5.0
	2.93	3.1	4.0	63	20	27.4	4.55
	2.38	2.66	5.0	46	17	27.0	3.7
	2.07	2.24	6.0	37	9	19.5	2.7
	1.9	1.98	7.0	30	7	19.0	2.08
	1.81	1.85	7.5	28	4	13.5	1.57
	1.63	1.72	10.0	20	3.2	11.4	1.18

is found to be true also for the streamer velocity of propagation.

The results are illustrated in Figure 42 which shows that the propagation velocity varies anywhere between 2.0×10^7 cm/sec and 5.0×10^7 cm/sec in a field ranging from 1 kV/cm to 5 kV/cm. The curves have different slopes and therefore, intersect which means that there is no apparent relationship between streamer propagation velocity and the applied field. This is unlike the drift velocity of charged particles which is solely dependent upon E at any given pressure. Hence, it was quite astonishing to find this unexpected result.

The streamer intensity decline at various mean field intensities is plotted in Figure 43. The streamer intensity decline varies from 5% to 35% at fields between 1 and 3.5 kV/cm. Again here, the external field does not seem to govern either the streamer intensity or the decline thereof.

The apparent lack of correlation between the field intensity on one hand and streamer intensity on the other hand leads us to assume that it must be the initial conditions which determine the intensity decline. A comparison of the decline of streamer intensities is made in Figure 44 for varying gap configurations at different applied voltages. It actually shows a consistent rate of decline of streamer intensity to to about 10% of maximum observable with the photomultiplier circuit, provided the initial intensity at the anode is approximately the same. This is supporting the above assumption.

If the streamers propagate mainly on account of their own space charge, the space charge field intensity must be sufficient to entertain

the streamer process. The results from the theoretical study listed in Table11 suggest that space charges of only 3.5×10^5 particles can produce a field intensity which will support a streamer process by fulfilling Equation 9. It is important to note, however, that extremely strong field intensities prevail only over a short distance around the space charge, shorter than the photoionizing free path in air. Photoelectrons, therefore, will drift towards the space charge and it is expected that the external field is an important factor in controlling the drift velocity of the photoelectron.

In this connection it is significant that the minimum field of streamer propagation was determined to be 600 V/cm in agreement with earlier studies (Nasser, et al., 1968; Nasser and Shah, 1969). It seems to contradict the theory that the length of the streamer depends on the initial intensity as outlined above. In view of the findings of Ollendorf (Ollendorf, 1932), however, this result only emphasizes the importance of the electron drift velocity in front of the space charge for the streamer propagation in the low field region. Ollendorf determined that the drift velocity of electrons due to the influence of an electric field significantly exceeds the thermal motion of electrons in air at normal pressure and temperature if the electric field is larger than approximately 600 V/cm. The photoelectrons will be able to drift into the high field region only if the external field is strong enouth to overcome the random thermal motion. The minimum field to achieve this is approximately 600 V/cm.

Also some observations of propagation patterns of streamers on Lichtenberg figures can be interpreted in the light of this condition. The lack of small tips on the sides of the streamer immediately after branching, the deflection of the streamers if they approach each other, the minimum branching angle, and also the suppression of one branch if three branches are generated simultaneously reflect the fact that a low field region is present from which photoelectrons cannot drift towards the space charge. In these cases the low field region is induced by the unipolar space charges themselves. Since this effect is isolated from previous propagation processes and is not related in any way to the initial conditions of the streamer it also does not contradict the findings from above that streamer propagation is governed mainly by the initial conditions of the space charge. Streamers may actually not reach the minimum field region as it is the case at onset conditions, where the field intensity at the streamer tip was found to be around 1100 V/cm (Table 4). They never will penetrate into a field region lower than 600 V/cm however because the photoelectrons will not be able to reach the ionization region of the space charge.

Since all the results from the experiments and theoretical studies suggest that the initial streamer intensity is the predominant factor governing the streamer propagation, it is important now to investigate the factors that influence the initial intensity. The results of the theoretical study in Table 8 indicate that the number of particles in the space charge is not proportional to the field gradient in the high field region around the anode or the anode field, but to the energy which

the electrons can extract from the external field as defined by Equation 7.

The measurements of intensities agree with the findings of the theoretical study if we relate the results from Figure 33, for instance, for V = 44 kV to the field distribution above 22.8 kV/cm shown in Figure 40a. We find that the field intensity at R = 3.0 mm is always higher than that at R = 5.0 mm and that for most of the region at R = 0.5 mm the field is considerably higher. If the potential is increased the point E = 22.8 KV will be shifted to the right and consequently the ionization region will increase considerably in length for R = 5.0 mm and less so for R = 3.0 and R = 0.5. With this field distribution in mind, we then can estimate that at 44 KV the space charge will be largest for R = .5 mm due to the very high field region within 1 mm of the anode. Although the field distribution according to Figure 40a suggest a higher energy for R = 3.0 than for R = 5.0 one can not rule out, however, that the opposite may occur for the following reason. For example, the radial field off the axis must be considered because it tends to increase the space charge density whenever the streamer is not exactly on the axis. Therefore, we estimate a decreasing space charge over a variation of the point radii from .5 to 5.0 and 3.0, which is analogous to the variation of the streamer intensity as shown in Figure 33.

If the voltage is increased to 61 KV, the intensity of the streamer should increase faster for R = 5.0 than for r = 3.0, or .5 mm, because of the significant increase in length of the initial avalanche. This

fact is reflected in the results of Figure 33. At 61 kV the highest intensity is found for R = 5.0 and the lowest for R = 3.0. From both theoretical and experimental results we may conclude then that the streamer intensity is proportional to the high field region around the anode.

Some researchers suggested that a partial influence of the external field exists leading to a constant energy of the streamer space charge if the external field intensity is approximately 4 to 7 kV/cm (Acker and Penney, 1969 and Phelps, 1971). In this case, one would expect a region of constant streamer intensity. For this d = 10 cm and for R = 3.0 and 5.0 mm the streamer intensity was measured within 1.5 cm of the anode at 40 KV. No peak could be observed in either case, however, as shown in Figure 34.

VIII. CONCLUSIONS

Both experimental and computer studies yield a relationship between initial avalanche length and the gradient of the electric field above 22.8 KV/cm, which has to be fulfilled for streamer onset in air. The relationship can be described by the equation

$$Y = 12.8 * L_{min}^{-1.76}$$

with

Y = Average rate of decrease of the field

L_{min} = Length of initial electron avalanche

The streamer propagation studies did not yield any direct relationship between external field and streamer velocity or streamer intensity. Instead, the results indicate that streamer propagation is essentially governed by the streamer intensity produced in the high field region around the anode. The initial streamer intensity is proportional to the integral over the initial avalanche length $e \int_{x_1}^{d} n(x)E(x)dx$. No evidence could be found which indicates that a field intensity around 4 to 7 KV/cm there is an energy balance in the space charge reproduction process as suggested by Acker and Penney as well as Phelps. The external field influences the streamer velocity in the low field region at large distances from the anode since it determines the drift velocity of the photoelectrons as they approach the streamer head. The streamer advance, therefore, seizes if the drift velocity of the electrons due to the external field does not significantly exceed their thermal velocity.

The theoretical limit for this boundary is approximately 600 V/cm. In excellent agreement with the theory the experimental results yield values around 600 V/cm for the field intensity at the location where a streamer terminates. Streamers may stop earlier if their space charge energy is insufficient to propagate into the low field region. However, they will never advance beyond a limit given by the field intensity.

IX. LITERATURE CITED

Abou-Seada, M. S.
1970 Digital computer calculation of corona thresholds in nonuniform fields. Unpublished Ph.D. thesis. Ames, Iowa, Library, Iowa State University of Science and Technology.

Abou-Seada, M.S. and Nasser, E.
1968 Digital computer calculation of the electric potential and field of a rod gap. Proc. IEEE 56: 813-820.

Abou-Seada, M. S. and Nasser, E.
1969 Digital computer calculation of the potential and its gradient of a twin cylindrical conductor. Trans. IEEE on Power App. and Syst. PAS-88: 1802-1814.

Acker, F. E. and Penney, G. W.
1968 Influence of previous positive streamers on streamer propagation and breakdown in a positive point to plane gap. J. of Appl. Phys. 39: 2364-2369.

Acker, F. E. and Penney, G. W.
1969 Some experimental observations of the propagation of streamers in "low field" regions of an asymmetrical gap. J. of Appl. Phys. 40: 2397-2400.

Aked, A. and McAllister, I. W.
1970 Impulse voltage breakdown of long point/plane gaps. Int. Conf. on Gas Discharges London Conf. Proc. 70: 279-283.

Alexandrov, G. N.
1969 Peculiarities of spark discharge development in long air gaps. Int. Conf. on Phenomena in Ionized Gases Bucharest Conf. Proc. 9: 283.

Alexandrov, G. N., Redkov, V. P., Gorin, B. N., Stekolnikov, I. S., and Shkilyov, A. V.
1970 Peculiarities of spark discharge in long air gaps of high voltage structures. Int. Conf. on Gas Discharges London Conf. Proc. 70: 309-312.

Amin, M. R.
1954a Fast time analysis of intermittent point-to-plane corona in air I. The positive point burst pulse corona. J. of Appl. Phys. 25: 210-216.

Amin, M. R.
1954b Fast time analysis of intermittent point-to-plane corona in air II. The positive pre-onset streamer corona. J. of Appl. Phys. 25: 358-363.

Baker, J. H. and Williams, A. W.
1970 A new apparatus for the study of pre-breakdown ionization growth in gases. Int. Conf. on Gas Discharges London Conf. Proc. 70: 21-25.

Baldo, G. and Gallimberti, I.
1970 Charge and field measurements in rod plane gaps under impulse voltage. Int. Conf. on Gas Discharges London Conf. Proc. 70: 576-580.

Banford, H. M., Chalmers, I. D., Chalmers, P., and Tedford, D. J.
1970 Sparkover phenomena in air and arcton 12 at high values of pd. Int. Conf. on Gas Discharges London Conf. Proc. 70: 273-278.

Baumann, W.
1957 Statistische fehler bei der bestimmung der 50% uberschlagsstoss-spannung. Elektrotechn. Zeitschr. ETZ-A 78: 369-375.

Bazelyan, E. M., Brago, E. N., and Stekolnikov, I. S.
1961 The large reduction in mean breakdown gradients in long discharge gaps with an oblique-sloping voltage wave. Soviet Physics Doklady 5: 794-796.

Blackett, J., Mattingley, J. M., and Ryan, H. M.
1970 Breakdown voltage estimation in gases using a semi-empirical concept. Int. Conf. on Gas Discharges London Conf. Proc. 70: 293-297.

Blair, D. T. A., Whittington, H. W.
1970 Absorption of radiation in a Townsend discharge. Int. Conf. on Gas Discharges London Conf. Proc. 70: 1-5.

Boylett, F. D. A., Williams, B. G.
1968 A new process observed in the development of a long spark. Brit. J. of Appl. Phys. Ser. 2, 1: 1505-1507.

Bronstein, I. and Semendjajew, K.
1962 Taschenbuch der mathematik. 6th ed. Frankfurt, Germany, Harri Deutsch Verlag.

Brown, S. C.
1966 Basic data of plasma physics. 2nd ed. Cambridge, Massachusetts, The M.I.T. Press.

Buchet, G. and Goldman, M.
1969a Stability of positive continuous corona discharges in electronegative and non-electronegative gaseous mixtures. Int. Conf. on Phenomena in Ionized Gases Bucharest Conf. Proc. 9: 291.

Buchet, G. and Goldman, M.
1969b On the stability of continuous positive corona discharges. Int. Conf. on Phenomena in Ionized Gases Bucharest Conf. Proc. 9: 292.

Buchet, G. and Goldman, M.
1970 Considerations sur l'entretien des decharges couronnes positives continues. Mimeographed Copy. Ivry, France, Laboratoire de Synthese Atomique et d'Optique Protonique, CNRS.

Cavenor, M. C.
1970 An experimental test of the streamer breakdown criterion. Austr. J. of Appl. Phys. 23: 953-956.

Csernatony and Hoffer, A.
1962 Uber den mechanismus des polaritaoseffektes in der durchschlagsspannung von gasen. Arch. fur Elektrotechn. 47: 207-218.

Dawson, G. A.
1965a Temporal growth of suppressed corona streamers in atmospheric air. J. of Appl. Phys. 36: 3391-3395.

Dawson, G. A.
1965b The lifetime of positive streamers in a pulsed point-to-plane gap in atmospheric air. Zeitschr. fur Physik 183: 172-183.

Dawson, G. A. and Winn, W. P.
1965 A model for streamer propagation. Zeitschr. fur Physik 183: 159-171.

DeGeeter, D. J.
1963 Photographic observations of a pre-breakdown discharge transition between metal electrodes in vacuum. J. of Appl. Phys. 34: 919-920.

Dimitry, D. and Mott, Th.
1966 Introduction to fortran IV programming. New York, N.Y., Holt, Rinehart, and Winston, Inc.

Dutton, J. and Harris, F. M.
1970 High voltage breakdown in uniform fields. Int. Conf. on Gas Discharges London Conf. Proc. 70: 544-548.

Elliott, R. S.
1966 Electromagnetics. New York, N.Y., McGraw-Hill Book Co., Inc.

English, W. N. and Loeb, L. B.
1949 Point-to-plane corona onsets. J. of Appl. Phys. 20: 707-711.

Etzel, O. and Helmchen, G.
1964 Berechnung der elemente des stosspannungskreises fur die stosspannungen 1.2/50 und 1.2/200. Elektrotechn. Zeitschr. ETZ-A 85: 578-582.

Feser, K.
1970 Inhomogene luftfunkenstrecken bei verschiedener spannungsbeanspruchung. Unpublished Dr.-Ing. thesis. Munich, Germany, Bibliothek, Technische Hochschule Munchen.

Flegler, E.
1967 Probleme des elektrischen durchschlags. Koln, Germany, Westdeutscher Verlag.

Fruengel, F. B. A.
1965a High speed pulse technology I. New York, N.Y., Academic Press.

Fruengel, F. B. A.
1965b High speed pulse technology II. New York, N.Y., Academic Press.

Gallimberti, I. and Rea, M.
1970 Leader development in positive rod-plane gap discharges. Int. Conf. on Gas Discharges London Conf. Proc. 70: 298-302.

Giao, T. N. and Jordan, J. B.
1968 Modes of corona discharges in air. Trans. IEEE on Power App. and Syst. PAS-87: 1207-1212.

Hamouda, E. D. and Meek, J. M.
1967 Space charge fields in positive point-plane discharge. Int. Conf. on Phenomena in Ionized Gases Vienna Conf. Proc. 8: 207.

Heiszler, M. and Nasser, E.
1968 Voltage and field threshold for positive streamer onset (Abstract). Gaseous Electronics Conf. Boulder Conf. Ann. Proc. 21: 13.

Henrici, P.
1964 Elements of numerical analysis. New York, N.Y., John Wiley and Sons.

Hermstein, W.
1960a Die stromfadenentladung und ihr ubergang in das glimmen. Arch. fur Elektrotech. 45: 209-224.

Hermstein, W.
1960b Die entwicklung der positiven vorentladungen in luft zum durchschlag. Arch. fur Elektrotech. 45: 279-288.

Hoegl, A.
1963 Messung von konzentration und beweglichkeit atmospharischer jonen. Zeitschr. fur Angew. Physik. 16: 252-258.

Howatson, A. M.
1965 An introduction to gas discharge. London, England, Pergamon Press.

Hudson, G. G. and Loeb, L. B.
1961 Streamer mechanism and main stroke in the filamentary spark breakdown in air as revealed by photomultipliers and fast oscilloscopic techniques. Phys. Review 123: 29-43.

Kip, A. F.
1938 Positive point-to-plane discharge in air at atmospheric pressure. Phys. Review 54: 139-146.

Kip, A. F.
1939 Onset studies of positive point-to-plane corona in air at atmospheric pressure. Phys. Review 55: 549-556.

Knoll, M., Ollendorf, F., and Rompe, R.
1935 Gasentladungstabellen. Berlin, Germany, Springer Verlag.

Koppitz, J.
1967 On the axial and radial development of the luminous spark channel (in H_2 and N_2). Int. Conf. of Phenomena in Ionized Gases Vienna Conf. Proc. 8: 201.

Krätzig, E.
1967 Vorentladungen im feld kugel-platte in luft bei gleichspannung. Wiss. Zeitschr. der TU Dresden 16: 211-221.

Kuffel, E.
1959 Electron attachment coefficients in oxygen, dry air, humid air, and water vapour. Proc. of the Phys. Soc. London 74: 297-308.

Kuffel, E. and Abdullah, M.
1966 Corona breakdown voltage characteristics in sphere-to-plane and rod-rod gaps under impulse voltages of various wavefront durations. Proc. IEEE 113: 1113-1119.

Laboratoire de Synthese Atomique et d'Optique Protonique.
1971 Rapport d-activite de l'equipe de recherches sur la physique des decharges. Depuis la Creation de la RCP. Mimeographed report of Research Center for the period 1969-1970. Irvy, France, author.

Lampe, W. L.
1963 Der durchschlagmechanismus positiver, langer funken in atmospharischer luft bei stosspannung. Arch. fur Elektrotech. 47: 388-408.

Leloup, J.
1967 Influence on the spark formation of the initiating avalanche electron distribution. Int. Conf. on Phenomena in Ionized Gases Vienna Conf. Proc. 8: 196.

Lemke, E.
1968 Der durchschlagsmechanismus von luftfunkenstrecken bei schaltspannungen. Wiss. Zeitschr. der TU Dresden 17: 105-115.

Lesch, G.
1959 Lehrbuch der hochspannungstechnik. Berlin, Germany, Springer Verlag.

Levitov, V. I., Liapin, A. G., and Shevtzov, E. N.
1969 On transition of corona into the spark breakdown. Int. Conf. on Phenomena in Ionized Gases Bucharest Conf. Proc. 9: 279.

Loeb, L. B.
1965 Electrical corona. Berkeley, Calif., Univ. of California Press.

Lozansky, E. D. and Firsov, O. B.
1969 A model of streamer propagation. Int. Conf. on Phenomena in Ionized Gases Bucharest Conf. Proc. 9: 275.

Marode, E. G.
1967 The preionization to spark transition in a point to plane discharge in air at atmospheric pressure. Int. Conf. on Phenomena in Ionized Gases Vienna Conf. Proc. 8: 192.

Marode, E. Goldman M.
1969 On the streamer to spark transition of a positive point to plane discharge in air at atmospheric pressure. Int. Conf. on Phenomenain Ionized Gases Bucharest Conf. Proc. 9: 270.

Marode, E.
1970 Nature of the primary-secondary streamer sequence in a positive point to plane discharge. Int. Conf. on Gas Discharge London Conf. Proc.: 525-529.

Menes, M. and Fisher, L. H.
1954 Positive point-to-plane corona studies in air. Phys. Review 94: 1-6.

Merrill, F. H. and Hippel, A. von
1939 The atom physical interpretation of Lichtenberg figures and their application to the study of gas discharge phenomena. J. of Appl. Phys. 10: 873-887.

Mesjatz, G. A. Bichkov, Y. I., and Iskol'dskij, A. M.
1967 On the increase of spark current during pulse breakdown of air gaps in nanosecond time range. Int. Conf. on Phenomena in Ionized Gases Vienna Conf. Rep. 8: 210.

Mesjatz, G. A. and Bichkov, Y. I.
1969 Development of impulsive nanosecond discharge in air at one electron initiation. Int. Conf. on Phenomena in Ionized Gases Bucharest Conf. Proc. 9: 262.

Miyoshi, Y. and Hosokawa, T.
1970 Pre-corona discharge in air. Int. Conf. on Gas Discharges London Conf. Proc. 70: 26-70.

Mulcahy, M. J. and Zumich, Z.
1967 Influence of electrode diameter on corona and breakdown in air. Int. Conf. of Phenomena in Ionized Gases Vienna Conf. Proc. 8: 197.

Nasser, E.
1963 Die ionisierten potentialwellen beim funkendurchschlag. Zeitschr. fur Physik 172: 405-428.

Nasser, E.
1966 Role of the cathode field emission in the streamer-spark transition. J. of Appl. Phys. 37: 4712-4716.

Nasser, E.
1967 The propagation of cathode directed streamers in asymmetrical field configuration. Int. Conf. on Phenomena in Ionized Gases Vienna Conf. Proc. 8: 194.

Nasser, E.
1971 Fundamentals of gaseous ionization and plasma electronics. New York, N.Y., John Wiley and Sons, Inc.

Nasser, E. and Manthiram, C.
1967 The shock-excited discharges from a stressed cathode. Int. Conf. on Phenomena in Ionized Gases Vienna Conf. Proc. 8: 195.

Nasser, E., Heiszler, M., and Abou-Seada, M. S.
1968 Field criterion for sustained streamer propagation. J. of Appl. Phys. 39: 3707-3713.

Nasser, E. and Shah, R.
1969 Analysis of streamer branching in atmospheric air. Int. Conf. on Phenomena in Ionized Gases Bucharest Conf. Proc. 9: 271.

Nasser, E. and Schroder, D. C.
1969 Secondary leader channels in low pressure air and nitrogen. Int. Conf. on Phenomena in Ionized Gases Bucharest Conf. Proc. 9: 272.

Newi, G.
1968 A high impedance, nanosecond rise time probe for measuring high voltage impulses. Trans. IEEE Power App. and Syst. PAS-87: 1779-1786.

Ollendorf, F.
1932 Über die kanalbreite von elektronenlawinen. Arch. fur Elektrotech. 26: 193-199.

Oshige, T.
1967 Positive streamer spark breakdown at low pressures in air. J. of Appl. Phys. 38: 2528-2534.

Park, T. H. and Cones, H. N.
1956 Surge voltage breakdown of air in a nonuniform field. Res. Nat. Bur. Stand. 56: 201-224.

Pedersen, A.
1949 Calculation of spark breakdown voltages in air at atmospheric pressure. Appl. Scientific Res. B1, No. 4: 299-305.

Pedersen, A.
1967 Calculation of spark breakdown or corona starting voltages in non-uniform fields. Trans. IEEE Power app. and Syst. PAS-86: 200-206.

Penney, G. W. and Hemmert, G. T.
1970 Photoionization in air, oxygen, and nitrogen. J. of Appl. Phys. 41: 572-577.

Perelman, L. S.
1969 Study of negative and positive point corona pulses in the air. Int. Conf. on Phenomena in Ionized Gases Bucharest Conf. Proc. 9: 286.

Peschke, E.
1968 Der durch- und uberschlag bei hoher gleichspannung in luft. Unpublished Dr.-Ing. thesis. Munich, Germany, Bibliothek, Technische Hochschule Munchen.

Phelps, C. T.
1971 Field-enhanced propagation of corona streamers. Unpublished mimeographed report, State University of New York.

Phelps, C. T. and Vonnegut, B.
1970 Charging of droplets by impulse corona. J. of Geophysical Res. 75: 4483-4490.

Plinke, W.
1967 Die ausbildung von teilentladungen an spitzen in luft. Elektrotech. Zeitschr. ETZ-A 88: 287-291.

Raether, H.
1939 Die entwicklung der elektronenlawine in den funkenkanal. Zeitschr. fur Physik 112: 464-489.

Raether, H.
1964 Elektron avalanches and breakdown in gases. Washington D.C., Butterworths, Inc.

Remde, Heinrich
1969 Stossdurchschlag einer spitze-platte funkenstrecke mit isolierschirm. Unpublished Dr.-Ing. thesis. Stuttgart, Germany, Bibliothek, Technische Hochschule Stuttgart.

Rogowski, W.
1936 Uber durchschlag und gasentladung. Zeitschr. fur Physik 100: 1-49.

Ruthloh, F. W. and Marheinecke, H. J.
1967 Allgemeine berechnung von stosschaltungen mit zwei energiespeichern. Elektrotech. Zeitschr. ETZ-A 88: 237-241.

Saint-Arnaud, R.
1969 Initiatory electrons for impulse corona. Int. Conf. on Phenomena in Ionized Gases Bucharest Conf. Proc. 9: 290.

Schroder, D. C.
1970 Development of leader channels in nonuniform fields. Unpublished M.S. thesis. Ames, Iowa, Library, Iowa State University of Science and Technology.

Schwab, A.
1963 Uber die anstiegszeiten von koronaentladungsimpulsen. Zeitschr. fur Angew. Physik 16: 23-27.

Schwab, A. and Zentner, R.
1968 Der ubergang von der impulsformigen in die impulslose koronaentladung. Elektrotech. Zeitschr. ETZ-A 89: 402-407.

Schwaiger, A.
1954 Uber elektrische entladungen in der luft. Elektrotech. Zeitschr. ETZ-A 75: 293-299.

Shah, R. M.
1969 The growth and attenuation of impulse streamer branching. Unpublished M.S. thesis. Ames, Iowa, Library, Iowa State University of Science and Technology.

Snedecor, G. and Cochran, W. G.
1967 Statistical methods. 6th ed. Ames, Iowa, Iowa State University Press.

Stassinopoulos, C. A. and Meek, J. M.
1967 The influence of space charges on spark growth in rod-plane gaps. Int. Conf. on Phenomena in Ionized Gases Vienna Conf. Proc. 8: 206.

Stassinopoulos, C. A.
1969 The influence of waveform on impulse breakdown of positive rod-plane gaps. Int. Conf. on Phenomena in Ionized Gases Bucharest Conf. Proc. 9: 261.

Steinbigler, H.
1969 Anfangsfeldstarken und ausnutzungsfaktoren rotationssymmetrischer elektrodenanordnungen in luft. Unpublished Dr.-Ing. thesis. Munich, Germany, Bibliothek, Technische Hochschule Munchen.

Tholl, H.
1967 Spectroscopic measurements of the temporal development of the radial density and temperature distribution in a spark channel in hydrogen. Int. Conf. on Phenomena in Ionized Gases Vienna Conf. Proc. 8: 198.

Trichel, G. W.
1939 The mechanism of the positive point-to-plane corona in air at atmospheric pressure. Physical Review 55: 382-390.

Virr, L. E., Lucas, J., and Kontoleon, N.
1970 Measurement of D/μ for electron swarms in gases at high E/p. Int. Conf. on Gas Discharges London Conf. Proc. 70: 530-533.

Vondenbusch, A.
1959 Beitrag zur berechnung von stosschaltungen mit zwei energiespeichern. Elektrotech. Zeitschr. ETZ-A 80: 617-622.

Wagner, C. F. and Hileman, A. R.
1964 Predischarge current characteristics of parallel electrode gaps. Trans. IEEE Power App. and Syst. PAS-83: 1236-1242.

Wagner, K. H.
1965 Die entwicklung der elektronenlawine in den plasmakanal, untersucht mit bildverstarker und wischverschluss. Zeitschr. fur Physik 189: 465-515.

Wagner, K. H.
1970 The effect of the second Townsend generation on the primary streamer. Int. Conf. on Gas Discharge London Conf. Proc. 70: 11-15.

Waters, R. T., Richard, T. E. S., and Stark, W. B.
1965 Influence of atmospheric ions on impulse corona discharge I. Proc. IEEE London 112: 1431-1438.

Waters, R. T., Richard, T. E. S., and Stark, W. B.
1968 Electric field and current densities in the impulse corona discharge in a rod/plane gap. Proc. of the Roy. Soc. London, A, 304: 187-210.

Waters, R. T., Richard, T. E. S., and Stark, W. B.
1970 The structure of the impulse corona in a rod/plane gap I. The positive corona. Proc. of the Royal Soc. London, A, 315: 1-25.

Wesendonk, K.
1890 Einige beobachtungen uber buschelentladungen. Ann. der Physik and Chemie 40: 481-488.

Winkelnkemper, H.
1965 Die aufbauzeit der vorentladungskanale im homogenen feld in luft. Elektrotech. Zeitschr. ETZ-A 86: 657-663.

Winkelnkemper, H.
1966 Die entwicklung der vorentladungskanale bis zum durchschlag im homogenen feld in luft. Arch. fur Elektrotech. 51: 1-15.

Wright, J. K.
1964 A contribution to the theory of impulse corona and the long spark. Proc. of the Roy. Soc. London, A, 280: 23-36.

Zeleny, J.
1920 Electrical discharges from pointed conductors. Physical Review 16: 102-125.

Zentner, R.
1970 Der raumlich-zeitliche aufbau der negativen impulsformigen koronaentladung. Abhandlungen des Instituts fur Hochspannungstechnik und elektrische Analgen, Karlsruhe, Germany, University of Karlsruhe, No. 14.

X. ACKNOWLEDGMENTS

I am most grateful to my major professor Dr. Essam Nasser for providing the opportunity to this study and for his guidance throughout the development of this thesis. I wish to thank the Power Affiliate Program and the National Science Foundation for their financial support which helped me to carry out this project.

Special thanks go to Darrell Schroder and James Schultz for their many suggestions they offered to the laboratory work, and to Dr. M. S. Abou-Seada for his initial contribution to the programming work.

XI. APPENDIX A

It is assumed that a trigger electron is available at distance x_1 from the cathode, in a point-to-plane gap of distance d (Figure 45), and that the external electric field at x_1 is larger than 30 V/cm-Torr. Then the trigger electron will be able to generate an avalanche as it advances towards the anode, and the total number of electrons or ions generated at a distance x from the cathode will be

$$n_x = n_o * e^{\int_{x_1}^{x} \alpha(x)dx} \tag{A-1}$$

where n_o in this case is equal to 1. In a slab of thickness dx at x the number of positive ions generated is then

$$dn = n_x * \alpha(x) * dx \tag{A-2}$$

and substituting Equation A-1 into Equation A-2

$$dn = n_o * \alpha(x) * e^{\int_{x_1}^{x} \alpha(x)dx} * dx \tag{A-3}$$

The positive ion density in the slab can be determined by assuming that all the ions are contained in a cylindrical volume of length dx and radius r, where r is equal to the space charge radius. Then we get for the ion density

$$\begin{aligned} n' &= dn/(\pi r^2 * dx) \\ &= n_o * \alpha(x) * e^{\int_{x_1}^{x} \alpha(x)dx} / \pi r^2 \end{aligned} \tag{A-4}$$

Since we assume that the positive ion space charge of an avalanche has approximately spherical shape and uniform charge distribution throughout the volume of radius r, the total number of ions contained in the volume is

$$N = n' * (4 \pi r^3/3)$$
$$= (4/3) * n_o * \alpha(x) * r * e^{\int_{x_1}^{x} \alpha(x)dx} \quad \text{(A-5)}$$

The field intensity produced by this space charge is given by

$$E_y = e * N/(4 \pi \epsilon_o y^2)$$
$$= e * n_o * \alpha(x) * r/(3 \pi \epsilon_o u^2) * e^{\int_{x_1}^{x} \alpha(x)dx} \quad \text{(A-6)}$$

where e is equal to the electron charge, and y equal to the radial distance from the space charge center. The production of photons and the amount of photoionization is proportional to the size of the ion space charge. If f denotes the proportion of excited states produced per ionization by collision, then the number of excited states produced as the avalanche arrives at x is equal to

$$N_e = f * N$$
$$= f * (4/3) * \alpha(x) * n_o * r * e^{\int_{x_1}^{x} \alpha(x)dx} \quad \text{(A-7)}$$

As the photons travel through the gas they will be absorbed at a rate described by the equation

$$I = I_o * e^{-\mu\rho} \quad \text{(A-8)}$$

where

I = Intensity of radiation at a distance ρ from the source

I_o = Intensity of radiation at the source

μ = Absorption coefficient of the gas

The decrease of intensity of radiation within a slab of length $d\rho$ is found by differentiating Equation A-8

$$dI = - \mu * I_o * e^{- \mu\rho} * d\rho \qquad \text{(A-9)}$$

Since I_o in this case is equal to the number of excited states as described in Equation A-7, the number of photons absorbed in a spherical shell of thickness $d\rho$ at a distance ρ from the space charge center is equal to

$$dN_{pe} = N * f * - \mu * e^{-\mu\rho} \, d\rho \qquad \text{(A-10)}$$

The amount of radiation absorbed, however, is proportional to the number of photoelectrons generated in these absorption processes. The proportionality is given by an empirical factor p, which is a measure of the probability of photoionization for a given photon absorption. Therefore, the number of photoelectrons generated in the shell is equal to

$$p * dN_{pe} = p * N * f * -\mu * e^{- \mu\rho} \, d\rho \qquad \text{(A-11)}$$

One can assume that right in front of the anode approximately one-half of the photoelectrons generated will not contribute to the streamer onset process, as they are produced to the right of the anode tip so that the total number of photoelectrons produced in a shell $d\rho$ and contributing to the streamer onset process will be

$$dN_{pe} = \tfrac{1}{2} * p * N * f * -\mu * e^{-\mu\rho}\, d\rho \qquad \text{(A-12)}$$

and the total number of active photoelectrons generated in semispherical volume of radius R around the avalanche space charge is

$$\begin{aligned} N_{pe} &= \int_{r}^{R} (\tfrac{1}{2}) * p * N * f * -\mu * e^{-\mu\rho}\, d\rho \\ &= (\tfrac{1}{2}) * p * f * N * (e^{-\mu r} - e^{-\mu R}) \end{aligned} \qquad \text{(A-13)}$$

These photoelectrons will now trigger avalanches themselves since R is such that all the field region where the intensity is above 30 V/cm-Torr is enclosed. Equations A-1 through A-4 also hold for these avalanches as illustrated in Figure 46. The space charge density in the tips of these photoelectron avalanches, as they arrive at the space charge of the initial avalanche, is

$$n'' = \alpha(x,\rho)/(\pi r'^{2}) * e^{\int_{\rho}^{r} \alpha(x,\rho)d\rho} \qquad \text{(A-14)}$$

where r' = space charge radius of the photoelectron avalanche. Then r' can be estimated from r if we assume that the drift velocity remains the same for both the initial avalanche and the photoelectron avalanches. Then

$$r'/r = (\rho - r)/(d - x_1) \simeq \rho/(d - x_1) \qquad \text{(A-15)}$$

for $\rho \gg r$.

The total number of positive ions from one photoelectron avalanche is then with Equation A-5

$$N_p = (4/3 * \alpha(x,\rho) * r' * e^{\int_{\rho}^{r} \alpha(x,\rho)d\rho}$$
$$= (4/3) * \rho * r * \alpha(x,\rho)/(d-x_1) * e^{\int_{\rho}^{r} \alpha(x,\rho)d\rho} \quad \text{(A-16)}$$

and the total number of ions due the whole photoelectron avalanche generation is equal to

$$N_t = N_p * N_{pe}$$
$$= \int_{r}^{R} (\tfrac{1}{2}) * p * f * N * - \mu * e^{-\mu\rho} * (4/3)$$
$$* \rho r\alpha(x,\rho)/(d-x_1) * e^{\int_{\rho}^{r} \alpha(x,\rho)d\rho} * d\rho \quad \text{(A-17)}$$
$$= \int_{r}^{R} (2/3)pfN\rho r\alpha(x,\rho)(-\mu e^{-\mu\rho})/(d-x_1)$$
$$* e^{\int_{\rho} \alpha(x,\rho)d\rho} * d\rho$$

The streamer onset condition is fulfilled if

$$N_t = N$$

Under this condition the space charge of the initial critical avalanche will be duplicated by one generation of photoelectron avalanches and no other trigger electrons are necessary to sustain the discharge. The ionization process is selfsustained and will continue as long as the potential is applied to the anode. The onset criterion for N_t equal to N therefore is

$$\int_{r}^{R} (2/3) * pf\rho r * \alpha(x,\rho) * - \mu e^{-\mu\rho}/(d-x_1)$$
$$* e^{\int_{\rho}^{r} \alpha(x,\rho)d\rho} * d\rho = 1 \quad \text{(A-18)}$$

XII. APPENDIX B

In selecting the gap dimensions, a compromise had to be made between large gap distances which provide a good time resolution for propagation measurements, and the limitations which are set by the maximum output voltage of the impulse generator so that the gas can be stressed up to the breakdown level. Therefore, a maximum gap length of 50 cm could be set for hemispherically capped cylinders with 1.0 mm, 3.0 mm, and 5.0 mm diameter, the ground plate diameter being 81.0 cm. Both electrodes are shown in Figures 47 and 48. The hemispherically capped cylinders, made of stainless steel, have a cylindrical portion of 9.5 cm, and are attached to a brass cone of 4.25 cm. Machined from the same piece of brass on the wide side of the cone there is a cylinder of 1.5 cm length and 1.0 cm diameter, and a 2.0 cm long thread to secure the seat of the electrode in a matching hole of the suspension platform described below. The ground plate was pressed from a 3.0 mm gauge aluminum sheet, the radius on the edges is 1.58 cm, and the height of the side walls 4.0 cm. The plate rests on a plastic socket of 5.0 cm diameter. The surfaces of all the electrodes were sanded and polished, and regularly cleaned with alcohol. In addition they were polished after every 3 to 5 complete breakdowns of the gap.

The cylinder electrodes were suspended in a plastic plate of 1.6 cm thickness through a hole in the center of the plate. The plate, referred to as the "working platform," has the shape of an equilateral triangle, and is suspended itself in the mainframe (Figure 49). In part, the main frame consists of three plastic rods of 1.0 m length and 2.0 cm diameter,

which reach through holes in the corners of the working platform. The rods are screwed to a wooden base plate on a circle of 85.0 cm diameter at an angle of 120^{o}. For reasons of stability, they are connected on top by another triangular plastic plate. On these rods, the working platform can be moved vertically into any position. If adjusted, it rests on three pins which can be plugged into horizontal holes in the rods. The holes are drilled in the outward pointing side in 2 mm intervals over the whole length of the rods. The fine adjustment of the electrode position can be made with the screw which holds the electrode in position in the center of the platform. The distances between the cylinder tip and the ground plate were checked with gauges machined to $\pm$ .1 mm accuracy.

Since the Lichtenberg figure technique was to be applied in the studies, the whole gap structure was surrounded by a wooden frame, enclosing a cube of 1.1 m side length covered by a triple layer of packing paper painted on both sides with dull black paint. Included in the dark chamber on one side of the cube is a small niche, which houses one of the photomultiplier units. The other photomultiplier hangs in one corner of the working platform, such that it's window is at the same level as the electrode tip. Figure 50 shows a photograph of the whole electrode system.

XIII. APPENDIX C

In order to achieve a fast-rising pulse, low induction circuit components and short circuit dimensions are most important, as are good ground connections to avoid excessive electric noise. The arrangement of the impulse generator is shown in Figure 51. The whole apparatus is placed over an aluminum base plate of approximately 2.3 m^2. The HVDC power supply with a maximum output voltage of 150 kV is connected to this base plate by a 1 m wide and 1 m long aluminum plate attached to the top cover of the power supply. From the same joint of the power supply, a 1 x 0.5 m aluminum plate is connected to the ground plate of the hemispherically capped cylinder to plane gap and the suspension frame of one of the PM's. For shielding purposes, a 2 x 2 m aluminum plate is mounted vertically between the trigger gap of the impulse generator and the point to plane gap. The circuit connection is fed through the plate by means of a high voltage cable with a 6.8 mm copper conductor and proper insulation.

The control pannel for the HVDC power supply, the -1.0 kVDC power supplies for the photomultipliers, the 11 VDC power supply for a field effect transistor used in the measuring circuit, and the oscilloscope are connected to the base plate by 1 x 2 m aluminum sheath, mounted vertically, thus shielding the equipment from the electrical noise of the impulse generator. The small DC power supplies are housed in a 0.61 x 0.61 x 0.3 m aluminum box, grounded with the same aluminum sheath, together with two low-pass power line filters for the power supplies and the oscilloscope to keep electrical noise from entering the measuring

circuit over the 117 VAC power line. The oscilloscope is housed in a special ventilated shielding box also grounded by the 1 x 2 m aluminum sheath. Coaxial cables are used for both feeder lines and measuring cables. To keep electric noise from being induced in the shield of the coaxial cables, they are placed in copper tubes or, where flexibility is necessary, in a triple coaxial shield isolated by insulation tape. The extra shields for the coaxial cables are connected to the common ground on several places. On the coaxial connector piece of one PM, a ferrite ring is mounted to dampen eventual electric noise travelling in the shield.

The impulse generator circuit is shown in Figure 52. From the 150 kV power supply (ripple 2% rms), two charging capacitors of 0.25 μF, connected in series with damping resistors of 193 and 242 ohm inserted, are charged up to the desired voltage level. By activating the trigger gap, the input side of the capacitors is set to zero causing an equivalent potential change on the output point of the impulse generator across a 10225 ohm load resistor. The 280 ohm resistor between output point and the capacitor also serves as damping resistor. The capacitors then are discharged over the load resistor. The electrode of the test gap is connected to the output point of the generator. The capacitance in parallel to the load resistor approximately represents the stray capacitance of the circuit. Connected in series to the load resistor there is a 50 ohm metal film resistor which allows the use of the load resistor at the same time as voltage divider for oscilloscope recordings. The 50 ohm resistor matches the characteristic impedance of the measuring coax cable.

Generally, the pulse wave generated at the output of the impulse generator is described by the function

$$U_o = U_{dc} * (e^{-bt} - e^{-at}) \qquad (C\text{-}1)$$

The rise time of the pulse is defined by the constant a, and the decay by b. The constant can be approximately estimated from the damping resistors and the stray capacitance, and b from the charging capacitance and the load resistance (Vondenbush, 1959, Etzel and Helmchen, 1964). Then

$$a = 1/(\sum_i R_i)C_2 = 1/715 \times 10^{-10} = 1.4 \times 10^7$$

$$b = 1/R_1C_1 = 1/(10225 \times .125 \times 10^{-6}) = 7.88 \times 10^2$$

and for

$$t = 0 \qquad U_o = 0$$

$$= 75 \text{ ns} \qquad = .65\ U_{dc}$$

$$= 900\ \mu s \qquad = .495\ U_{dc}$$

Figures 3 and 4 show the voltage pulse as measured with the oscilloscope. Applying the standard procedure of determining the rise time of a pulse, we can deduce a rise time of 75 ns, and a tail half time of 900 μs from the measurement. The wave has no considerable overshoot which indicates the low induction level of the components. All resistors are carbon resistors rated for a maximum voltage of 75 kV (120 kV for the 10225 ohm resistor). The magnitude of the resistors was determined with a digital ohmmeter to $\pm$ .3% accuracy. According to the specifications, the resistors decrease in magnitude by 2% at 10 MHz and by 10% at 30 MHz. The low

inductance capacitors are rated at 100 kV at .125 μF. Considering the fact that the stray capacitance can be only estimated, the agreement between measured and calculated time constants of the voltage pulse is good.

The output potential of the impulse generator was calibrated with low voltage pulse generators. The voltage signal is picked up at the 50 ohm metal film resistor with a Tektronix high frequency probe P 6034 and transmitted to the oscilloscope over a 4 m 50 ohm coaxial cable terminated with a 50 ohm resistor at the oscilloscope. Figure 55 shows the response of the low voltage side of the measuring circuit to a 60 nsec pulse of 4 V at 5 MHz. A small reflection appears after 30 ns, but no attenuation occurs. To determine the efficiency factor of the pulse generator, a 1 KHz rectangular pulse was applied at the trigger gap of the generator and measured on the output point of the generator as well as at the divider output. The oscillograms are shown in Figure 56. When 59 volts were applied at the trigger gap, 56 volts were measured at the output point and 0.225 V at the divider output. The sag of the rectangular pulse was 91.5% on both locations. The efficiency factor, according to these measurements, is

$$n = 56/59 = .95$$

and the divider ratio

$$m = 56/.225 = 248:1 \ .$$

The divider ratio unfortunately does not agree with the theoretical value one would expect from the magnitudes of the resistors. Since the overall

resistance on the low voltage side of the divider was measured to be 45.5 ohm, the expected divider ratio is 10225/45.5, or 225:1. The discrepancy between measured and theoretical value is probably due to a variation of the total load resistance when the output point was connected to the oscilloscope; therefore, the measured efficiency factor should be somewhat high. Theoretically, it is defined by the ratio between the load resistance and the total series circuit resistance which in this case is 10271/10985 or 0.935. Although, the theoretical values could not be verified directly by measurements they are assumed to be the true values, since it was possible to measure a voltage ratio between trigger gap and divider output equivalent to the ratio of the circuit resistances, if no measurements were taken at the output point of the generator. For this case, Figure 57 shows the oscillogram of the divider voltage at 59 V applied to the generator input. The divider voltage rose slightly from 0.225 to 0.245 V so that the overall input/divider voltage ratio is equal to 241:1, which agrees very well with equivalent ratio of the resistances of 10985/45.5 or 241:1.

The divider ratio of 241:1 was then used to determine the voltage calibration curve of the impulse generator as shown in Figure 58. It gives the actual output voltage of the impulse generator at the test electrodes for a given setting of the voltmeter on the control pannel of the DC power supply. The plotted data points are given in Table 15.

Table 15. Calibration of the impulse generator.

Voltage at the Control Panel [kV]	Voltage measurement with the scope [V]	Voltage at the point [kV]
5	20	4.5
10	40	9.0
15	60	13.5
20	80	18.0
25	100	22.5
30	120	27.0
35	135	30.4
40	157.5	35.5
45	172.5	38.85
50	195.0	43.8
55	215.0	48.5
60	235.0	53.0
65	255.0	57.5
70	270.0	60.9
75	300.0	67.5
75	310.0	69.8
80	335.0	75.4
90	375.0	84.5
100	420.0	94.5
110	480.0	108.0

XIV. APPENDIX D

Sensitive photographic papers or films, brought close to a streamer discharge, are easily exposed by the light radiation of these processes. Utilizing this effect, one can record streamer events by inserting into the discharge area a piece of film either parallel (axial mode), or perpenticular (coplanar mode) to the longitudinal axis of the hemispherically capped cylinder as shown in Figure 59 a and b. The light emitted from the streamer head leaves a characteristic pattern on the film of narrow sharply contoured branches shown in Figures 60 and 61. To obtain these patterns, it is important to use impulse potentials so that only one generation of streamers is allowed to develop. The patterns on the film then represents a direct image of the spacial propagation of the streamers and can provide ample information on the characteristics of the streamer advance.

To position the film in the gap space, a platform is attached to the frame described in Appendix C between the working platform and the ground plate. It also can be adjusted to any position along the three plastic rods, and is supported by pins when in fixed position. As can be seen from Figure 62, the platform is U-shaped. It carries film drums on both sides of U, and the open space is bridged by a system of plastic bars. To keep the film in vertical position underneath the cylinder electrode (axial mode), it is held by two U-shaped plastic clamps which are attached to two plastic guide bars bridging the platform. The guide bars are positioned at a distance slightly less than the width of the film, and have on their opposite side V-shaped cuts at the joint of the clamps

so that the film can be placed perpendicularly between the guide bars. Over the ground plate the film is held in position by one plastic bar, reaching in from one of the three rods of the gap frame. The film is pulled between the bar and a rubber band, which is attached to one side of the bar and held in position by pins through the bar. Details of the film adjustment are given in Figures 63 and 64.

In the coplanar mode the film is pulled from one drum to the other across the U underneath the guide bars. Two paper plates on both sides of the U prevented early exposure of the film.

Throughout the studies a Kodak TRI-X Pan black and white film 70 mm wide (ASA 320) was used together with a Kodak D76 developer. The maximum sensitivity lies in the ultraviolet region.

XV. APPENDIX E

Figure 65 shows the general arrangement of photomultipliers for measurements of light radiation from streamers. Set I is used to trigger the oscilloscope, Set II is adjustable in both horizontal and vertical direction and measures the light intensity in the gap space. The larger the gap distances and the applied voltages at the electrodes, the more it becomes a problem to achieve adequate sensitivity of the PM's because of the increasing distances between the window of the PM and the location of the events to be observed. Some means has to be used, therefore, to transmit the light to the PM without disturbing the ionization processes. Very often this is done with lense systems, or only slit arrangements are made at lower voltage levels. Most recently light pipes were used for this purpose with very good results. They transmit light very efficiently, also in the ultraviolet region if quartz glass is used they can be pointed to the locations where an event shall be observed, and, by varying the cross section of the pipe, allow maximum selectivity; however, the dimensions still can be kept small enough so that the ionization processes remain undistorted.

The PM's used for these studies are arranged at an angle of approximately 60°, thus allowing short distance between the two light pipe tips. Set I is permanently fixed underneath the working platform, which also holds the cylinder electrode, at a distance of approximately 35.5 cm from the center. The PM tube, which has its window on the side, is vertically mounted in an upside down position and the bottom of the set lies at the level of the electrode tip. The LP, which reaches from

the electrode tip to the window of the tube, therefore, is mounted at an angle of ca. 5^{o}. Its diameter is 4 mm and its length is 35.5 cm. Set II is suspended between two L-shaped metal tracks of 80 cm length and can be adjusted at any vertical level from 0 to 60 cm with respect to the ground plate of the gap. The center of the set can be moved horizontally $\pm$ 2.3 cm and lies about 58.4 cm away from the cylinder electrode. The exact position of the tip of the LP was checked with gauges machined to $\pm$ 0.1 mm accuracy. All distances given refer to the center of the pipe tip.

Fused quartz glass rods with diameters of 1.0 mm, 3.0 mm, 6.0mm and 58.4 cm length are used for Set II. Both ends of the rods are fire polished. The index of refraction of fused quartz glass at 3500 $\mathring{A}$ is 1.4775, and air is used as the reflecting medium on the rod boundaries. Therefore, the aperture half angle of the rods is approximately 90^{o}. At half angles larger than 85^{o}, however, less than 20% of the incident light will be refracted into the rod. A glass tube with an inner diameter of 8 mm and 55.8 cm was pulled over all quartz rods and covered with black insulation tape to prevent light from entering the LP at any place other than the tip. The LP's are centered in the glass tubes with silicon glue on both ends, also preventing dust from entering the tube and spoiling the surface of the LP's. A sketch of the LP's is shown in Figure 66. To limit the effective aperture half angle of the light pipes to ca. 50^{o}, a shield made of black insulation tape was pulled 0.5 cm over the tip of the rods.

For both sets, an RCA 1P28A PM tube is used. Its spectral response is of Type S-5 with a maximum sensitivity around 3400 $\mathring{A}$, $\pm$ 500 $\mathring{A}$. A

relative sensitivity of 70% is maintained within the range from 2100 Å to 4600 Å. With a maximum rise time of 1.7×10^{-9} sec, and an electron transit time of 17.0×10^{-9} sec, the tube is very suitable for observing fast ionization events. Figure 67 shows the anode current characteristics taken from the RCA specifications, relating the light intensity entering the PM to the anode current.

Both PM's are supplied with -1000 V from two independent power supplies. The circuit for the PM and the DC power supply is shown in Figure 68. Since the capacitance between anode and all the other electrodes of the PM is only 6 pF, a 1000 ohm resistor could be used for the anode load resistor without affecting the rise time of the tube noticeably. A large load resistance is most desirable since it raises the signal voltage level well above the noise level, which could not be eliminated from the impulse generator circuit. The anode load resistor was decoupled from the characteristic impedance termination of the coaxial cable on the photomultiplier side by a field effect transistor as shown in Figure 69. A 125 ohm coaxial cable was chosen for Set II to gain as much signal strength as possible at the oscilloscope (75 ohm for Set I). Since in spite of all precautions, the noise level of the impulse generator was still quite high, the coaxial calbes were terminated on both sides with their characteristic impedance. The use of the FET also has the advantage that the gain of the measuring circuit can easily be changed by varying the load resistance at the anode. With a rise time of 4×10^{-9} sec, a turn on time of 8×10^{-9} sec, and a fall time of 20×10^{-9} sec, the FET--2N4093--is the weakest link as far as frequency response is concerned, although its performance almost equalled the one of the

other components.

The PM measuring circuit was tested with a square wave pulse generator with an internal impedance of 50 ohm producing pulses from 1 to 5 MHz at durations from 1 to 100 ns. Figure 70 shows a 30 ns pulse applied to 50, 75, and 125 ohm coaxial cables of 4 m length each terminated with their characteristic impedance. Both the 75 and 125 ohm cable show a somewhat distorted signal due to reflections. Figure 71 a and b allow a comparison of the transmission characteristics of the coaxial cable alone, and the FET stage connected to the anode. The test pulse for these oscillograms was applied directly at the load resistance of the anode. In both cases, there is no actual gain in signal strength due to the FET circuit as it was expected. The response to the 30 ns pulse at 1 MHz is satisfactory for both PM circuits, although, somewhat better with the 125 ohm coax. Varying the pulse width from 1 ns to 50 ns at 2 MHz, the graph of Figure AV.9 was obtained. Some sample oscillograms are shown in Figure 72. A comparison of Figure 73 with Figure 4 shows that the overall response of the measuring circuit to the pulses is almost as good as the one of the oscilloscope.

Since the field effect transistor is not exactly linear, the input/output voltage ratio was determined. A 30 nsec pulse at 2 MHz of varying amplitude was applied to the load resistance at the photomultiplier anode and measured there with a Tektronix P6034 probe. Simultaneously, the signal was also measured through the 125 ohm coax. Samples of the measurements are given in Figure 74 a and b; the results are shown in Figure 75. From Figure 75 we can deduce a cutoff voltage of the field

effect transistor of -2.0 V, and an approximately linear region up to -1.0 V. The oscillograms of Figure 74a also indicate that around the cutoff level the pulse tail becomes very much distorted due to saturation of the FET.

No calibrated light source was available to determine the characteristics of the whole measuring circuit equivalent to Figure 67. To estimate the increase in gain due to the FET stage, a comparison was made between the measuring circuit as described in Figure 69 and a 75 ohm coax terminated on both ends directly connected to the PM anode (Figure 76) measuring the change of intensity of the artificial room light. From the measurements an improvement of the overall gain by a factor of 50 can be estimated. An attempt to increase the gain further by adding a transistor follower stage was abandoned since the impulse response deteriorated too much (Figure 77).

The recommendations for the photomultiplier tube prescribe an ambient temperature less than room temperature. Due to the shielding of the whole tube and circuit connections, the temperature limit could not be met. This resulted in a somewhat higher dark current than expected from the specifications. Figures 78 shows several dark current pulses of the PM measured with a completely enclosed tube over a period of 0.5 sec and a medium sensitivity level of the oscilloscope trigger. Figure 79 shows the difference in signal strength between the dark current and a typical streamer signal (lower traces). To obtain the upper trace, a cap was pulled over the tip of the light pipe to prove that all the measured light entered through the tip of the quartz glass rod. In both cases the oscilloscope was triggered with the second photomultiplier.

XVI. APPENDIX F

```
C
C CORONA ONSET IN A HEMISPHERICALLY CAPPED CYLINDER TO PLANE GAP
C
C  THE PROGRAM COMPUTES THE POTENTIAL AND FIELD FOR  CORONA ONSET
C  IN HEMISPHERICALLY CAPPED CYLINDER TO  PLANE GAPS USING
C  ' LOEBS CRITERION '.
C  EACH DATA HAS TO BE SUBMITTED ON A SINGLE CARD IN THE FOLLOWING ORDER
C  VPU              FORMAT F  9.4       ENTER 1.0 FOR UNIT POTENTIAL
C  GPL              FORMAT 10.4         GAP DISTANCE
C  PTRAD            FORMAT 10.4         CYLINDER RADIUS
C  PRES             FORMAT 10.4         GAS PRESSURE
C  EDIFC            FORMAT 10.4         ELECTRON DIFFUSION COEFFICIENT
C  UEW              FORMAT 10.4         ABSORPTION COEFFICIENT
C  ISWI             FORMAT  I1          FLAG FOR INPUT OF ESTIMATED POTENTIAL
C                                       1  IF ESTIMATED POTENTIAL IS GIVEN
C                                       ON DATA CARD
C  VKV              FORMAT 10.4         ESTIMATED CORONA ONSET POTENTIAL
C                                       REQUIRED ONLY IF ISWI EQUAL 1
C  PRESLI           FORMAT 10.4         PRESSURE LIMIT FOR THE INITIAL AVALANCHE
C  THE LAST CARD OF THE DATA SET HAS TO BE A 9999.0  IN THE FIRST SIX COLUMNS
C
      IMPLICIT REAL*8(A-H,O-Z)
      DIMENSION A(9),Z(7),V(10,10),Y(100),ZD(100),SF(100),ROR(20),U(10)
      DIMENSION REDVX(100),EP(100),YY(100),EF(100),ROINTD(20),ROINTL(20)
 1111 READ (1,11) VPU
   11 FORMAT (F9.4)
      IF(VPU.EQ.9999.0D0) GO TO 901
      Z4=0.0D0
      READ (1,5) GPL,PTRAD,PRES,EDIFC,UEW
    5 FORMAT (F10.4)
      RPTRAD=1.0D0/PTRAD
      G=GPL*RPTRAD
      WRITE (3,6) GPL,PTRAD,G,VPU,PRES,EDIFC,UEW
```

```
    6 FORMAT ('1',//,10X,'GAP DISTANCE',5X,'=',F7.2,' (CM)',//,10X,'CYLI
     1NDER RADIUS',2X,'=',F7.2,' (CM)',//,10X,'GAP RATIO D / R',2X,'=',F
     27.2,//,10X,'CYLINDER VOLTAGE',1X,'=',F7.2,' (PU)',//,10X,'GAS PRES
     3SURE',5X,'=',F7.2,' (TORR)',//,10X,'ELECT. DIF. COEF.=',F7.2,' (CM
     4**2/SEC)',//,10X,'ABSORPTION COEF. =',F7.2,' (CM-1)')
      READ (1,7) ISWI
    7 FORMAT (I2)
      REPR=1.0D0/PRES
C
C     COMPUTE GAP LENGTH/POINT RADIUS, Z-COORDINATES OF POINTS AT WHICH
C     AXIAL LINE CHARGES START, Z-COORDINATES OF POINTS ON CYL. PORTION
C     OF BOUNDARY AT WHICH POTENTIAL IS SET = UNITY, POTENTIAL AND
C     FIELD FACTORS.
C
      F=G+1.0D0
      A(1)=F
      A(2)=F+.1D0
      A(3)=F+.2D0
      A(4)=F+.5D0
      A(5)=F+1.0D0
      A(6)=F+9.0D0
      A(7)=F+24.0D0
      A(8)=F+89.0D0
      A(9)=F+239.0D0
      Z(1)=F
      Z(2)=F+1.0D0
      Z(3)=F+4.0D0
      Z(4)=F+14.0D0
      Z(5)=F+39.0D0
      Z(6)=F+139.0D0
      Z(7)=F+439.0D0
```

```
C
C      FORM MATRIX OF COEFFICIENTS
C
C      COMPUTE V(0,G;A(J)) AND LOCATE POSITION IN MATRIX OF COEFFICIENTS
C
       DO 14 J=1,9
       X=A(J)
       B=X+G
       C=X-G
       V(8,J)=DLOG10(B/C)
   14  CONTINUE
C
C      COMPUTE P(0,G) AND LOCATE POSITION IN MATRIX OF COEFFICIENTS
C
       V(8,10)=1.0D0-1.0D0/(F+G)
C
C      COMPUTE V(1,Z(I);A(J)) AND LOCATE POSITION IN MATRIX OF COEFFT'S
C
       DO 23 I=1,7
       DO 23 J=1,9
       X=Z(I)
       B=A(J)+X
       C=A(J)-X
       V(I,J)=DLOG10((B+DSQRT(1.0D0+B*B))/(C+DSQRT(1.0D0+C*C)))
   23  CONTINUE
C
C      COMPUTE P(1,Z(I)) AND LOCATE POSITION IN MATRIX OF COEFFICIENTS
C
       J=10
       DO 28 I=1,7
       D=F-Z(I)
       E=F+Z(I)
       V(I,J)=1.0D0/(DSQRT(1.0D0+D*D))-1.0D0/(DSQRT(1.0D0+E*E))
   28  CONTINUE
C
```

```
C     COMPUTE SECOND AND FOURTH DERIVATIVES OF V(C;A(J)) AT C= 0 AND
C     LOCATE POSITION IN MATRIX OF COEFFICIENTS
C
      DO 33 J=1,9
      X=A(J)
      B=1.0D0/(X-G)
      C=1.0D0/(X+G)
      V4=C+B
      B=B*B
      C=C*C
      V(9,J)=.43429D0*(.5D0*(C-B)+V4)
      V4=5.0D0*(B-C)-V4
      B=B*B
      C=C*C
      V4=V4+2.25D0*(B-C)
      B=(X-G)*B
      C=C*(X+G)
      V(10,J)=.43429D0*(V4-6.0D0*(B+C))
   33 CONTINUE
C
C     COMPUTE SECOND AND FOURTH DERIVATIVES OF P(C) AT C= 0 AND LOCATE
C
      T=2.0D0*F
      P2=(T/(T-1.0D0)**3.0D0)
      V(9,10)=P2
      V(10,10)=-9.0D0*P2*P2*(T-1.0D0)-P2
C
C     FORM VECTOR OF ORIGINAL CONSTANTS
C
      DO 73 I=1,10
      IF (I-8) 71,71,72
   71 U(I)=1.0D0
      GO TO 73
   72 U(I)=0.0D0
   73 CONTINUE
```

```
C
C      SOLVE FOR POTENTIAL COEFFICIENTS
C
       CALL DGELG (U,V,10,1,0.,IER)
       WRITE (3,49) U(10)
    49 FORMAT('0',///,10X,'POINT CHARGE    = ',E11.5,' (COUL)')
       DO 47 I=1,9
       WRITE (3,48) I,U(I)
    47 CONTINUE
    48 FORMAT('0',10X,'LINE CHARGE ',I1,' = ',E11.5,' (COUL)')
C
C      ESTIMATION OF THE ONSET VOLTAGE
C
       GO TO (850,851),ISWI
   851 CONTINUE
       CALL ECTIHK(KRAT)
       IF(KRAT.EQ.3) GO TO 1111
       GO TO 852
   850 READ (1,11) VKV
       WRITE (3,801) VKV
   801 FORMAT ('0',///,10X,'ESTIMATED VOLTAGE =',F9.4,' (KV)')
   852 CONTINUE
C
C      COMPUTATION OF THE INTEGRAL OF ALPHA W, R, T. X
C      BET. VARIABLE LIMITS (SPACE CHARGE NOT INCLUDED)
C
   221 READ(1,11) PRESLI
       IF(PRESLI.EQ.9999.) GO TO 901
       WRITE(3,222) PRESLI
   222 FORMAT('0',10X,'IT IS ASSUMED, THAT FREE ELECTRONS IN THE FIELDRAN
      1GE E/P G.T.  ',F5.2,'  V/CM*TORR CONTRIBUTE TO THE ONSET PROCESS')
       ITEST=1
       ILT=0
       IGT=0
```

```
102 XX=G
    X1=G-.1D0
    NM=99
    OUTP=XX*PTRAD
    KK=1
    MN=NM+1
    KRAT=1
101 HH=(XX-X1)/DFLOAT(NM)
    CALL EXTFLD (G,A,U,EF,F,HH,MN,YY,KRAT,VKV,PTRAD,RPTRAD,DERZ)
    EBYP=EF(100)*REPR
    IF(EBYP-PRESLI)144,144,155
155 X1=X1-.1D0
    IF(X1.LT.0.0D0) GO TO 145
    GO TO 101
145 X1=X1+0.10D0*G
144 CONTINUE
    KRAT=2
    AA=EF(1)*1.0D-03
    YYY=AA/DERZ
    WRITE (3,104) AA,DERZ,YYY
104 FORMAT ('0',///,10X,'THE ANODE FIELD IS EA =',F9.3,' (KV/CM)',/,10
   1X,'THE CATH. FIELD IS EC =',F9.3,' (KV/CM)',/,10X,'THE FIELD RATIO
   2 IS ER =',F9.3)
    IF(YYY.GT.11.0D0) GO TO 105
    WRITE (3,9)
  9 FORMAT (' ',/////,10X,'THE FIELD RATIO E(ANODE)/E(CATH.) IS SMALLE
   1R THAN 11',/,10X,'**********************************************
   2****',//,10X,'NO CORONA IS EXPECTED BEFORE BREAKDOWN OCCURS',/,10X
   3,'**********************************************')
105 CONTINUE
    WRITE (3,8) OUTP,NM
  8 FORMAT(' ',///,10X,'EVALUATION OF THE INTEGRAL OF ALPHA W.R.T. X B
   1ETWEEN X =',F7.4,' AND X = X',/,25X,'USING TRAPEZOIDAL RULE (N =',
   2I2,')',//,21X,'X',22X,'INTEGRAL',15X,'EXP(INTEGRAL)*10E8')
    CALL ALPHAC (EP,EF,PRES,REPR,Y,MN,EBYP)
    HH=HH*PTRAD
    CALL DQSF (HH,Y,ZD,MN)
```

```
      AREA=ZD(MN)
      EALPHX=1.0D-08*DEXP(AREA)
      CURR=EALPHX*1.0D+08
      OUTP=X1*PTRAD
      WRITE (3,10) OUTP,AREA,EALPHX
   10 FORMAT ('0',3(14X,F12.6))
C
C     CALCULATION OF THE AVALANCHE ENERGY
C
      DO 40 KM=1,MN
      AREA=DEXP(ZD(KM))
      SF(KM)=EF(KM)*AREA
   40 CONTINUE
      CALL DQSF (HH,SF,ZD,MN)
      AREA=ZD(MN)*1.6D-19
      WRITE (3,12) AREA
   12 FORMAT ('0',10X,'CORONA ONSET ENERGY OF CRITICAL AVALANCHE =',E9.3
     1,' (KJ)')
C
C     FIELD DISTRIBUTION AROUND THE ANODE
C
      WRITE (3,149)
  149 FORMAT ('1',14X,'X',10X,'FIELD',10X,'E/P',9X,'ALPHA',7X,'EL. DRIFT
     1 VEL.',/,14X,'(CM)',7X,'(KV/CM)',4X,'(VOLT/CM TORR)',3X,'(CM-1)',9
     2X,'(KM/SEC)',/)
      DO 152 K=1,MN
      FIELDK=EF(K)*1.0D-03
       IF (EP(K).LT.42.5D0) GO TO 30
      EDVX=2.08D0*EP(K)+65.0D0
      GO TO 31
   30 EDVX=3.3D0*EP(K)+12.5D0
   31 REDVX(K)=10.0D0/EDVX
      WRITE (3,92) YY(K),FIELDK,EP(K),Y(K),EDVX
   92 FORMAT (' ',9X,F10.6,3X,F10.6,3X,F10.4,4X,F11.6,3X,F13.6)
      IF(K.EQ.1) CEDVX=EDVX
  152 CONTINUE
      ALPHLI=Y(MN)
```

```
C
C      CALCULATION OF THE AVERAGE SLOPE
C
       SLOPE1=1.0D0/HH
       SLOPE=0.0D0
       DO 20 KL=1,NM
       KLL=KL+1
       SLOPE=(EF(KL)-EF(KLL))*SLOPE1+SLOPE
   20  CONTINUE
       SLOPE=1.0D-03*SLOPE/DFLOAT(NM)
       WRITE (3,21) SLOPE
   21  FORMAT (' ',///,10X,'THE AVERAGE GRADIENT OF THE FIELD IN THE IONI
      1ZATION REGION IS',//,10X,'AGRAD =',F9.2,' (KV/CM**2)')
C
C      CALCULATION OF TRANSIT TIME AND OF THE SPACE CHARGE RADIUS OF ELECTRONS
C
       CALL TRAPEZ (HH,NM,REDVX,AREA)
       RBAR=DSQRT(.0000060D0*EDIFC*AREA)
       WRITE (3,4) GPL,NM,OUTP,AREA,RBAR
    4  FORMAT ('0',//,5X,'EVALUATION OF T : TRANSIT TIME OF ELECTRONS FRO
      1M X =',F7.4,'TO X = X',/,25X,'USING TRAPEZOIDAL RULE (N=',I2,')',/
      2/,20X,'X',22X,'T (MIC SEC)',//,14X,F12.6,14X,F12.6,//,20X,'RADIUS
      3OF POSITIVE ION SPACE CHARGE =',F10.6,3X,'(CM)')
```

```
C
C       EFFECT OF SPACE CHARGE INCLUDED
C       ******************************
C
        DELROI=(YY(1)-YY(100))*RPTRAD*0.060D0
        DELRO=DELROI
        LMN=1
        NNN=40
        NNM=39
        XX=G-2.0D0*RBAR*RPTRAD
  401   IJK=LMN
        RO=RBAR+DELRO*PTRAD
        ROR(IJK)=RO
        HH=DELRO/DFLOAT(NNM)
        CALL EXTFLD (XX,A,U,EF,F,HH,NNN,YY,KRAT,VKV,PTRAD,RPTRAD,DERZ)
        DO 400 KL=1,NNN
        X=XX*PTRAD+RBAR-YY(KL)
        SF(KL)=19.17D0*RBAR*Y(1)*EALPHX/(X*X)
        REDVX(KL)=EF(KL)+SF(KL)
  400   CONTINUE
        CALL ALPHAC (EP,REDVX,PRES,REPR,Y,NNN,EBYP)
        HH=HH*PTRAD
        IF(Y(20).LT.ALPHLI)GO TO 350
        CALL DQSF (HH,Y,ZD,NNN)
        Z1=DSQRT(DELRO*PTRAD)
        Z2=1.0D0/DEXP(UEW*RO)
        Z3=DEXP(ZD(NNN))
        ROINTD(IJK)=.00134D0*UEW*RBAR*Y(1)*Z1*Z2*Z3
        DELRO=DELRO+DELROI
        IF(LMN.EQ.20) GO TO 470
        IF(DELRO.GT.XX) GO TO 470
        GO TO 471
  470   WRITE (3,201)
  201   FORMAT('1',//,14X,'X',15X,'EXT. FIELD',10X,'SP. CH. FIELD',6X,' RE
       1SULTANT FIELD',12X,'E/P',18X,'ALPHA',/,13X,'(CM)',15X,'(KV/CM)',14
       2X,'(KV/CM)',14X,'(KV/CM)',10X,'(VOLT/CM-TORR)',13X,'(CM-1)',/)
```

```
      DO 393 KL=1,NNN
      AREA=EF(KL)*1.0D-03
      EBYP=SF(KL)*1.0D-03
      FIELDK=REDVX(KL)*1.0D-03
      WRITE (3,302) YY(KL),AREA,EBYP,FIELDK,EP(KL),Y(KL)
  393 CONTINUE
  302 FORMAT(' ',9X,F10.6,10X,F10.6,3(11X,F10.6),11X,F12.6)
      WRITE (3,303) RO,Z1,Z2,ZD(NNN),Z3,ROINTD(IJK)
  303 FORMAT ('0',/,36X,'RO =',F8.6,/,24X,'(RO-RBAR)**1/2 =',F8.6,/,29X,
     1'EXP(-U*RO) =',F9.6,/,21X.'INT.(ALPHA PRIME) =',F9.6,/,16X.'EXP(IN
     2T.(ALPHA PRIME)) =',F12.4,/,23X,'INTEGRAND OR RO =',F12.4)
  471 CONTINUE
      DO 410 KL=1,NNN
      ZD(KL)=DEXP(ZD(KL))
      YY(KL)=REDVX(KL)*ZD(KL)
  410 CONTINUE
      CALL DQSF (HH,YY,ZD,NNN)
      Z4=Z4+ZD(NNN)
      IF(LMN.EQ.20) GO TO 461
      IF(DELRO.GT.XX) GO TO 460
      LMN=LMN+1
      GO TO 401
  350 WRITE (3,201)
      DO 395 KL=1,NNN
      AREA=EF(KL)*1.0D-03
      EBYP=SF(KL)*1.0D-03
      FIELDK=REDVX(KL)*1.0D-03
      WRITE (3,302) YY(KL),AREA,EBYP,FIELDK,EP(KL),Y(KL)
  395 CONTINUE
      WRITE (3,351) ALPHLI
  351 FORMAT('0',/,11X,'THE PHOTOELECTRONS TRAVEL FOR MORE THAN HALF THE
     1 DISTANCE IN A FIELD L.T.',F5.2,' V/CM*TORR',/,12X,'DO NOT CONTRIB
     2UTE TO THE PROCESS')
```

```
      ROINTD(IJK)=0.0D0
  460 LMN=IJK
  461 DELROI=DELROI*PTRAD
      CALL DQSF (DELROI,ROINTD,ROINTL,LMN)
      WRITE (3,304) RBAR
  304 FORMAT ('1',/,10X,'EVALUATION OF THE TOTAL INTEGRAL OF RO FROM RO
     1=',F8.6,' TO RO = R',//,21X,'R',17X,'INTEGRAL',/)
      DO 402 IJK=1,LMN
  402 WRITE (3,305) ROR(IJK),ROINTL(IJK)
      IF(DABS(ROINTL(LMN)-1.0D0)-.2D0) 500,500,501
  501 IF(ROINTL(LMN)-1.0D0) 502,500,503
  502 GO TO (601,602,603),ITEST
  601 ILT=1
  604 VKVV=VKV
      VKV=1.02D0*VKV
      ITEST=2
      GO TO 102
  602 GO TO (604),ILT
      VKV=(3.0D0*VKV-VKVV)/2.0D0
      VKVV=(2.0D0*VKV+VKVV)/3.0D0
      ITEST=2
      IGT=0
      GO TO 102
  603 VKV=(VKVV+VKV)/2.0D0
      VKVV=2.0D0*VKV-VKVV
      ITEST=2
      IGT=0
      GO TO 102
  503 GO TO (605,606,607),ITEST
  605 IGT=1
```

```
608 VKVV=VKV
    VKV=.98D0*VKV
    ITEST=3
    GO TO 102
606 VKV=(VKVV+VKV)/2.0D0
    VKVV=2.0D0*VKV-VKVV
    ITEST=3
    ILT=0
    GO TO 102
607 GO TO (608),IGT
    VKV=(3.0D0*VKV-VKVV)/2.0D0
    VKVV=(2.0D0*VKV+VKVV)/3.0D0
    ITEST=3
    ILT=0
    GO TO 102
500 CONTINUE
    WRITE (3,306) VKV
305 FORMAT (' ',17X,F8.6,8X,F12.4)
306 FORMAT (' ',///,16X,'CORONA ONSET VOLTAGE =',F9.4,/,16X,'*********
   1**********************')
    Z4=Z4*1.6D-19
    WRITE (3,411)Z4
411 FORMAT (' ',///,16X,'CORONA ONSET ENERGY =',E9.3,' (KJ)',/,16X,'**
   1****************************')
    CURR=CURR*CEDVX*1.2D-14/RBAR
    WRITE (3,121) CURR
121 FORMAT('0',10X,'THE PEAK CURRENT OF THE INITIAL ELECTRON AVALANCHE
   1 IS',//,11X,'I = ',E10.3,' (A)')
    GO TO 221
901 STOP
    END
```

```
      SUBROUTINE EXTFLD (G,A,U,EF,F,HH,MN,YY,KRAT,VKV,PTRAD,RPTRAD,DERZ)
      IMPLICIT REAL*8(A-H,O-Z)
      DIMENSION A(9),U(10),EF(100),YY(100)
      ZED=G
      DO 102 II=1,MN
      DERZ=0.0D0
      YY(II)=ZED*PTRAD
      DO 101 I=1,9
      X=A(I)
      B=1.0D0/(X+ZED)
      C=1.0D0/(X-ZED)
      DERZ=U(I)*.43429D0*(B+C)+DERZ
  101 CONTINUE
      DERZ=DERZ+U(10)*(1.0D0/((F-ZED)*(F-ZED))+1.0D0/((F+ZED)*(F+ZED)))
      EF(II)=DERZ*VKV*RPTRAD*1.0D+03
      ZED=ZED-HH
  102 CONTINUE
      GO TO (103,105),KRAT
  103 DERZ=0.0D0
      DO 106 I=1,9
      B=1.0D0/A(I)
      DERZ=U(I)*.86858D0*B+DERZ
  106 CONTINUE
      DERZ=DERZ+U(10)*2.0D0/(F*F)
      DERZ=DERZ*RPTRAD*VKV
  105 RETURN
      END
```

```
      SUBROUTINE TRAPEZ(H,N,Y,AREA)
      IMPLICIT REAL*8(A-H,O-Z)
      DIMENSION Y(100)
      SUM=0.0D0
      NN=N+1
      DO 10 I=2,N
   10 SUM=SUM+Y(I)
      AREA=(H/2.0D0)*(Y(1)+2.0D0*SUM+Y(NN))
      RETURN
      END
```



```
      SUBROUTINE ECTIHK (KRAT)
      WRITE (3,1)
    1 FORMAT (' ',10X,'NO PROGRAM IS DEVELOPED AS YET. ESTIMATE THE ONSE
     1T VOLTAGE')
      KRAT=3
      RETURN
      END
```

```
      SUBROUTINE ALPHAC (EP,EF,PRES,REPR,Y,MN,EBYP)
      IMPLICIT REAL*8(A-H,O-Z)
      DIMENSION EP(100),EF(100),Y(100)
      DO 94 K=1,MN
      EBYP=EF(K)*REPR
      IF(EBYP-32.5D0) 40,40,41
   40 Y(K)=.00000936D0*PRES*DEXP(.805D0*EBYP-20.0D0)
      GO TO 93
   41 IF(EBYP-42.5D0) 42,42,43
   42 Y(K)=.00000609D0*PRES*DEXP(.2D0*EBYP)
      GO TO 93
   43 IF(EBYP-64.0D0) 44,45,45
   44 Y(K)=.00159D0*PRES*DEXP(.07D0*EBYP)
      GO TO 93
   45 IF(EBYP-100.D0) 46,47,47
   46 Y(K)=.01283D0*PRES*DEXP(.039D0*EBYP)
      GO TO 93
   47 IF(EBYP-180.D0) 48,49,49
   48 Y(K)= 8.0D0*PRES*DEXP(-250.0D0/EBYP)
      GO TO 93
   49 Y(K)=15.0*PRES*DEXP(-365.0D0/EBYP)
   93 EP(K)=EBYP
   94 CONTINUE
      RETURN
      END
```

GAP DISTANCE = 10.00 (CM)

CYLINDER RADIUS = 0.05 (CM)

GAP RATIO D / R = 200.00

CYLINDER VOLTAGE = 1.00 (PU)

GAS PRESSURE = 760.00 (TORR)

ELECT. DIF. COEF.= 430.00 (CM**2/SEC)

ABSORPTION COEF. = 5.00 (CM-1)

ESTIMATED VOLTAGE = 9.3400 (KV)

IT IS ASSUMED, THAT FREE ELECTRONS IN THE FIELDRANGE E/P G.T.

30.00 V/CM*TORR CONTRIBUTE TO THE I

THE ANODE FIELD IS EA = 110.241 (KV/CM)
THE CATH. FIELD IS EC = 0.153 (KV/CM)
THE FIELD RATIO IS ER = 719.114

EVALUATION OF THE INTEGRAL OF ALPHA W.R.T. X BETWEEN X =10.0000 AND X = X
USING TRAPEZOIDAL RULE (N =99)

X	INTEGRAL	EXP(INTEGRAL)*10E8
9.930000	12.841589	0.003776

CORONA ONSET ENERGY OF CRITICAL AVALANCHE =0.710D-10 (KJ)

X (CM)	FIELD (KV/CM)	E/P (VOLT/CM TORR)	ALPHA (CM-1)	EL. DRIFT VEL. (KM/SEC)
10.000000	110.241494	145.0546	1084.930261	366.713561
9.999293	107.191423	141.0413	1033.007874	358.365999
9.998586	104.271929	137.1999	982.992315	350.375806
9.997879	101.475673	133.5206	934.853689	342.722895
9.997172	98.795820	129.9945	888.559567	335.388560
9.996465	96.225999	126.6132	844.075243	328.355367
9.995758	93.760268	123.3688	801.363986	321.607050
9.995051	91.393076	120.2540	760.387275	315.128419
9.994343	89.119237	117.2622	721.105034	308.905280
9.993636	86.933897	114.3867	683.475857	302.924351
9.992929	84.832515	111.6217	647.457215	297.173199
9.992222	82.810833	108.9616	613.005663	291.640175
9.991515	80.864860	106.4011	580.077029	286.314354
9.990808	78.990849	103.9353	548.626596	281.185481
9.990101	77.185281	101.5596	518.609275	276.243928
9.989394	75.444850	99.2695	468.183997	271.480642
9.988687	73.766444	97.0611	429.547637	266.887110
9.987980	72.147135	94.9304	395.296666	262.455317
9.987273	70.584165	92.8739	364.830002	258.177715
9.986566	69.074934	90.8881	337.641310	254.047189
9.985859	67.616990	88.9697	313.302308	250.057026
9.985152	66.208018	87.1158	291.449300	246.200892
9.984444	64.845833	85.3235	271.772263	242.472806
9.983737	63.528368	83.5900	254.005955	238.867114
9.983030	62.253671	81.9127	237.922651	235.378469
9.982323	61.019893	80.2893	223.326168	232.001814
9.981616	59.825285	78.7175	210.046950	228.732360
9.980909	58.668189	77.1950	197.937987	225.565571
9.980202	57.547035	75.7198	186.871432	222.497148
9.979495	56.460332	74.2899	176.735776	219.523013
9.978788	55.406667	72.9035	167.433487	216.639299

9.978081	54.384698	71.5588	158.879024	213.842332
9.977374	53.393151	70.2541	150.997163	211.128625
9.976667	52.430815	68.9879	143.721587	208.494862
9.975960	51.496538	67.7586	136.993684	205.937893
9.975253	50.589224	66.5648	130.761533	203.454718
9.974545	49.707831	65.4050	124.979026	201.042485
9.973838	48.851367	64.2781	119.605135	198.698477
9.973131	48.018885	63.1827	100.694299	196.420106
9.972424	47.209484	62.1177	93.460523	194.204904
9.971717	46.422306	61.0820	86.924147	192.050521
9.971010	45.656530	60.0744	81.004433	189.954714
9.970303	44.911375	59.0939	75.631370	187.915341
9.969596	44.186093	58.1396	70.744080	185.930359
9.968889	43.479971	57.2105	66.289489	183.997815
9.968182	42.792328	56.3057	62.221203	182.115846
9.967475	42.122513	55.4244	58.498571	180.282668
9.966768	41.469903	54.5657	55.085882	178.496575
9.966061	40.833901	53.7288	51.951695	176.755939
9.965354	40.213937	52.9131	49.068263	175.059197
9.964646	39.609467	52.1177	46.411047	173.404856
9.963939	39.019966	51.3421	43.958296	171.791485
9.963232	38.444933	50.5854	41.690691	170.217712
9.962525	37.883890	49.8472	39.591039	168.682225
9.961818	37.336375	49.1268	37.644009	167.183763
9.961111	36.801947	48.4236	35.835900	165.721118
9.960404	36.280183	47.7371	34.154453	164.293132
9.959697	35.770676	47.0667	32.588670	162.898692
9.958990	35.273036	46.4119	31.128675	161.536730
9.958283	34.786888	45.7722	29.765579	160.206220
9.957576	34.311873	45.1472	28.491370	158.906178
9.956869	33.847644	44.5364	27.298816	157.635657
9.956162	33.393869	43.9393	26.181374	156.393746
9.955455	32.950228	43.3556	25.133122	155.179571
9.954747	32.516413	42.7848	24.148686	153.992289
9.954040	32.092130	42.2265	21.536588	151.847405

9.953333	31.677092	41.6804	19.308256	150.045267
9.952626	31.271026	41.1461	17.351401	148.282086
9.951919	30.873668	40.6232	15.628643	146.556714
9.951212	30.484763	40.1115	14.108281	144.868049
9.950505	30.104066	39.6106	12.763361	143.215025
9.949798	29.731342	39.1202	11.570901	141.596617
9.949091	29.366363	38.6400	10.511250	140.011838
9.948384	29.008908	38.1696	9.567569	138.459733
9.947677	28.658767	37.7089	8.725387	136.939384
9.946970	28.315735	37.2575	7.972238	135.449903
9.946263	27.979615	36.8153	7.297360	133.990435
9.945556	27.650217	36.3819	6.691438	132.560152
9.944848	27.327356	35.9570	6.146394	131.158257
9.944141	27.010856	35.5406	5.655203	129.783980
9.943434	26.700545	35.1323	5.211747	128.436576
9.942727	26.396257	34.7319	4.810685	127.115327
9.942020	26.097832	34.3393	4.447342	125.819536
9.941313	25.805116	33.9541	4.117623	124.548532
9.940606	25.517959	33.5763	3.817930	123.301666
9.939899	25.236216	33.2055	3.545097	122.078308
9.939192	24.959748	32.8418	3.296333	120.877852
9.938485	24.688418	32.4848	3.335042	119.699709
9.937778	24.422096	32.1343	2.515305	118.543310
9.937071	24.160654	31.7903	1.906888	117.408104
9.936364	23.903971	31.4526	1.452942	116.293557
9.935657	23.651926	31.1210	1.112514	115.199154
9.934949	23.404406	30.7953	0.855941	114.124394
9.934242	23.161298	30.4754	0.661625	113.068792
9.933535	22.922493	30.1612	0.513759	112.031879
9.932828	22.687888	29.8525	0.400718	111.013198
9.932121	22.457381	29.5492	0.313909	110.012310
9.931414	22.230872	29.2511	0.246949	109.028787
9.930707	22.008267	28.9582	0.195077	108.062212
9.930000	21.789473	28.6704	0.154725	107.112185

THE AVERAGE GRADIENT OF THE FIELD IN THE IONIZATION REGION IS

AGRAD = 1263.60 (KV/CM**2)

EVALUATION OF T : TRANSIT TIME OF ELECTRONS FROM X =10.0000TO X = X
USING TRAPEZOIDAL RULE (N=99)

X	T (MIC SEC)
9.930000	0.004081

RADIUS OF POSITIVE ION SPACE CHARGE = 0.003245 (CM)

X (CM)	EXT. FIELD (KV/CM)	SP. CH. FIELD (KV/CM)	RESULTANT FIELD (KV/CM)	E/P (VOLT/CM-TORR)
9.993510	86.552240	24.512440	111.064680	146.137737
9.991356	80.437245	8.855547	89.292792	117.490515
9.989202	74.983904	4.524955	79.508859	104.616920
9.987048	70.099720	2.739614	72.839334	95.841230
9.984895	65.707747	1.834936	67.542683	88.871951
9.982741	61.743570	1.314256	63.057826	82.970824
9.980587	58.152944	0.987420	59.140364	77.816268
9.978433	54.889935	0.768912	55.658847	73.235325
9.976279	51.915446	0.615656	52.531102	69.119871
9.974125	49.196032	0.504039	49.700072	65.394831
9.971972	46.702957	0.420238	47.123194	62.004203
9.969818	44.411416	0.355722	44.767137	58.904128
9.967664	42.299914	0.304998	42.604912	56.059095
9.965510	40.349751	0.264398	40.614149	53.439670
9.963356	38.544596	0.231396	38.775992	51.021042
9.961202	36.870138	0.204209	37.074346	48.782035
9.959048	35.313794	0.181546	35.495339	46.704394
9.956895	33.864464	0.162456	34.026921	44.772264
9.954741	32.512330	0.146227	32.658557	42.971785
9.952587	31.248677	0.132313	31.380990	41.290777

9.950433	30.065752	0.120295	30.186047	39.718483
9.948279	28.956638	0.109842	29.066481	38.245369
9.946125	27.915148	0.100695	28.015843	36.862952
9.943972	26.935733	0.092645	27.028379	35.563656
9.941818	26.013410	0.085523	26.098933	34.340701
9.939664	25.143686	0.079192	25.222878	33.187997
9.937510	24.322507	0.073539	24.396046	32.100060
9.935356	23.546208	0.068470	23.614678	31.071944
9.933202	22.811464	0.063907	22.875371	30.099173
9.931048	22.115257	0.059786	22.175043	29.177688
9.928895	21.454841	0.056051	21.510892	28.303805
9.926741	20.827713	0.052656	20.880368	27.474169
9.924587	20.231587	0.049560	20.281147	26.685720
9.922433	19.664375	0.046729	19.711104	25.935663
9.920279	19.124161	0.044134	19.168295	25.221441
9.918125	18.609190	0.041749	18.650939	24.540709
9.915972	18.117847	0.039553	18.157400	23.891315
9.913818	17.648648	0.037525	17.686173	23.271280
9.911664	17.200224	0.035649	17.235874	22.678781
9.909510	16.771314	0.033911	16.805225	22.112138

```
                    RO =0.087245
          (RO-RBAR)**1/2 =0.289828
               EXP(-U*RO) = 0.646472
       INT.(ALPHA PRIME) = 8.404955
EXP(INT.(ALPHA PRIME)) =    4469.1584
         INTEGRAND OR RO =     20.0058

EVALUATION OF THE TOTAL INTEGRAL OF RO FROM RO =0.003245 TO RO = R

              R                    INTEGRAL

          0.007445                  0.0
          0.011645                  0.0006
          0.015845                  0.0033
          0.020045                  0.0107
          0.024245                  0.0259
          0.028445                  0.0511
          0.032645                  0.0865
          0.036845                  0.1316
          0.041045                  0.1858
          0.045245                  0.2473
          0.049445                  0.3160
          0.053645                  0.3894
          0.057845                  0.4662
          0.062045                  0.5438
          0.066245                  0.6242
          0.070445                  0.7054
          0.074645                  0.7876
          0.078845                  0.8697
          0.083045                  0.9529
          0.087245                  1.0350
THE PEAK CURRENT OF THE INITIAL ELECTRON AVALANCHE IS

I =  0.512D-03 (A)

CORONA ONSET VOLTAGE =    9.3400
*******************************
```

XVII. APPENDIX G

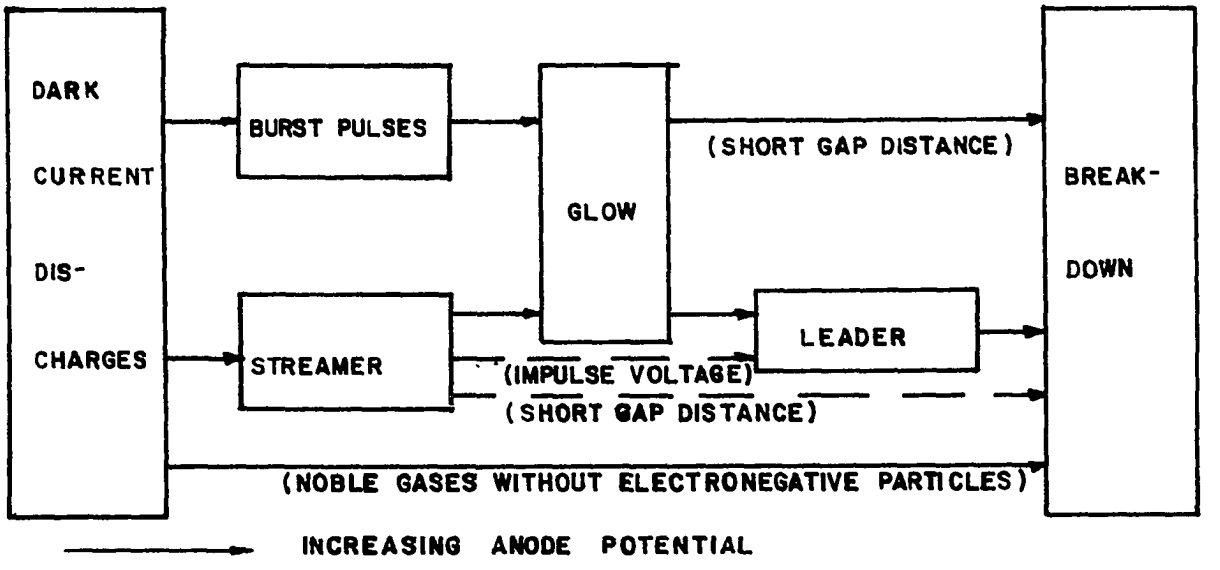

Figure 1. Modes of gas discharges in an nonuniform field.

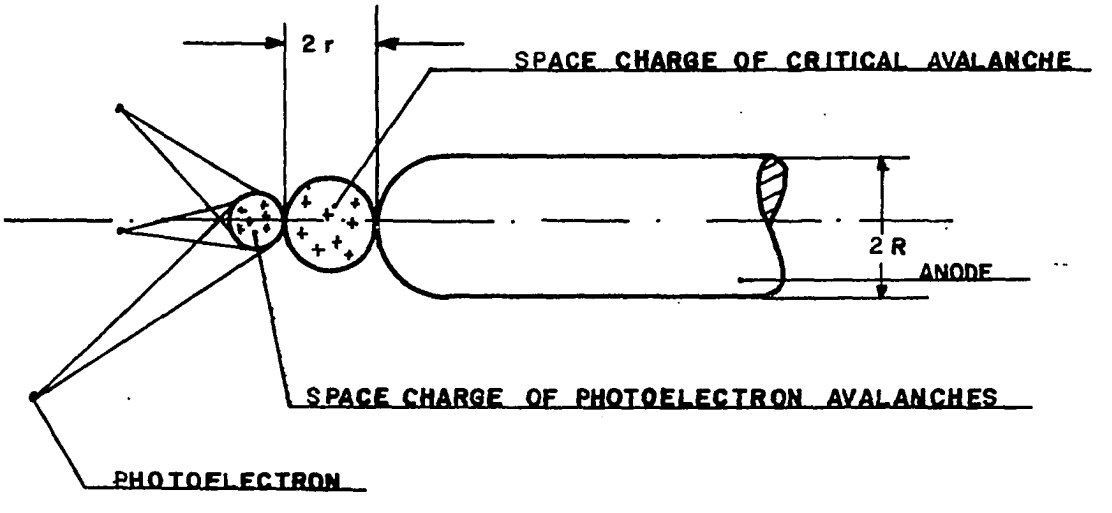

Figure 2. Criterion for streamer propagation.

Figure 3. Response of the scope to usec pulses of 4V peak and varying width, measured through a 10 foot 50 Ω coaxial cable.

horizontal: .05 μs/cm

	pulse width from top to bottom	vertical deflection
a)	90 ns	5 V/cm
b)	3 ns	2 V/cm
c)	4 ns	2 V/cm
d)	10 ns	2 V/cm

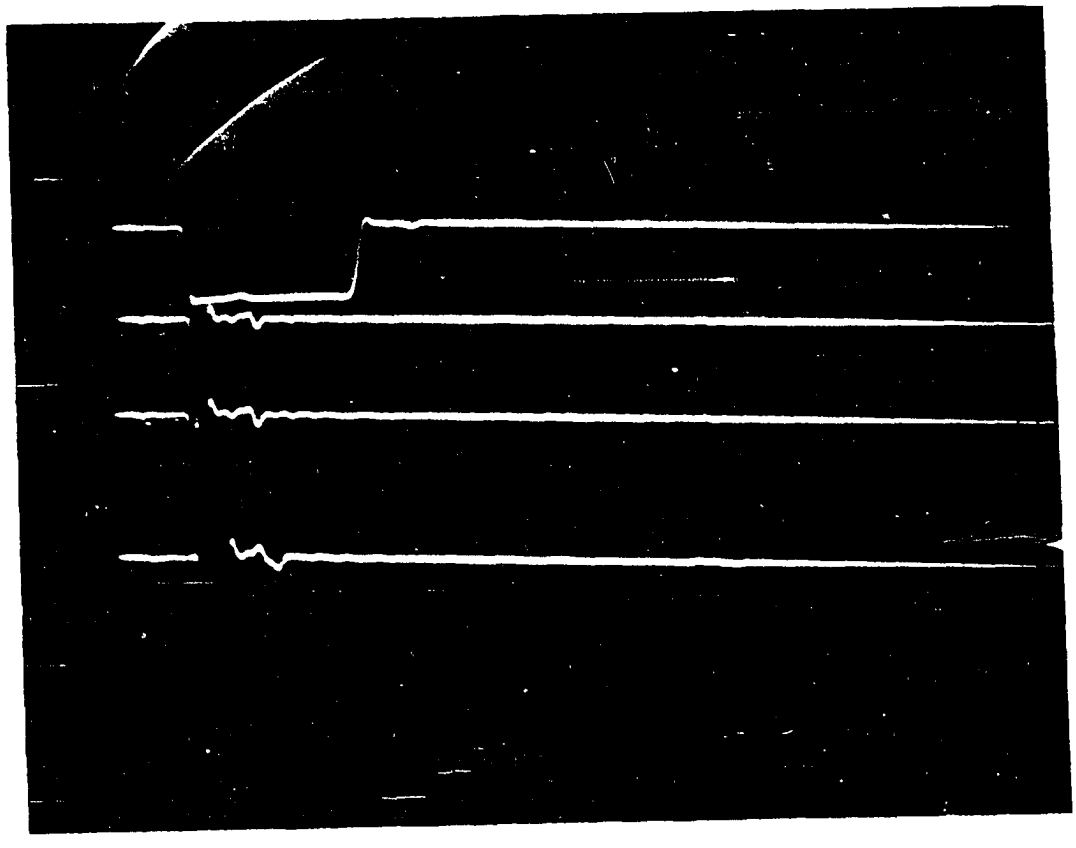

Figure 4. Oscilloscope response to nsec pulse.

Figure 5. Coordinate system describing the gap space.

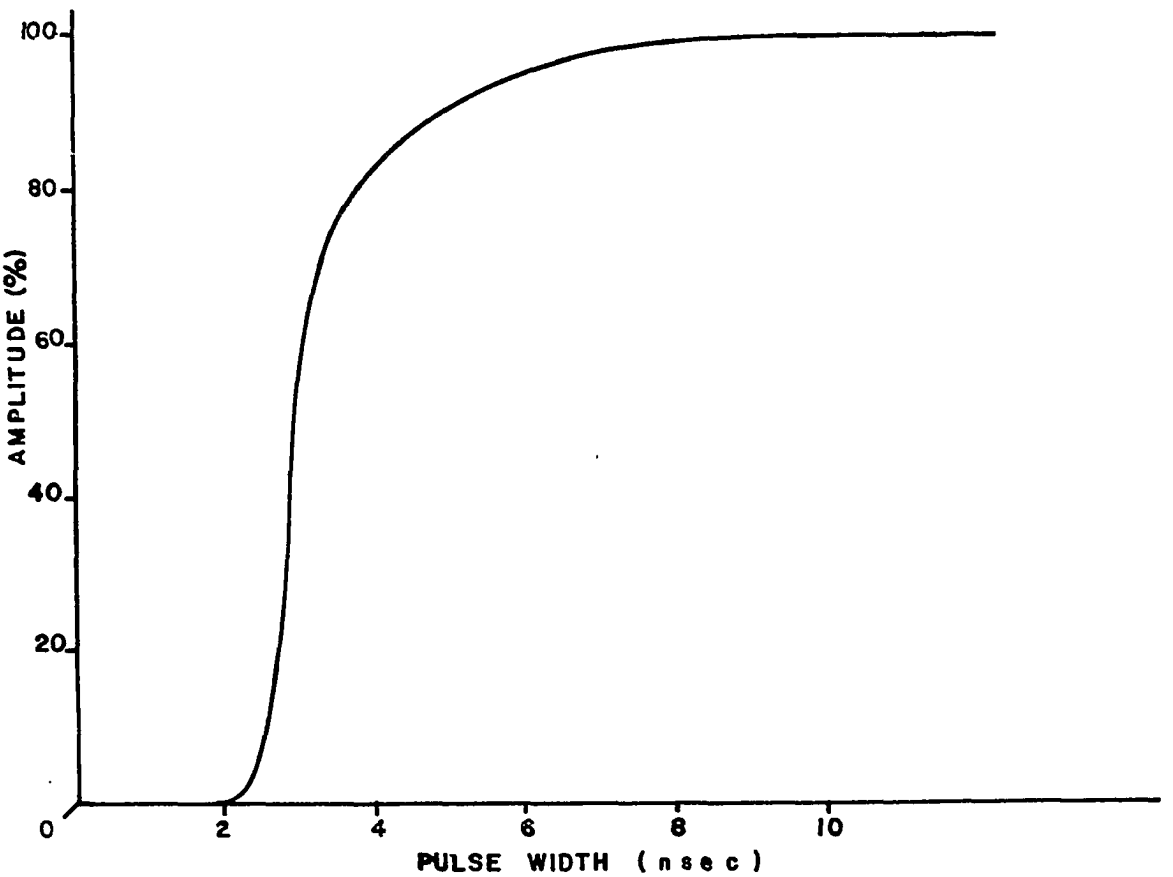
100
80
60
40
20
0
AMPLITUDE (%)
2
4
6
8
10
PULSE WIDTH (n s e c)

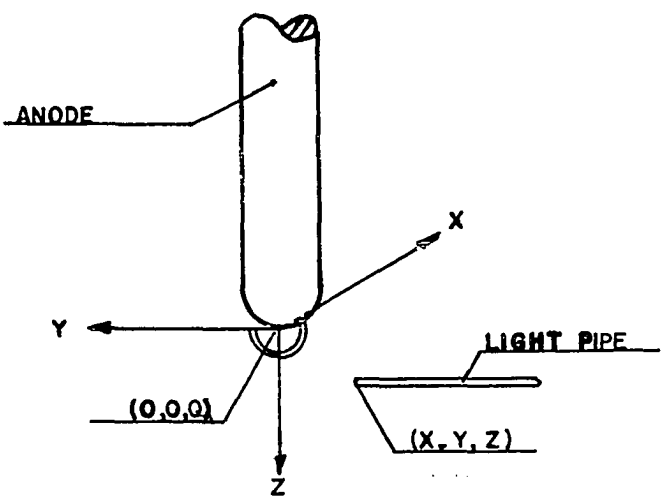
ANODE
X
Y
LIGHT PIPE
(0,0,0)
(X, Y, Z)
Z

Figure 6. Cathode reflections.

position (0, 0, 9.5), V = 58.0 KV, light pipe

diameter = 1.0 mm

horizontal: .2 μs/cm, vertical: 2 V/cm

Figure 7. Cathode reflections (with cloth over cathode).

position (0, 0, 9.5), V = 58.0 KV, light pipe

diameter = 1.0 mm

horizontal: .2 μs/cm, vertical: 2 V/cm

Figure 8. Cathode reflections (with shield over cathode).

position (0, 0, 9.5), V = 58.0 KV, light pipe

diameter = 1.0 mm

horizontal: .2 μs/cm, vertical: 2 V/cm

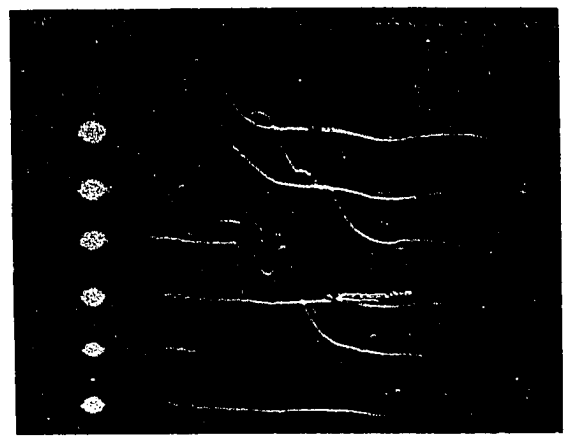

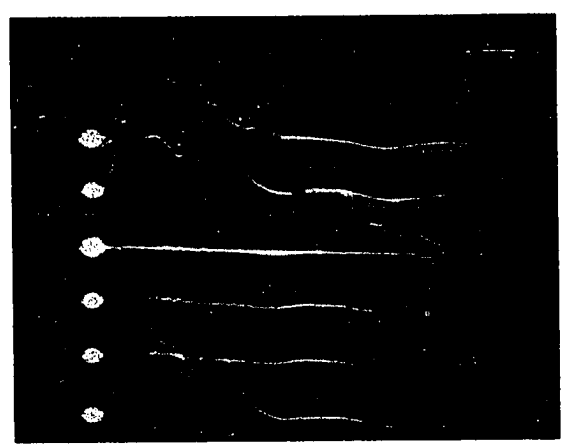

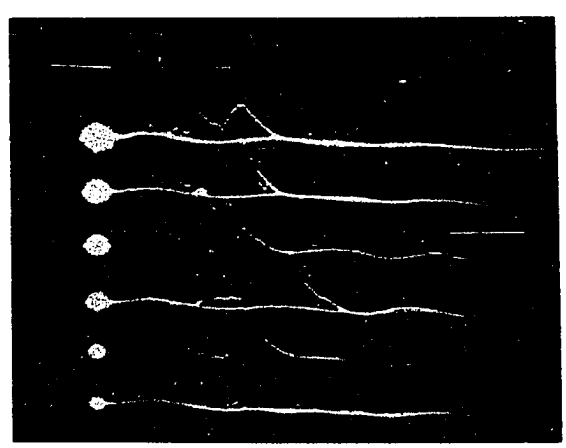

Figure 9. PM signal at (0, 0, .5) 13.5 kV, 1 mm point diameter, 10 cm gap.

horizontal: .05 μs/cm, vertical: .5 V/cm (without film)

Figure 10. PM signal at (0, 0, .5) 13.5 kV, 1mm point diameter, 10 cm gap.

horizontal: .05 μs/cm, vertical: .2 V/cm (with film)

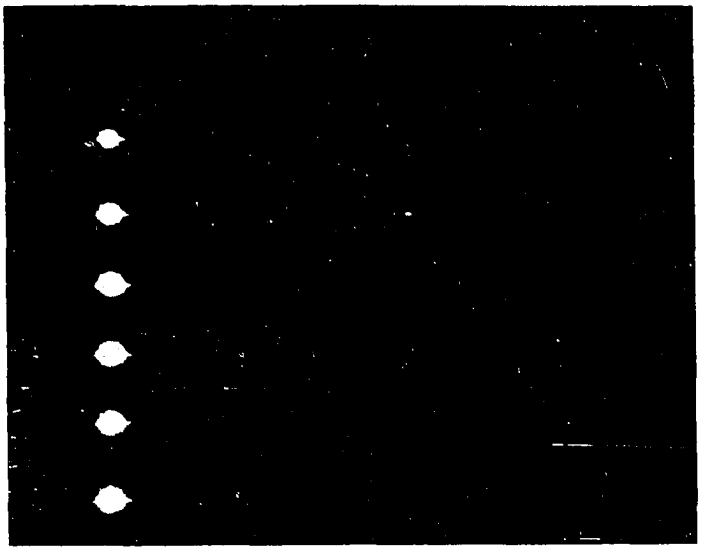

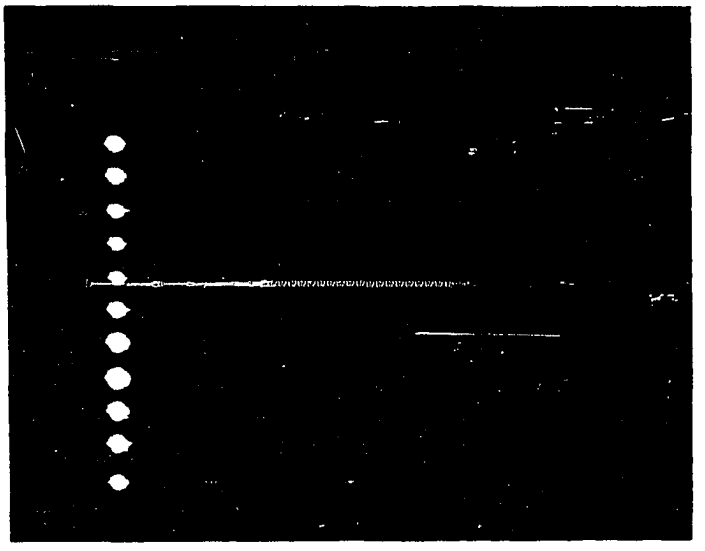

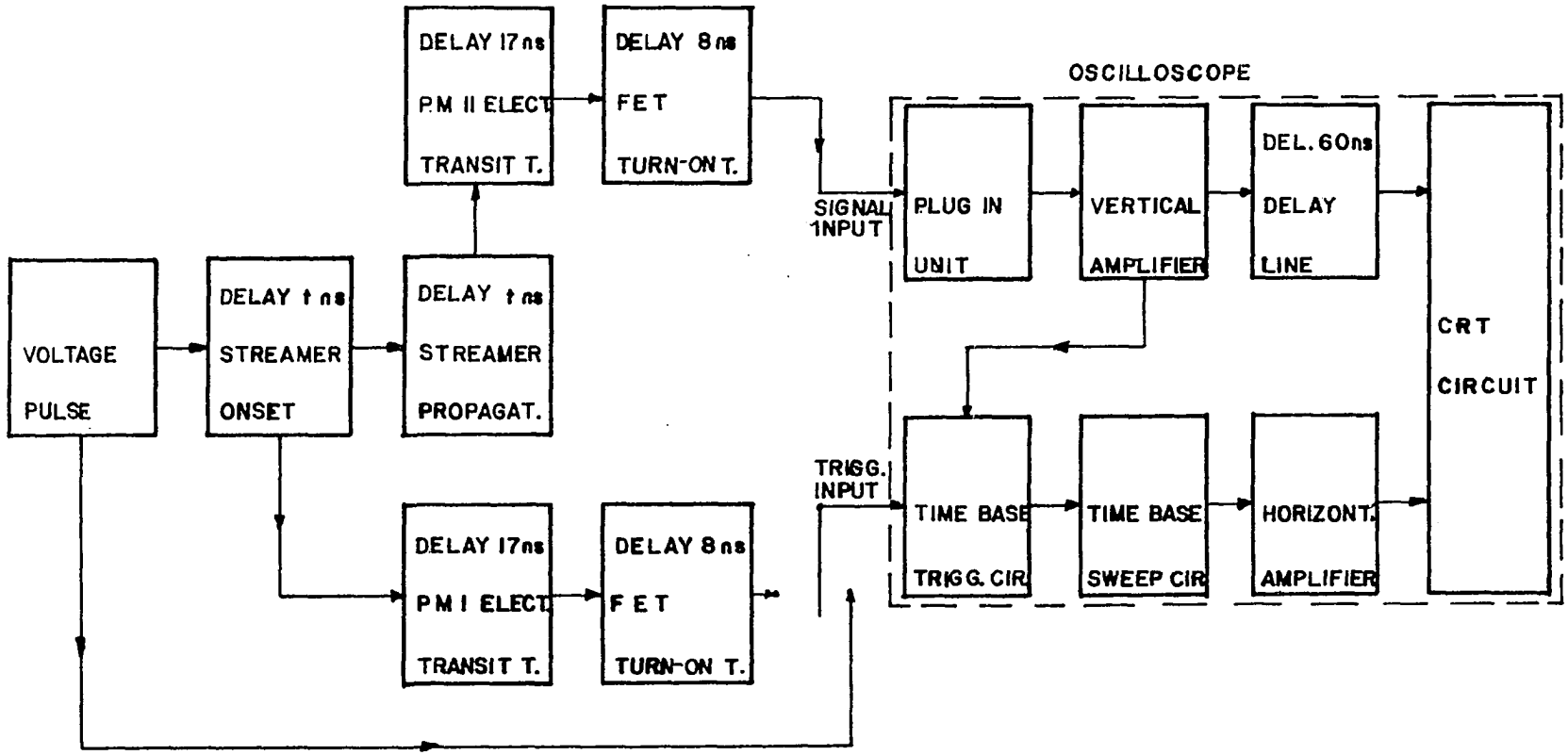

Figure 11. Block diagram of the measuring circuit.

Figure 12. Comparison of propagation measurement with previous results (Nasser et al., 1968).

1. Present results

2. Results of Nasser et al. (1968)

   d = 15 cm, R = .5 mm

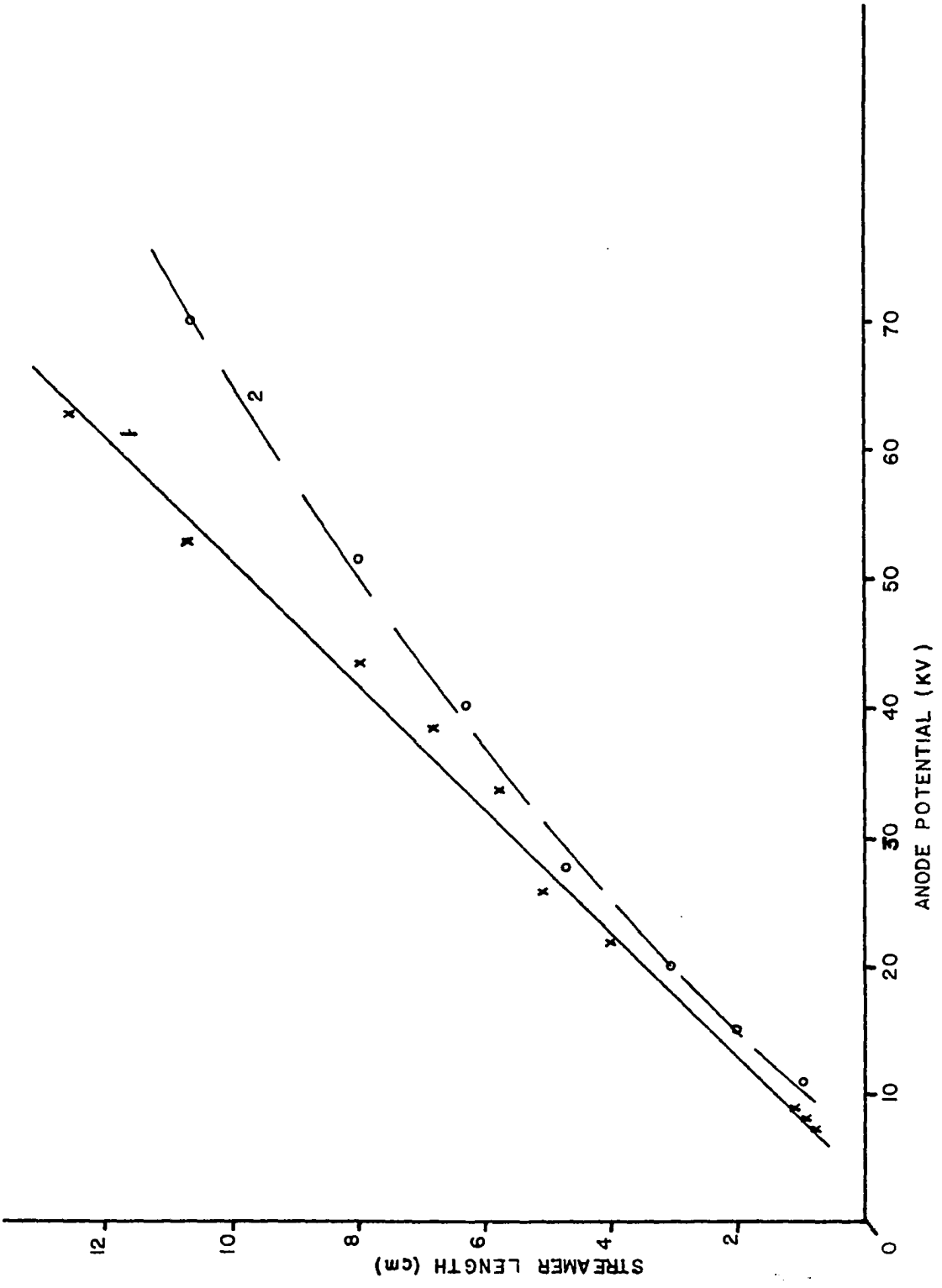
STREAMER LENGTH (cm)
ANODE POTENTIAL (KV)
0
10
20
30
40
50
60
70
2
4
6
8
10
12
1
2

Figure 13. Streamer onset anode potential.

1. R = .5 mm
2. R = 3.0 mm
3. R = 5.0 mm

Figure 14. Streamer onset anode field intensity.

1. R = .5 mm
2. R = 3.0 mm
3. R = 5.0 mm

Figure 15. Onset streamer length.

1. R = .5 mm
2. R = 3.0 mm
3. R = 5.0 mm

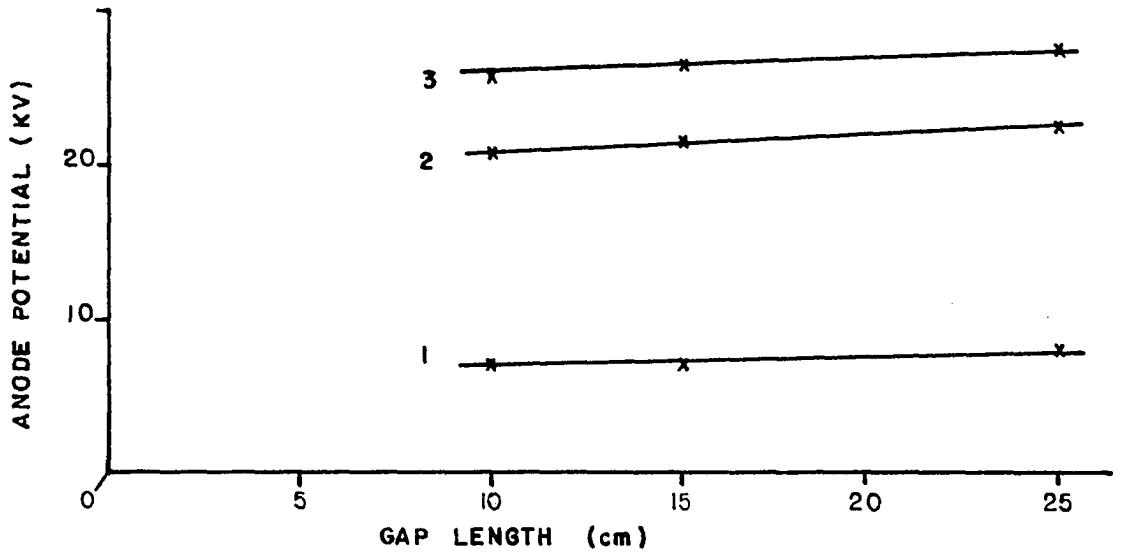
ANODE POTENTIAL (KV)
20
10
0
5
10
15
20
25
GAP LENGTH (cm)
3
2
1

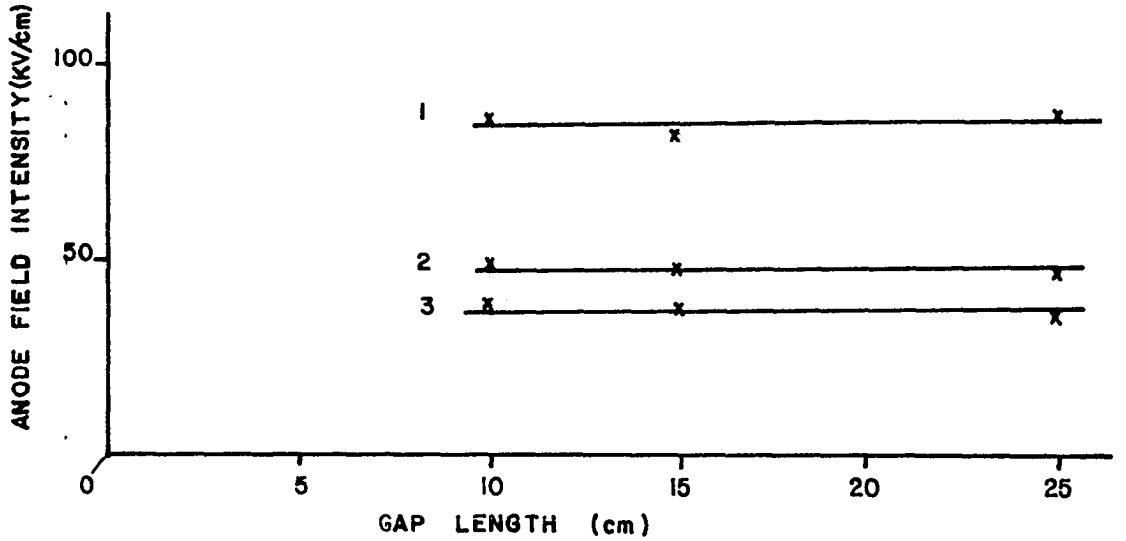
ANODE FIELD INTENSITY(KV/cm)
100
50
0
5
10
15
20
25
GAP LENGTH (cm)
1
2
3

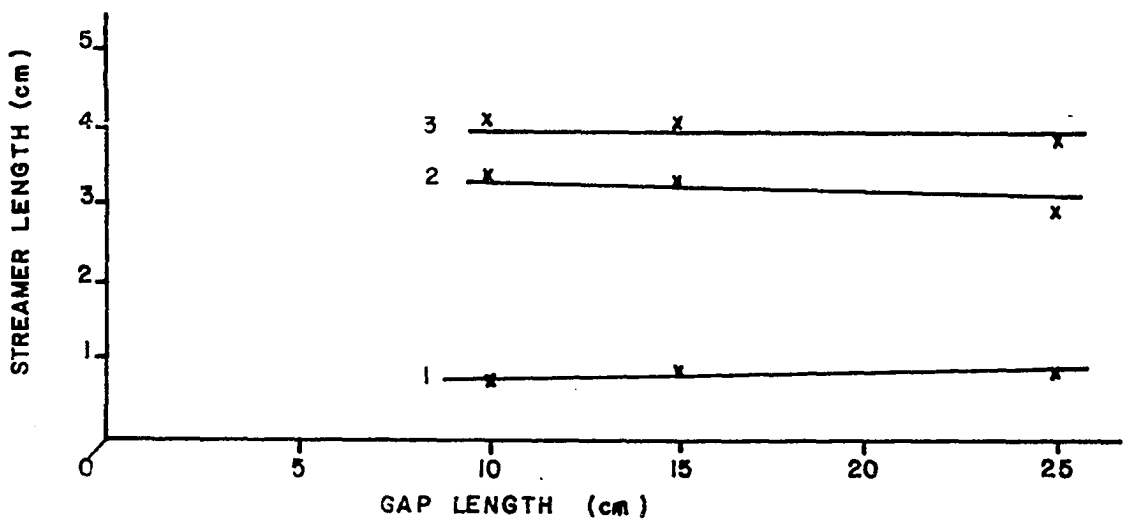
STREAMER LENGTH (cm)
5
4
3
2
1
0
5
10
15
20
25
GAP LENGTH (cm)
3
2
1

Figure 16. Burst pulse and streamer pulse recorded with a photomultiplier (d = 10 cm, R = 5 mm).

a. Burst pulse: horizontal: .05 μs/cm,
vertical: .5 V/cm

V = 28.5 KV

b. Streamer pulse: horizontal: .2 μs/cm,
vertical: .5 V/cm (FET saturated)

V = 28.5 KV

Figure 17. Time lag of burst and streamer pulses.

horizontal: 10 μs/cm (5 μs/cm 1^{st} and 2^{nd} trace from the top)

vertical: .5 V/cm

d = 10 cm, R = 5 mm, V = 32 KV

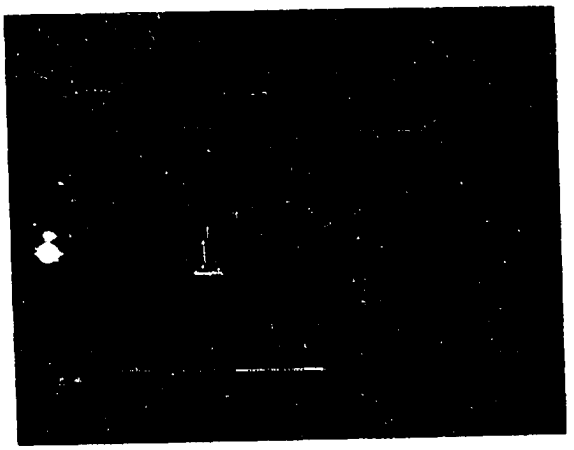

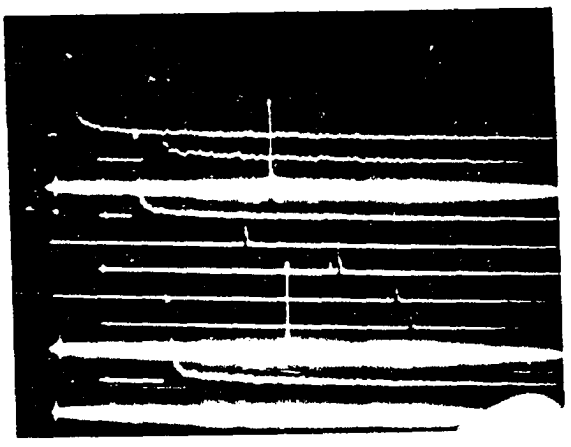

Figure 18. Double burst pulse (lower trace dark current signal).
horizontal: .2 μs/cm, vertical: .5 V/cm
d = 10 cm, R = 5 mm, V = 32 KV

Figure 19. Burst and streamer pulses observed from 2 mm distance.
light pipe diameter 6 mm, d = 15 cm, R = 5 mm, V = 33 KV
horizontal: 10 μs/cm, vertical: .5 V/cm

Figure 20. Burst and streamer pulses of large point radii.
d = 20 cm, R = 16 mm, V = 67 KV (upper trace) and 61 KV
horizontal: 5 μs/cm, vertical: .5 V/cm

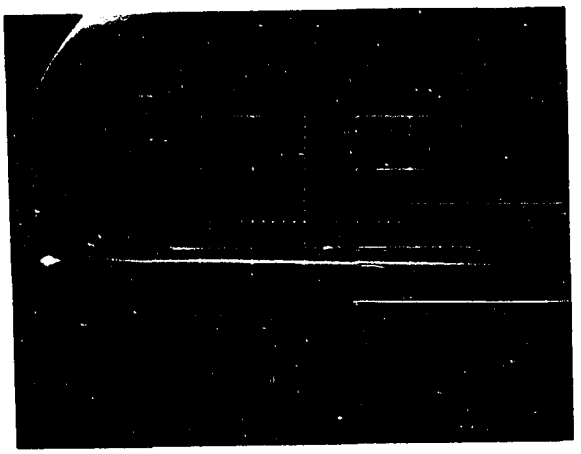

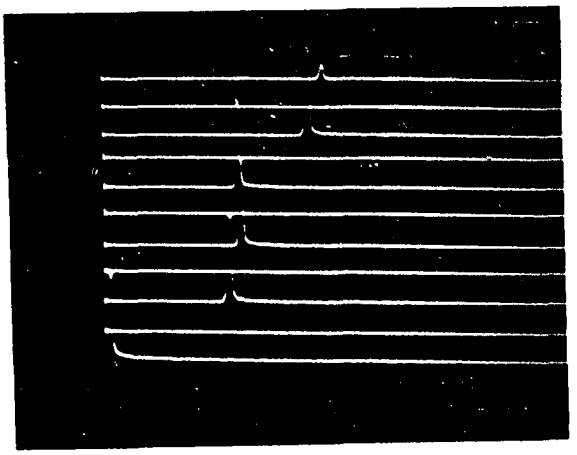

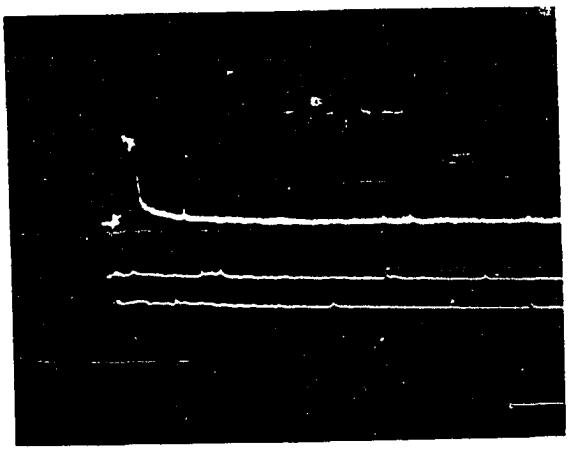

Figure 21. Development of a glow at the point.

d = 10 cm, R = 5 mm, V = 53, 58, 61 KV from top to bottom

horizontal: 50 μs/cm, 100 μs/cm, 100 μs/cm

vertical: .5 V/cm

light pipe diameter 12 mm

Figure 22. Flashover observed with a 1 mm light pipe.

position (0, 0, 7.5)

d = 10 cm, R = 5 cm, V = 76, 77, 78 KV from top to bottom

horizontal: 10 μs/cm

vertical: .5 V/cm

Figure 23. Streamer pulses observed with a 1 mm light pipe at the point electrode.

d = 10 cm, R = 5 cm, V = 34 KV

horizontal: 1 μs/cm

vertical: 5 V/cm

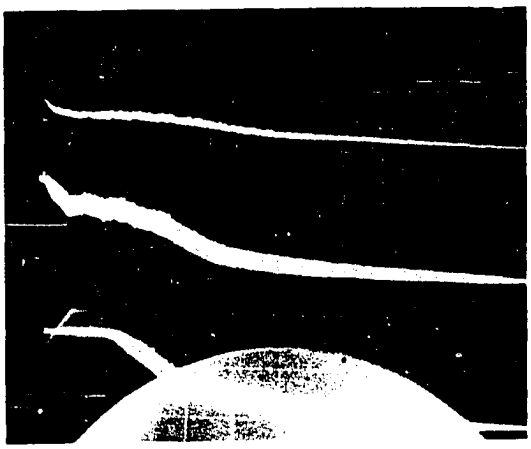

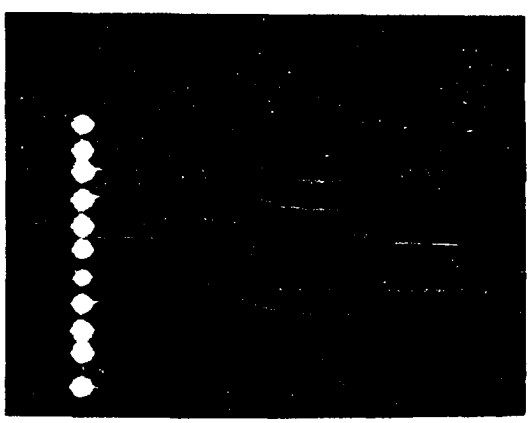

Figure 24. Variation of the statistical spread of the time lag with point radius increase at onset potential (d = 20 cm).

Horizontal: 5 μs/cm, vertical: .5 V/cm

a. R = .5 mm

b. R = 3.0 mm

c. R = 5.0 mm

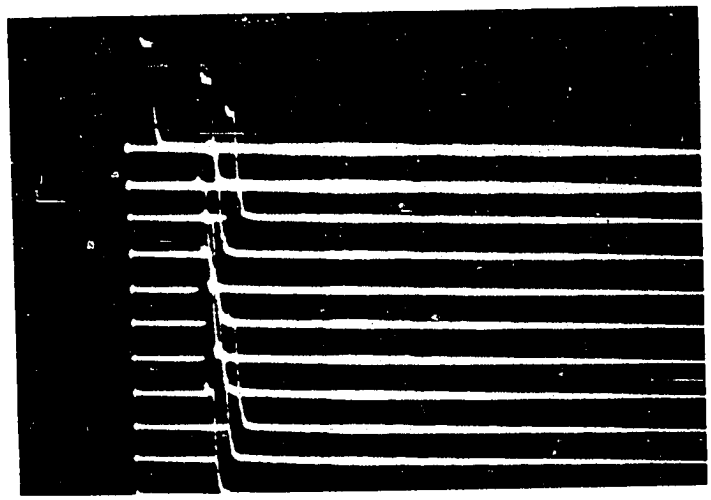

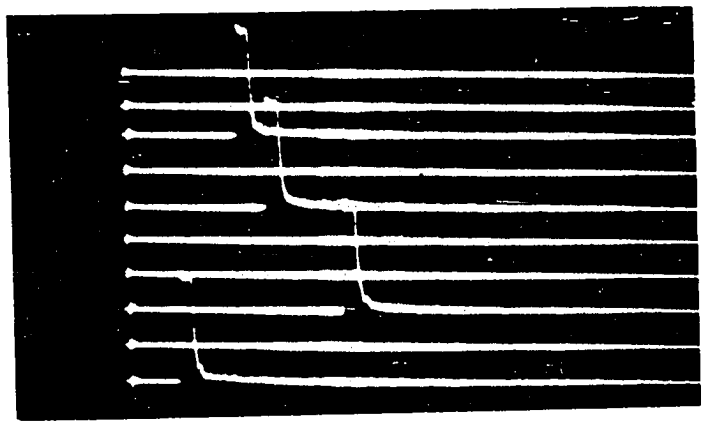

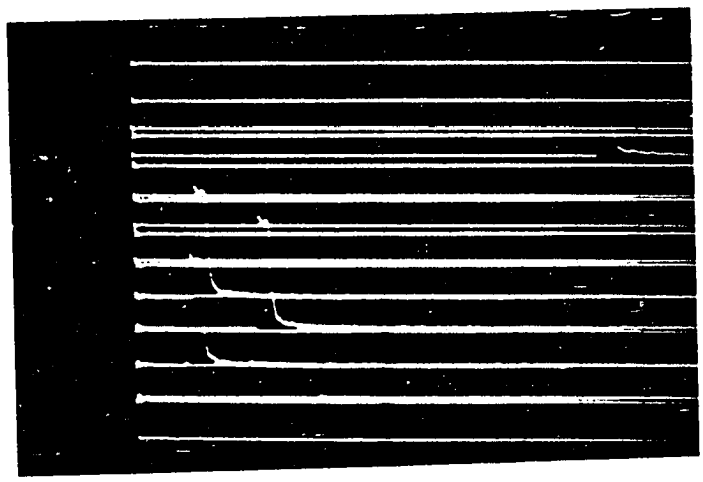

Figure 25. Variations of the time lag with the point radius at various potentials.

Figure 26a. Streamer pulse width.

d = 10 cm, R = .5 mm

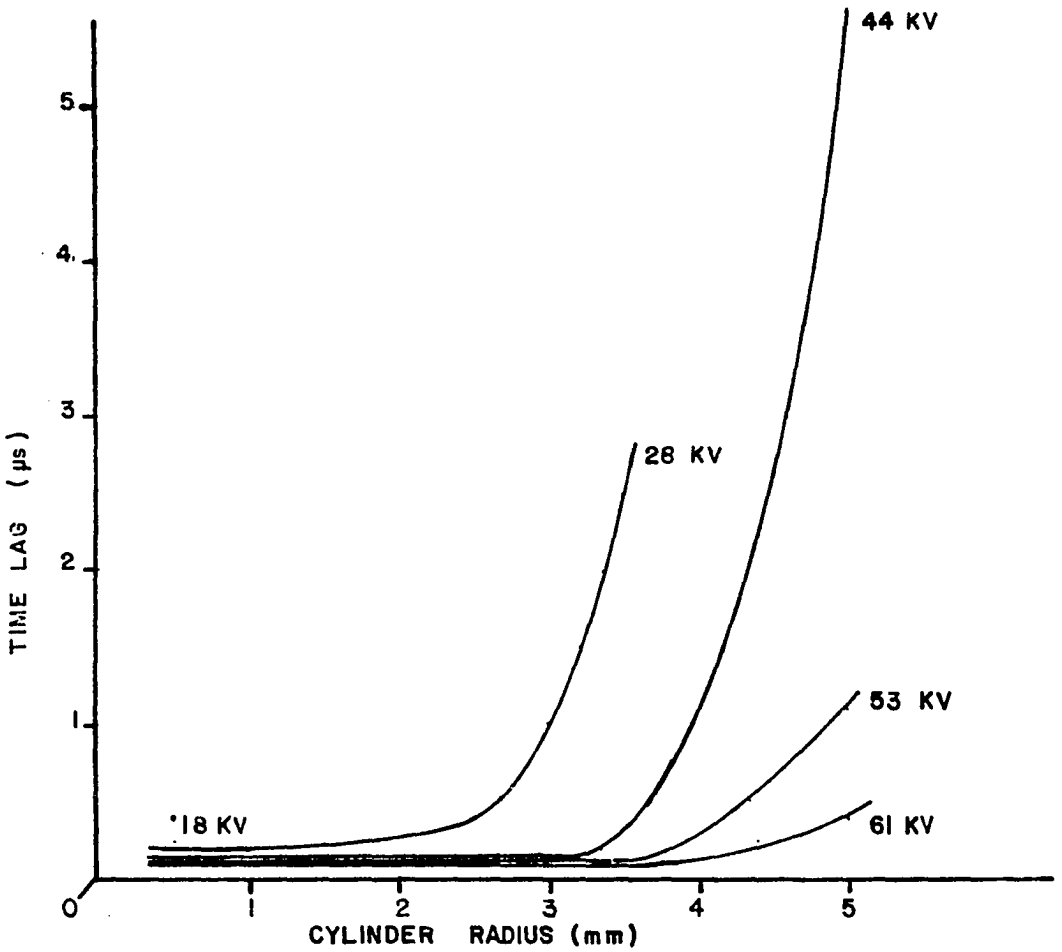
44 KV
28 KV
53 KV
61 KV
18 KV
TIME LAG (μs)
0
1
2
3
4
5
CYLINDER RADIUS (mm)

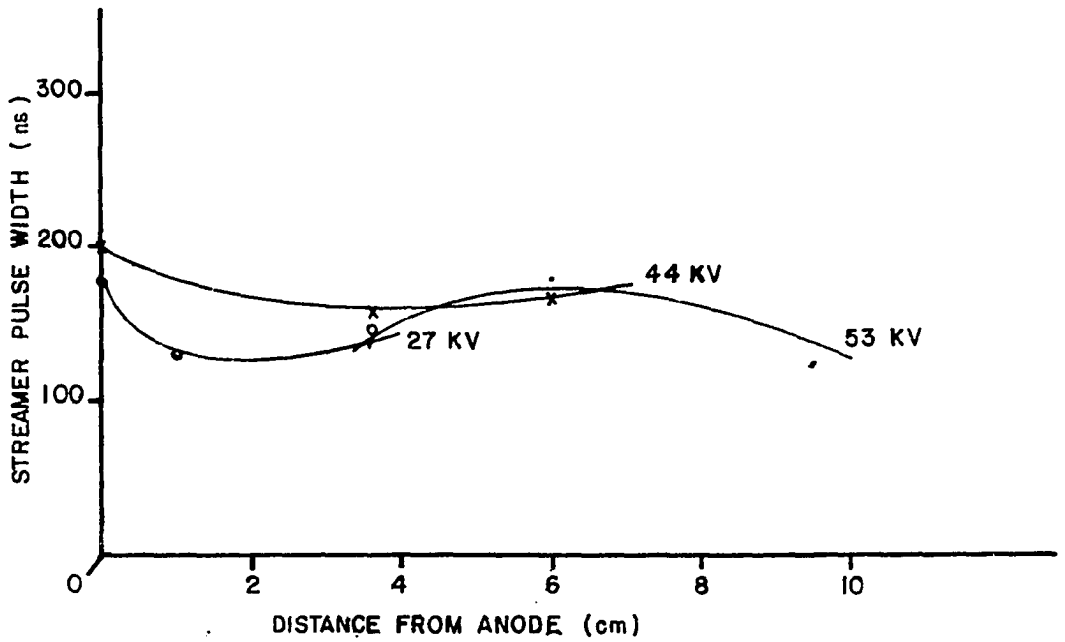
STREAMER PULSE WIDTH (ns)
100
200
300
44 KV
27 KV
53 KV
0
2
4
6
8
10
DISTANCE FROM ANODE (cm)

Figure 26b. Streamer pulse width.

d = 10 cm, R = 3.0 mm

Figure 26c. Streamer pulse width.

d = 10 cm, R = 5.0 mm

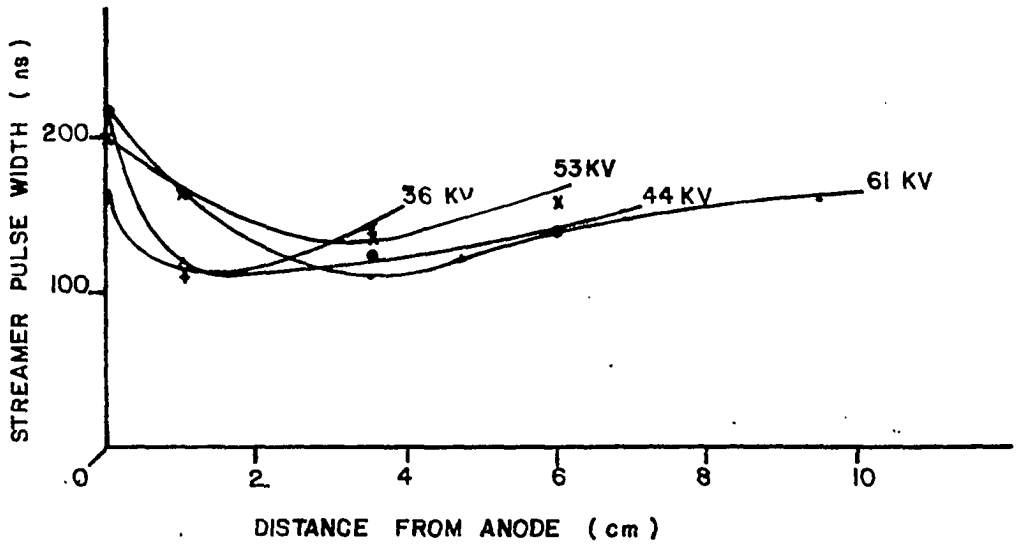
STREAMER PULSE WIDTH (ns)
200
100
0
2
4
6
8
10
DISTANCE FROM ANODE (cm)
36 KV
53KV
44 KV
61 KV

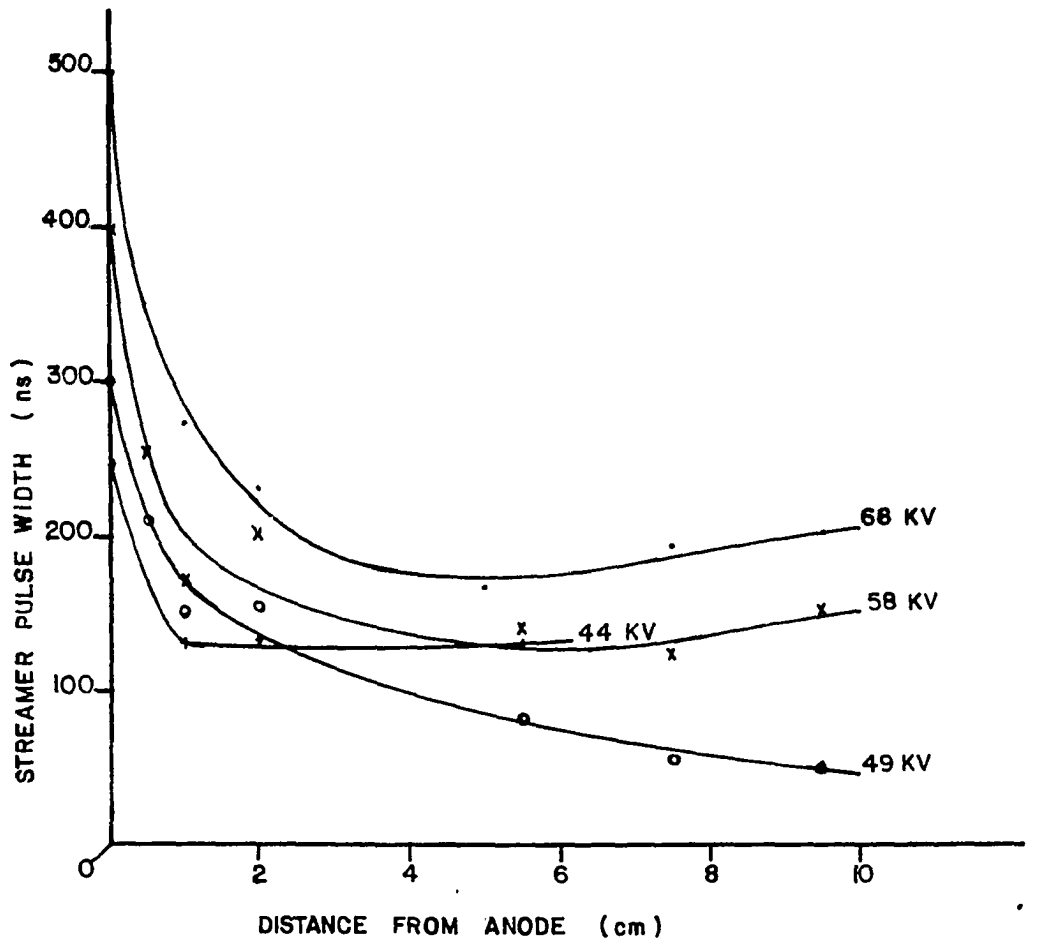
STREAMER PULSE WIDTH (ns)
500
400
300
200
100
0
2
4
6
8
10
DISTANCE FROM ANODE (cm)
68 KV
58 KV
44 KV
49 KV

Figure 26d. Streamer pulse width.

d = 15 cm, R = 5.0 mm

Figure 27. Comparison of pulse width at point and mid-gap for various point radii.

d = 10 cm, V = 44 kV

1. At point

2. At mid-gap

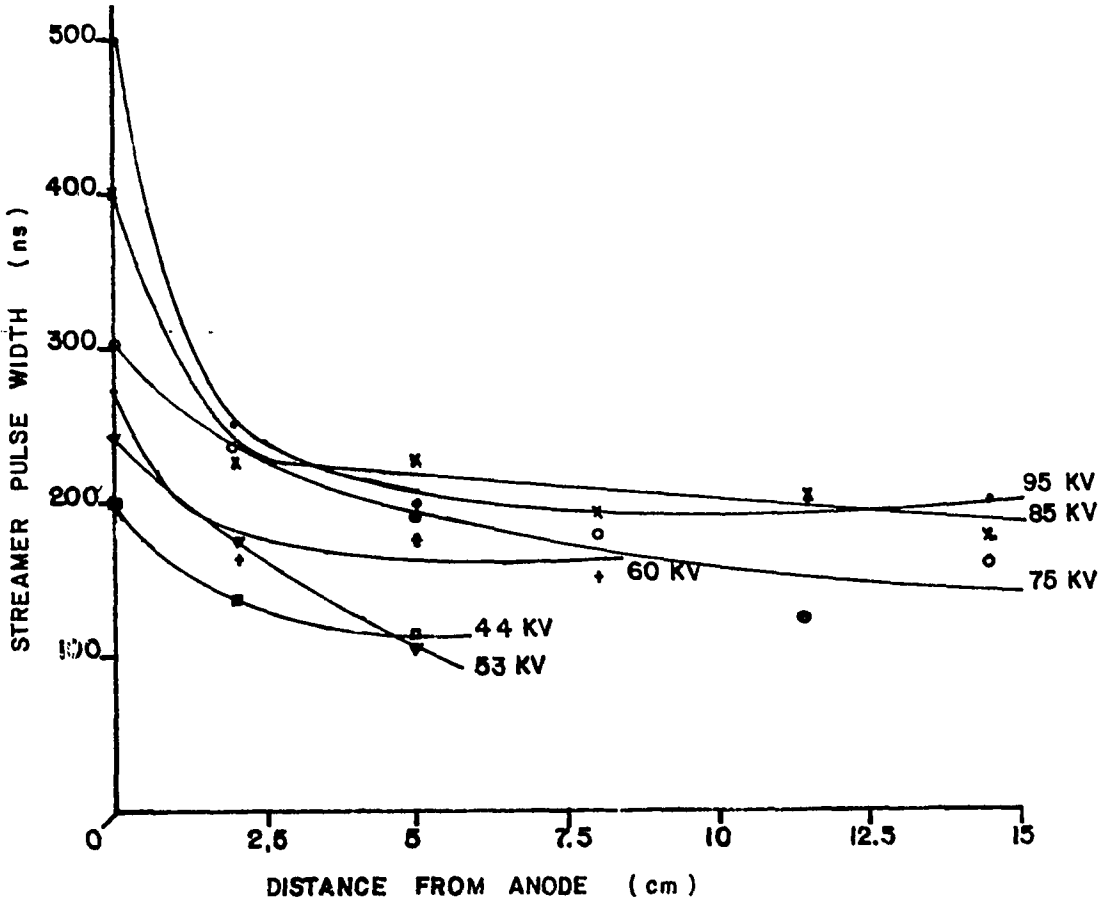
500
400
300
200
100
STREAMER PULSE WIDTH (ns)
95 KV
85 KV
75 KV
60 KV
44 KV
53 KV
0
2.5
5
7.5
10
12.5
15
DISTANCE FROM ANODE (cm)

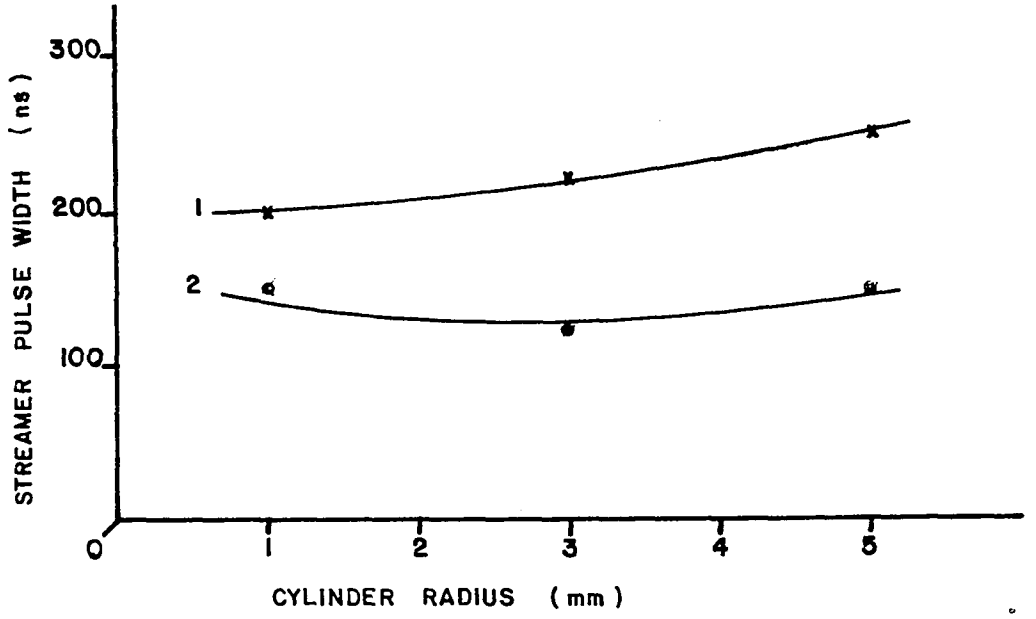
300
200
100
0
STREAMER PULSE WIDTH (ns)
1
2
1
2
3
4
5
CYLINDER RADIUS (mm)

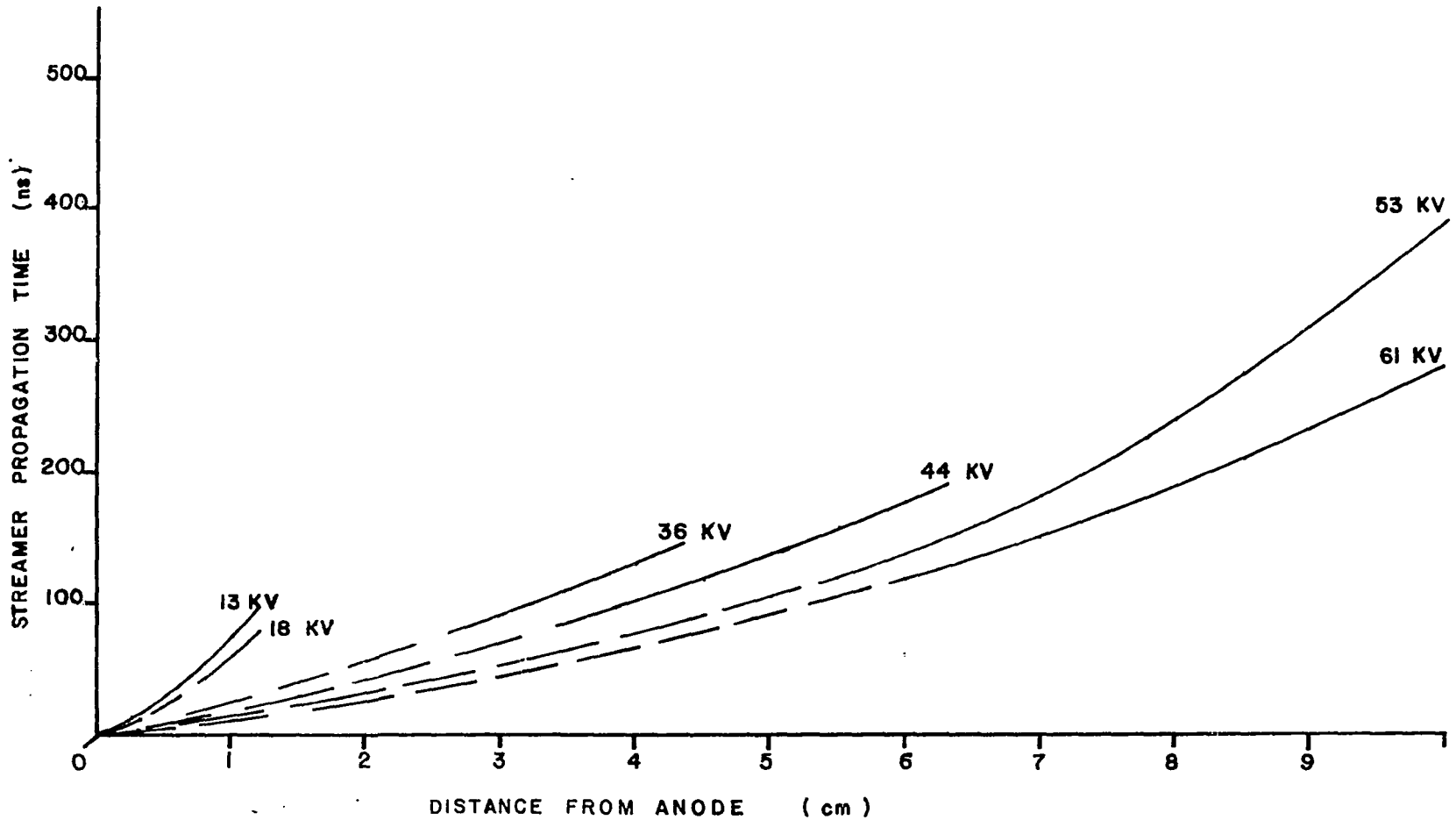

Figure 28a. Propagation time.

d = 10 cm, R = .5 mm

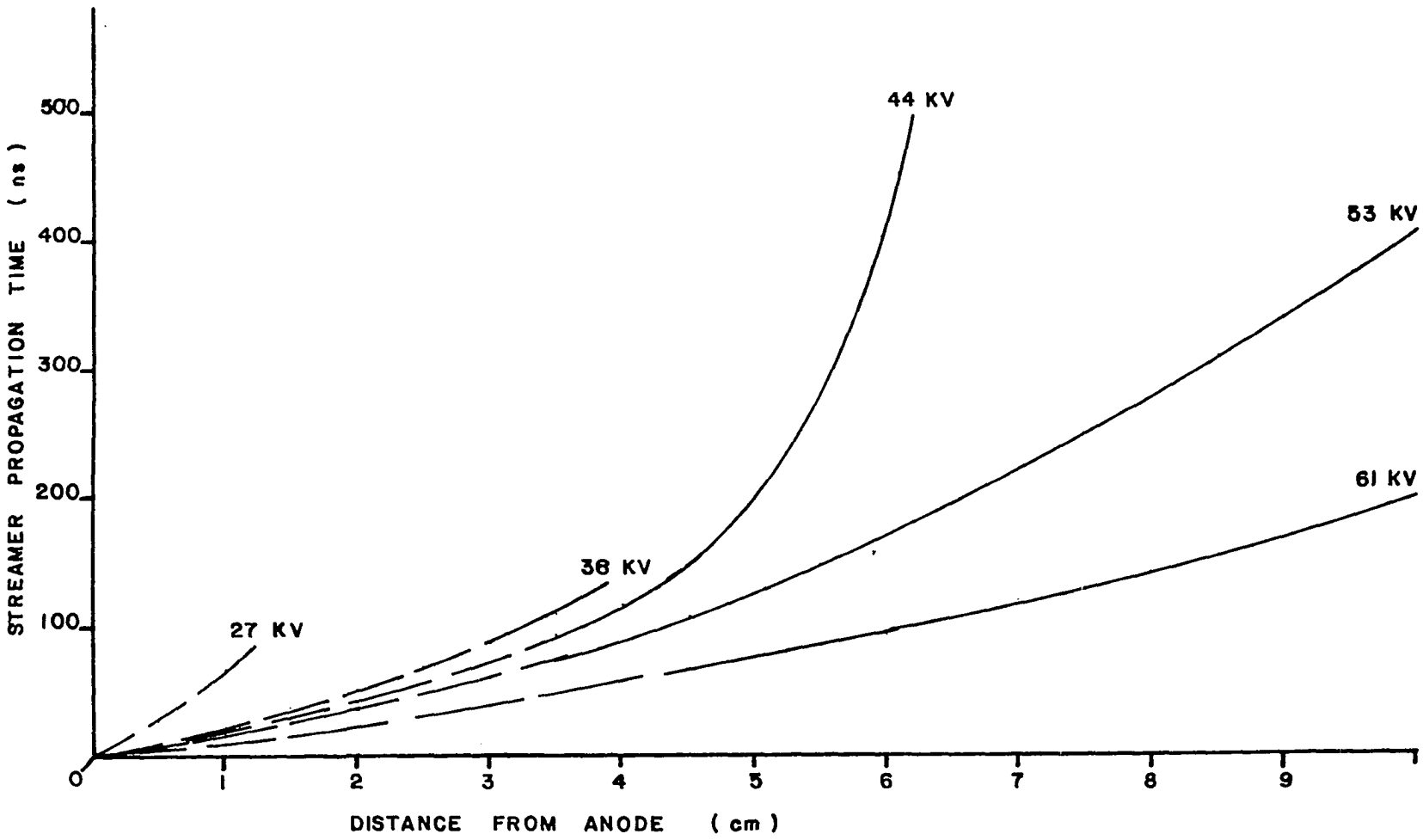

Figure 28b. Propagation time.

d = 10 cm, R = 3.0 mm

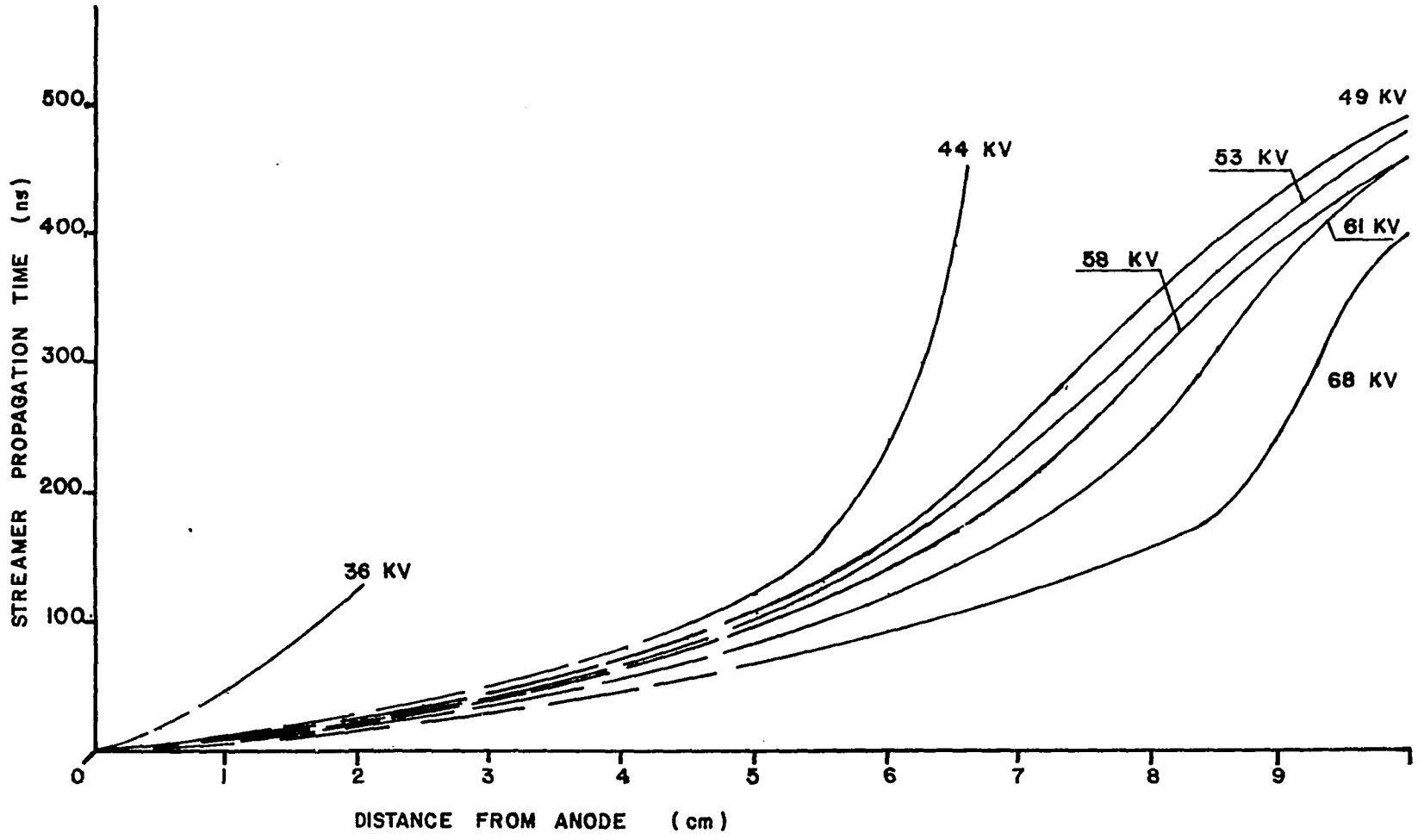

Figure 28c. Propagation time.

d = 10 cm, R = 5.0 mm

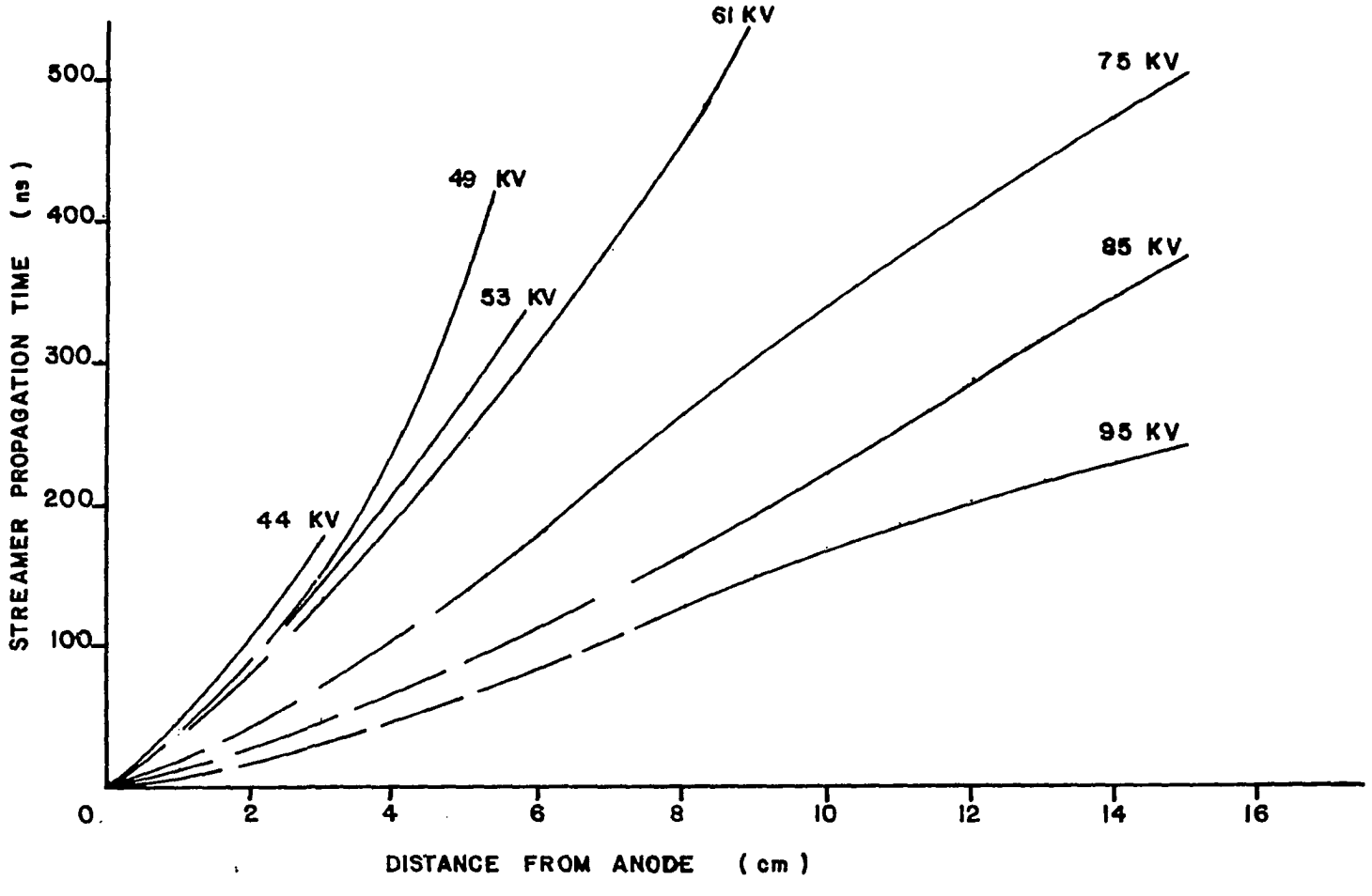

Figure 28d. Propagation time.

d = 15 cm, R = 5.0 mm

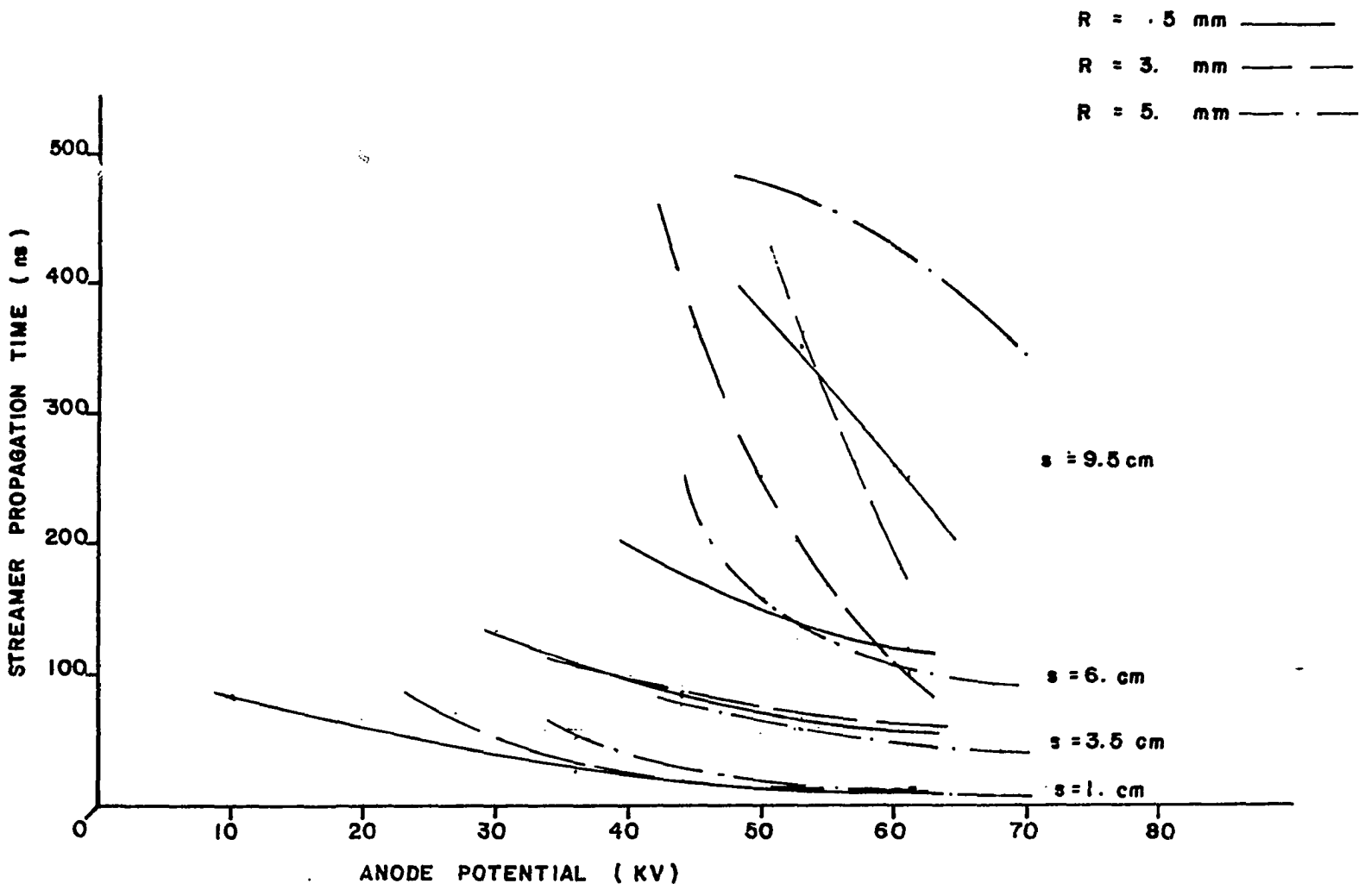

Figure 29. Propagation time versus potential at various locations in the gap.

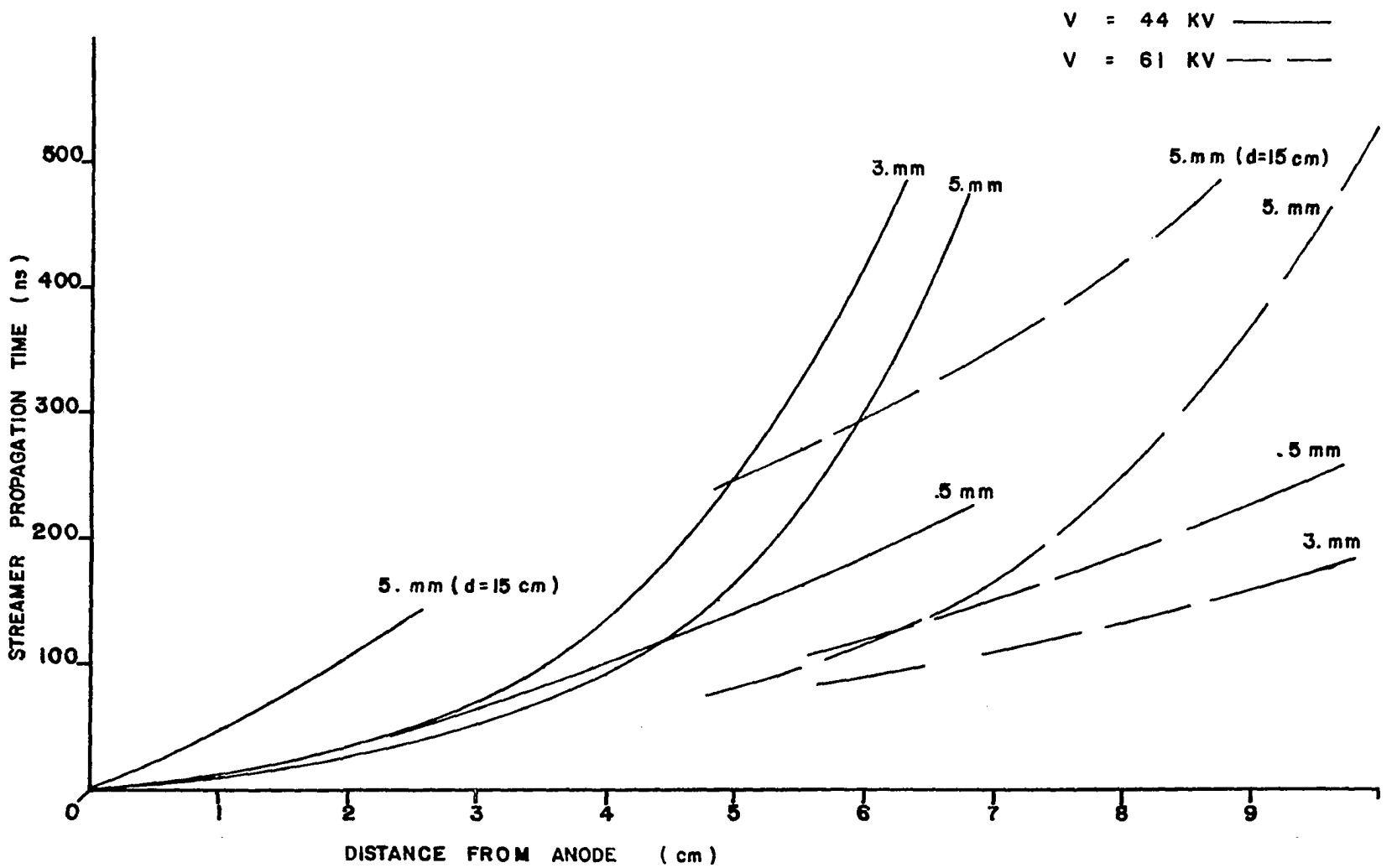

Figure 30. Propagation time of streamer for various point radii at 44 KV and 61 KV.

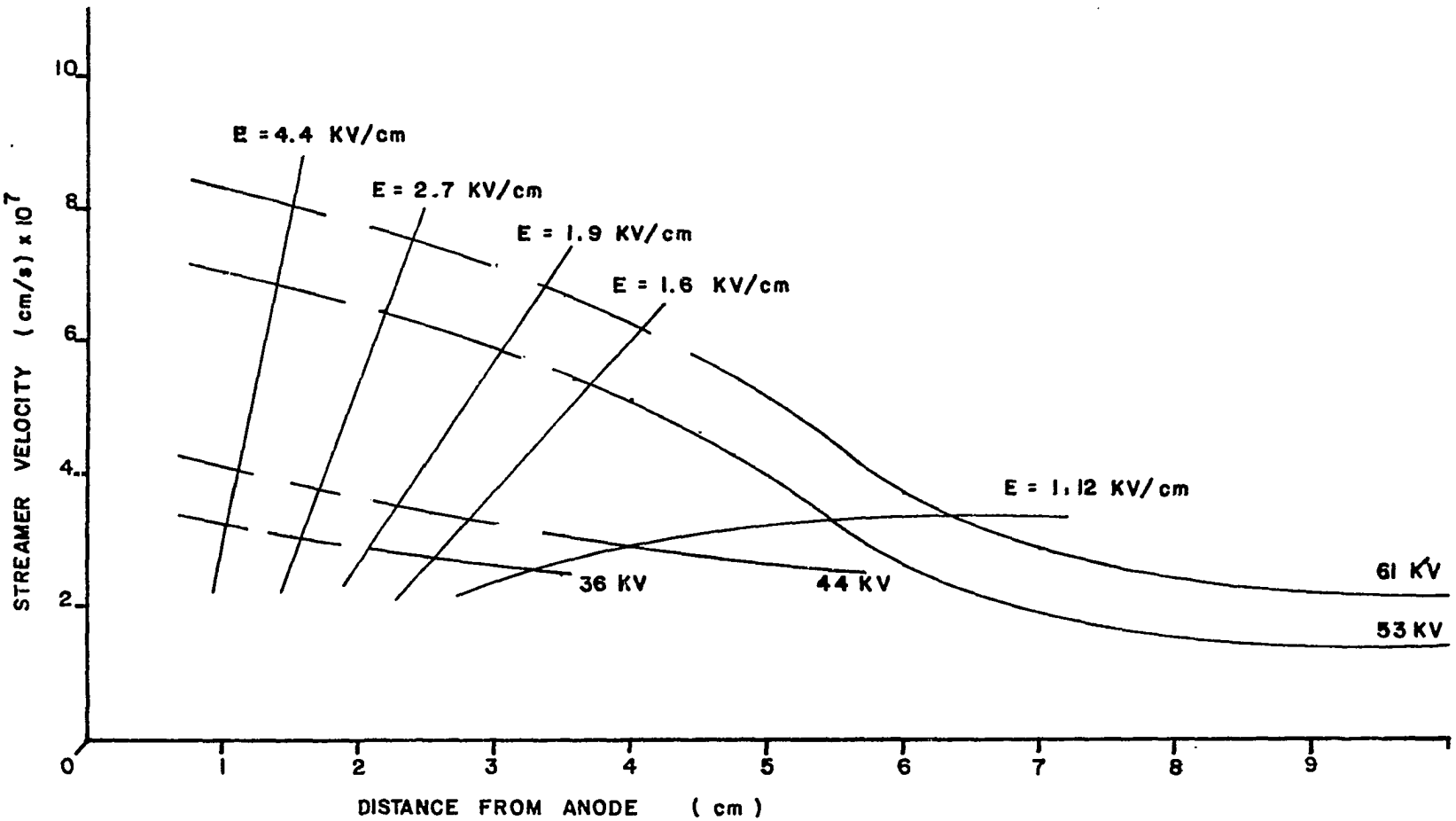

Figure 31a. Streamer velocity.

d = 10 cm, R = .5 mm

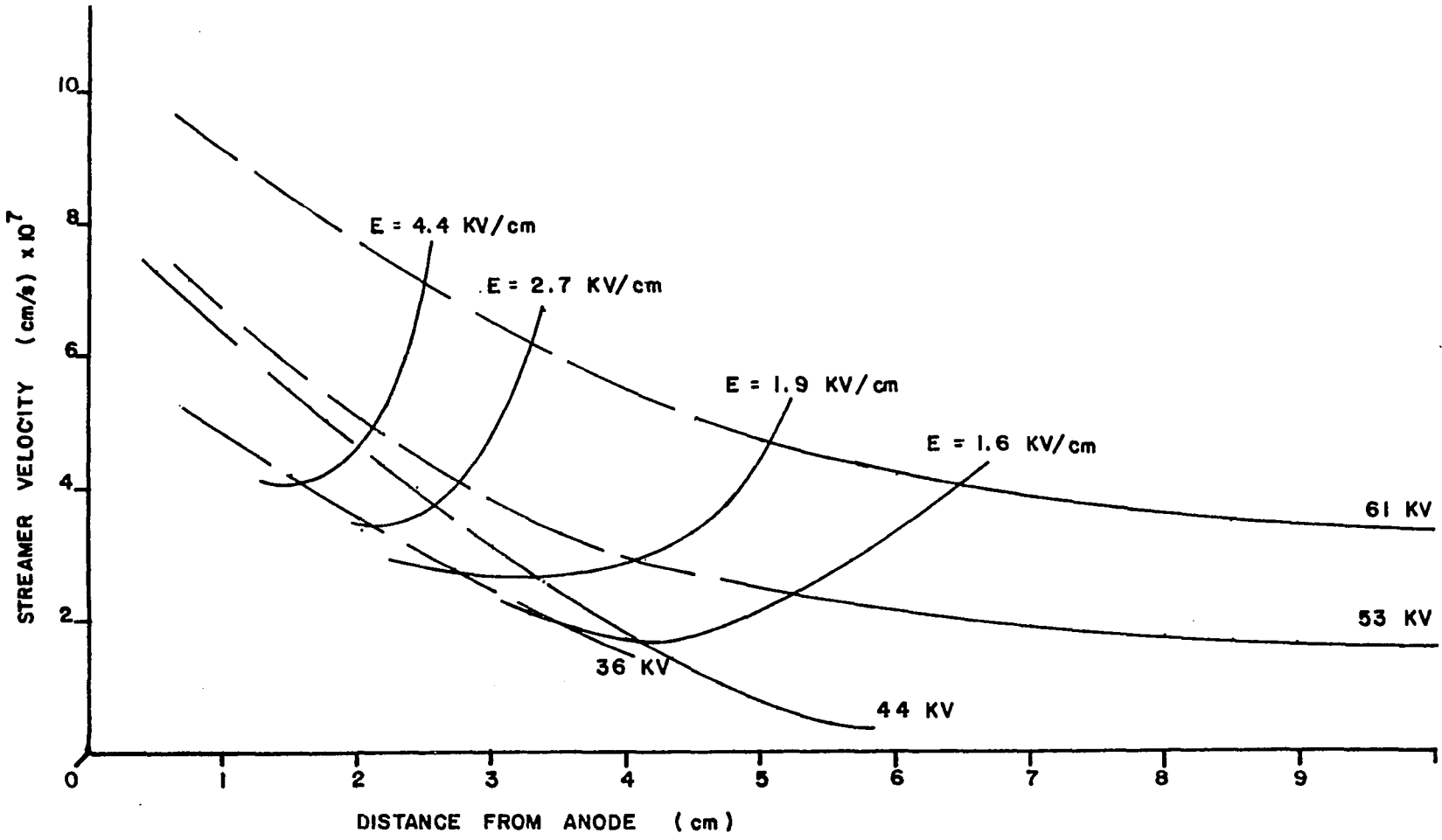

Figure 31b. Streamer velocity.

d = 10 cm, R = 3.0 mm

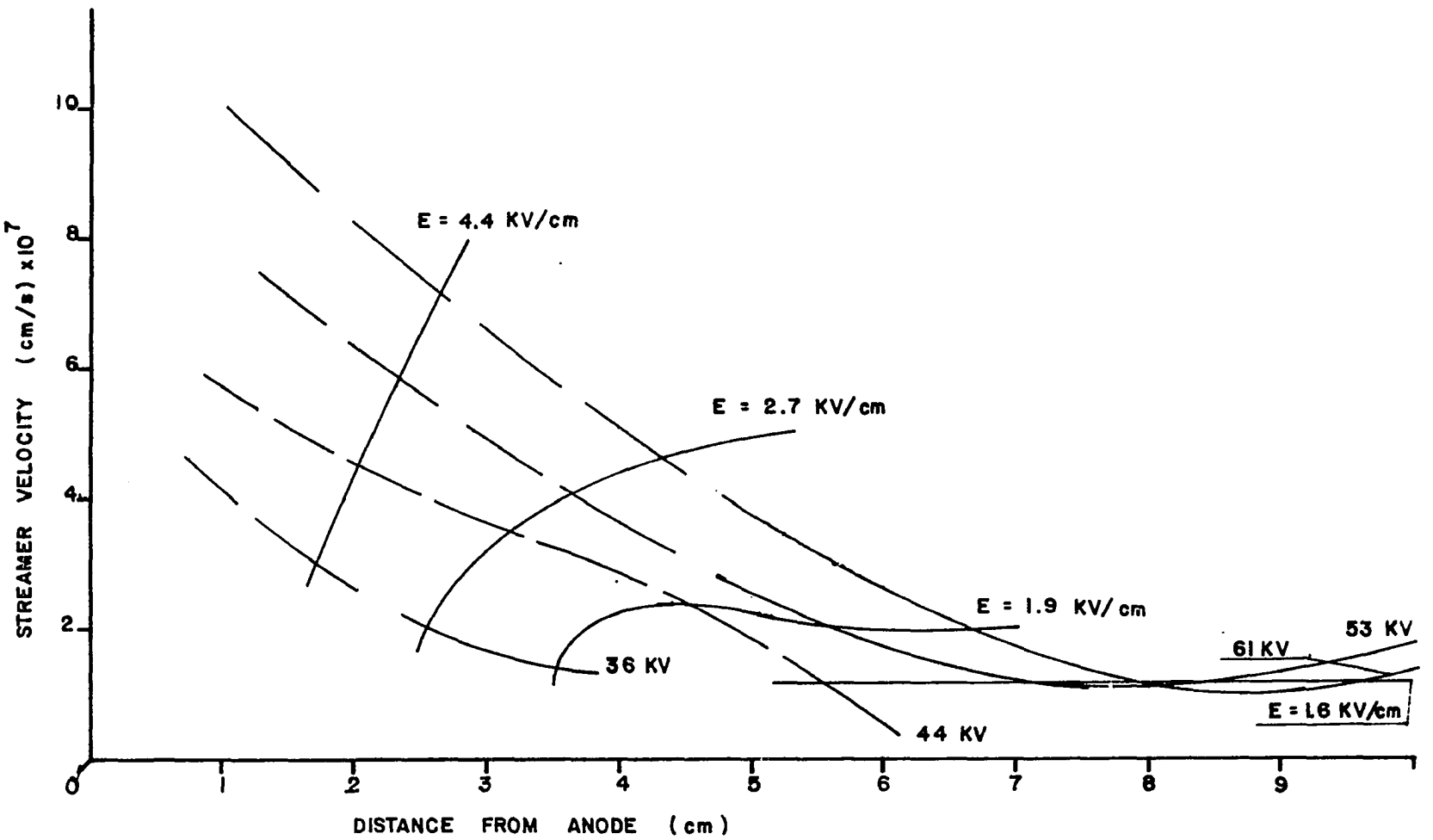

Figure 31c. Streamer velocity.

d = 10 cm, R = 5.0 mm

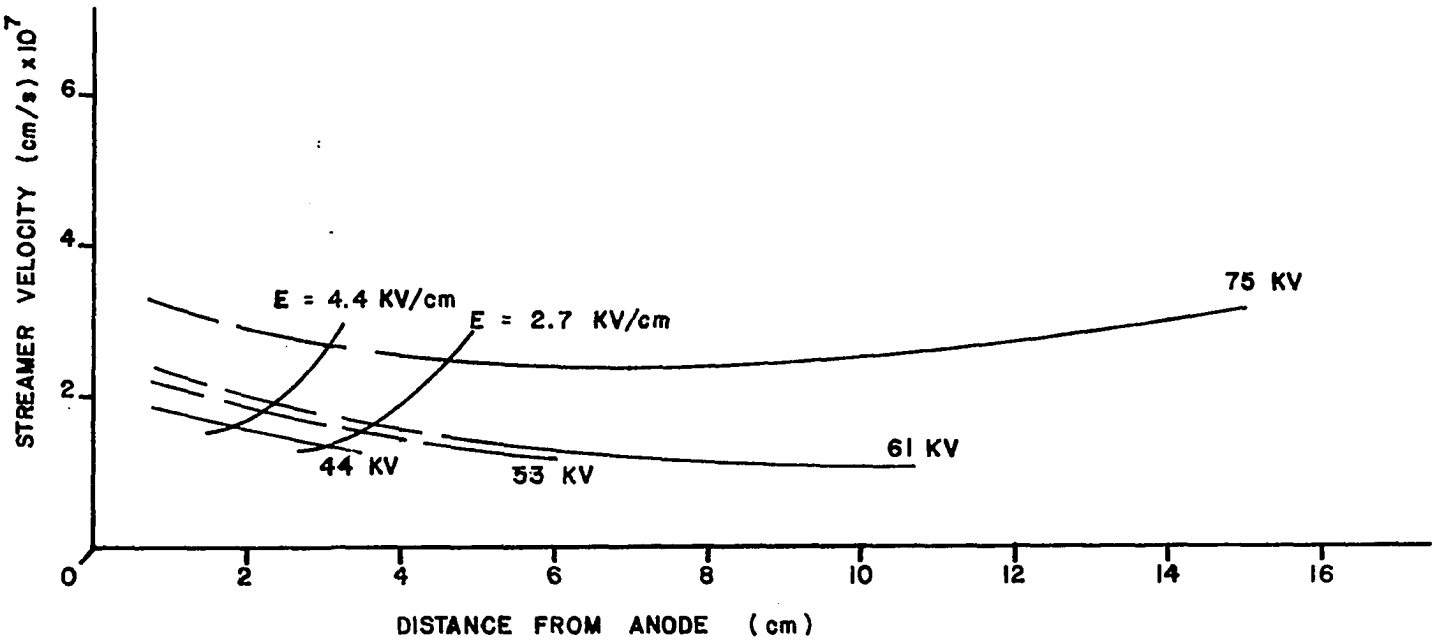

Figure 31d. Streamer velocity.
d = 15 cm, R = 5.0 mm

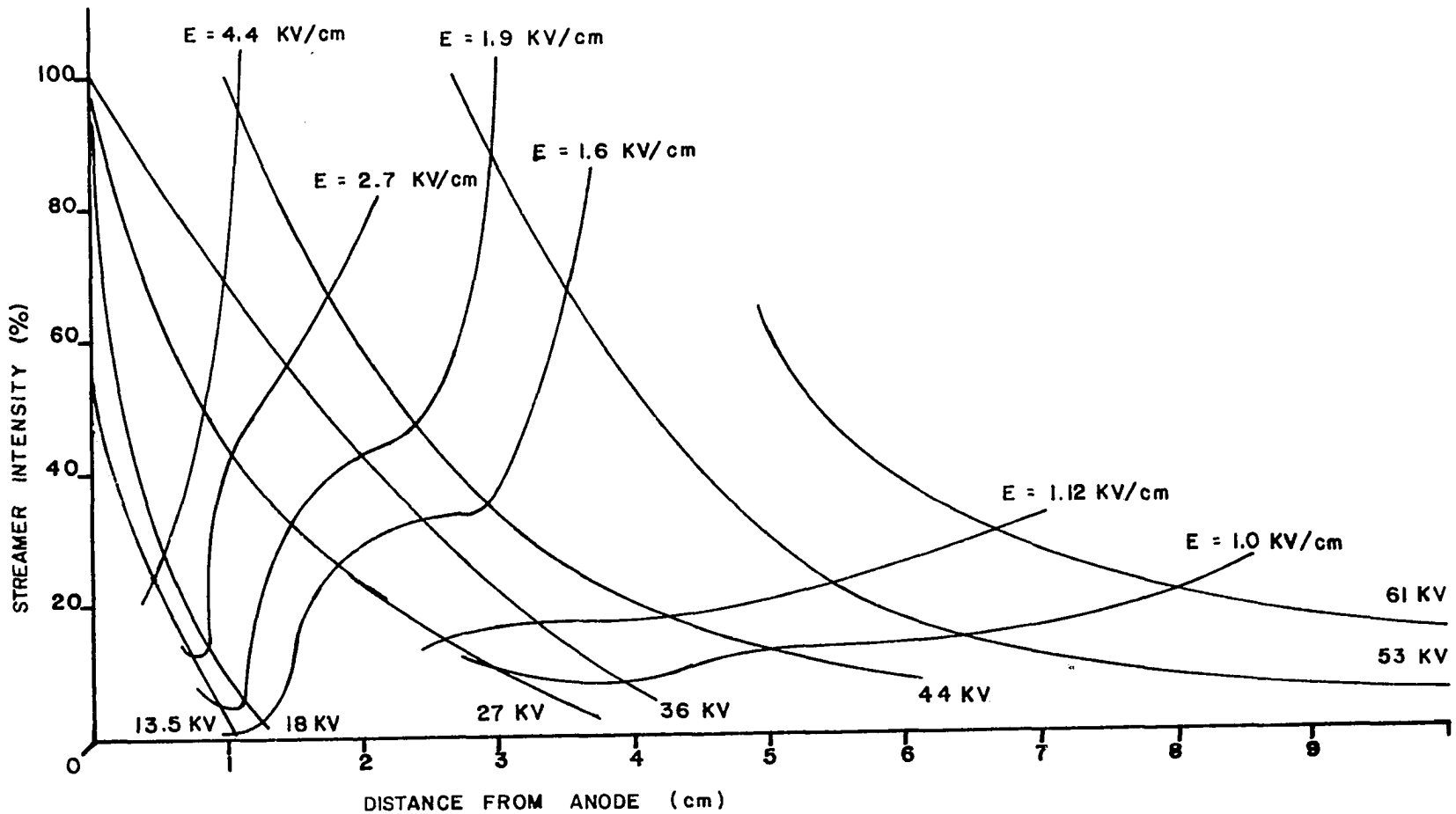

Figure 32a. Streamer intensity.

d = 10 cm, R = .5 mm

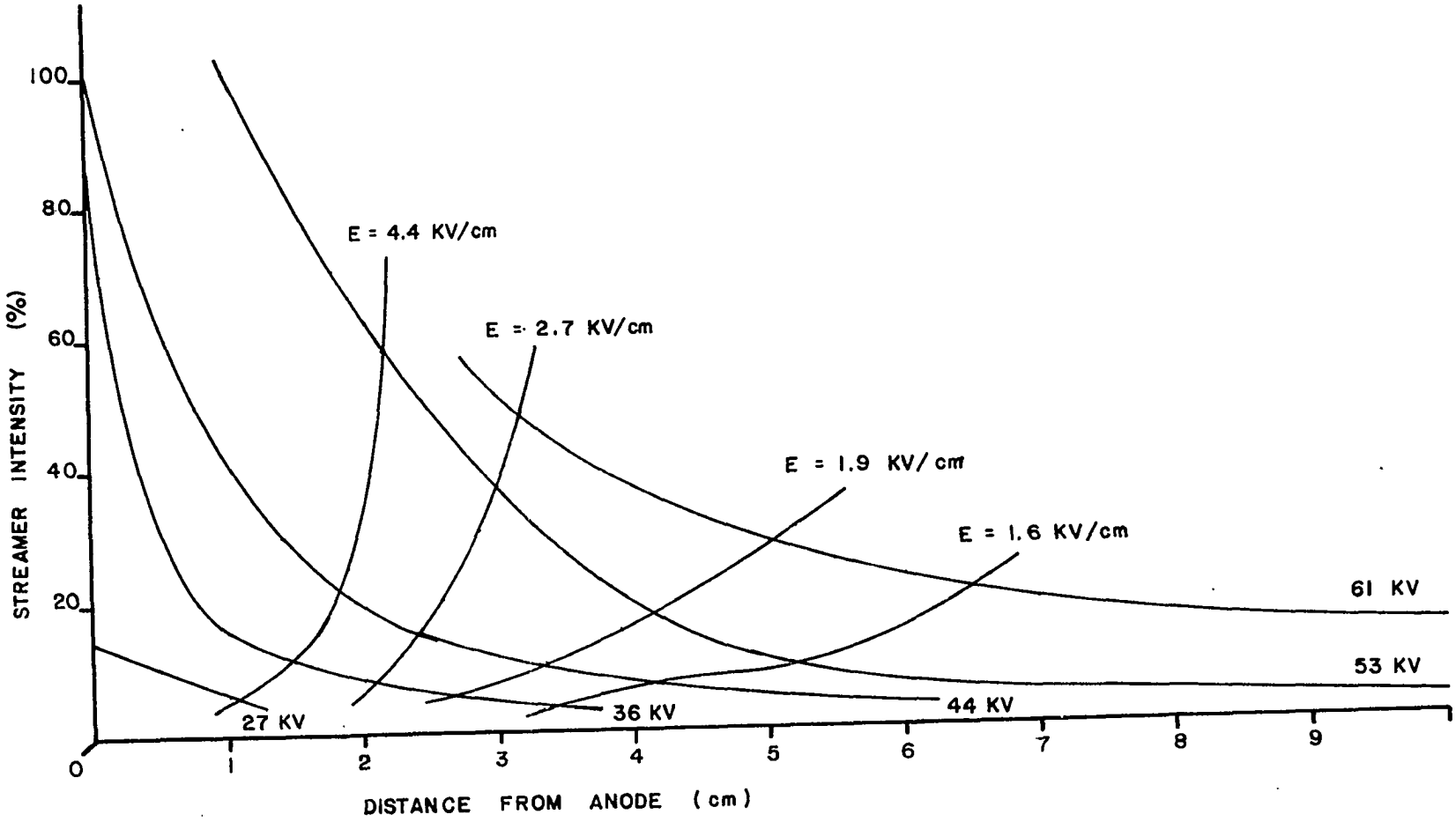

Figure 32b. Streamer intensity.

d = 10 cm, R = 3.0 mm

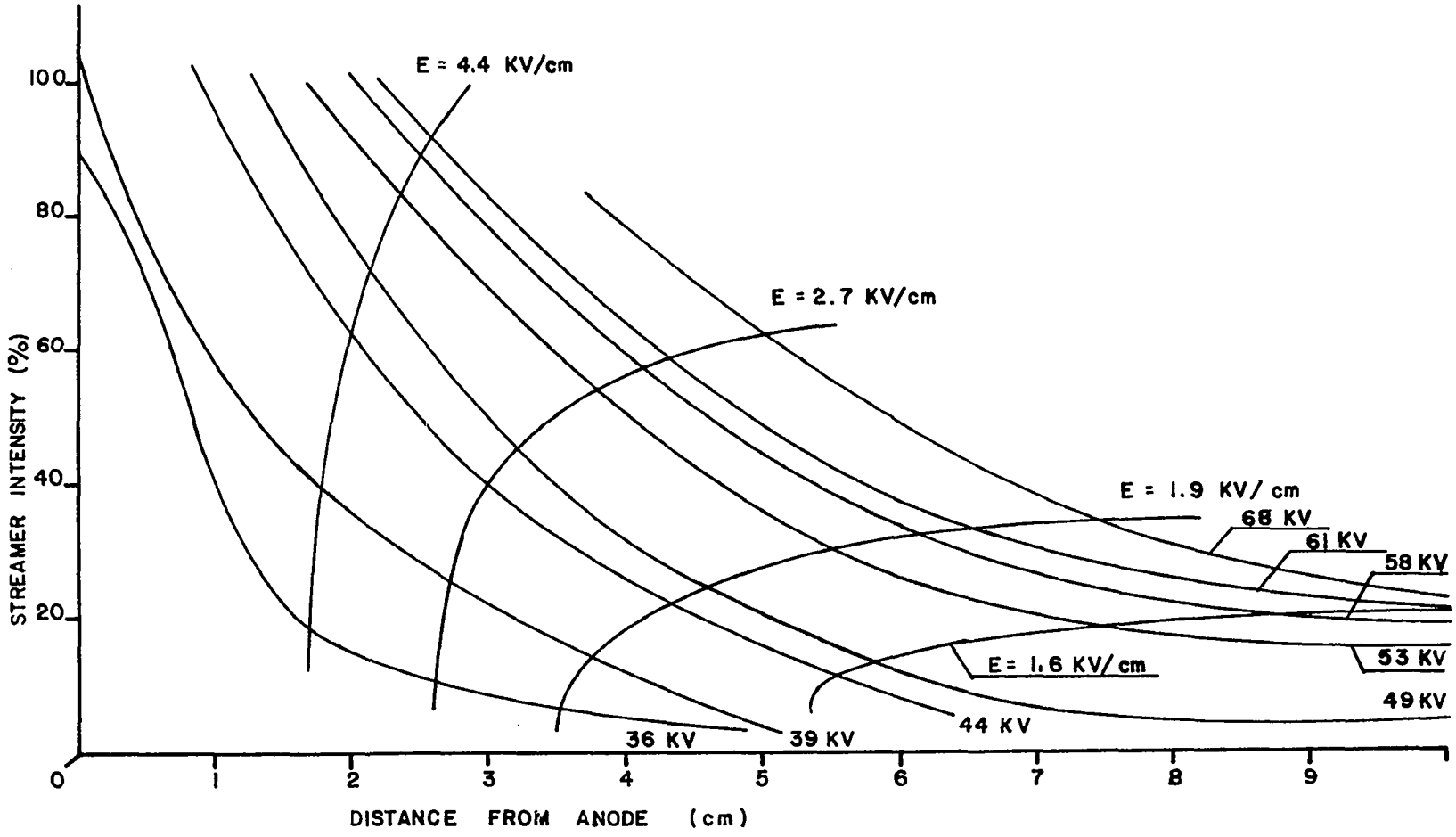

Figure 32c. Streamer intensity.

d = 10 cm, R = 5.0 mm

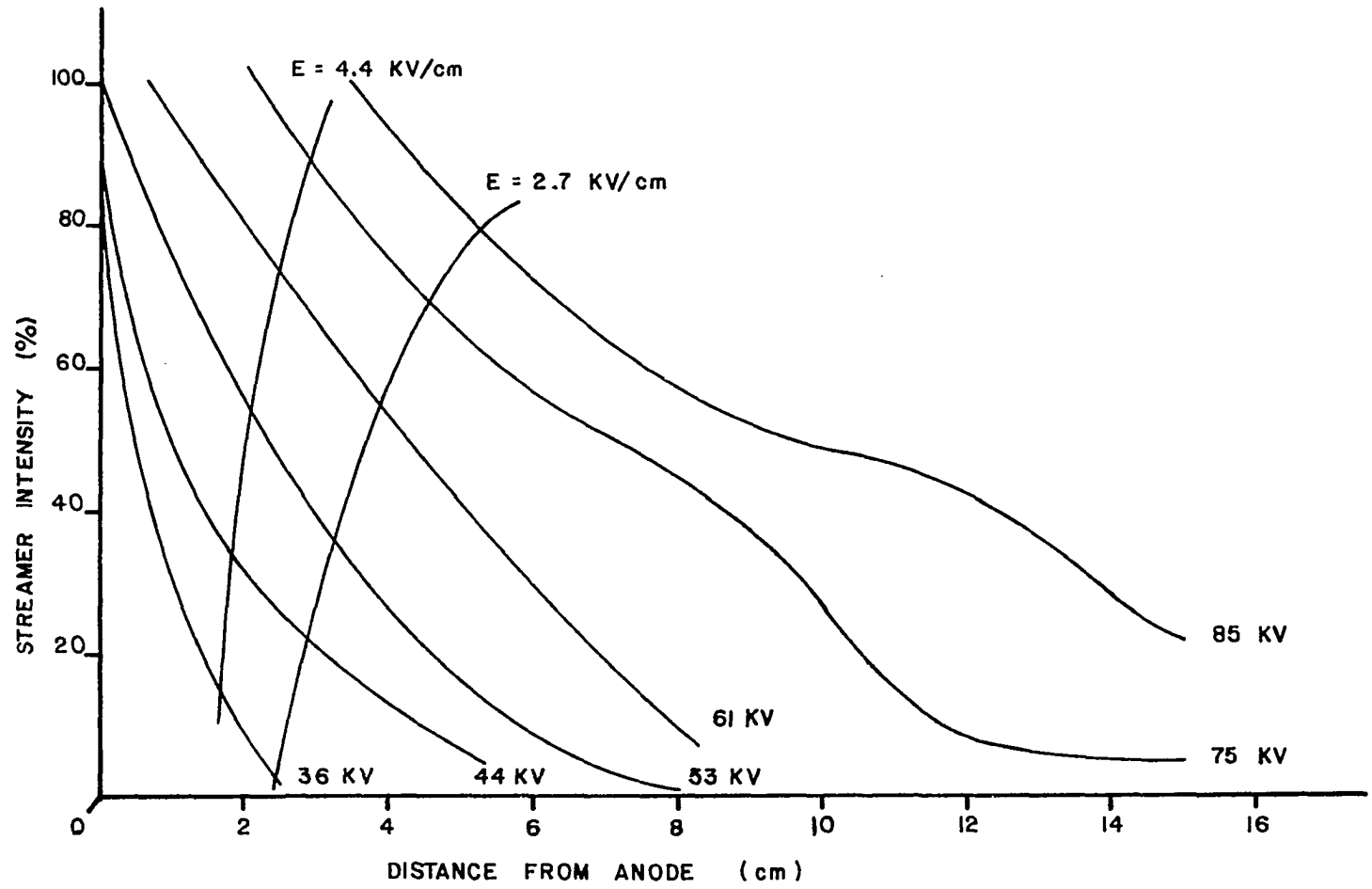

Figure 32d. Streamer intensity.

d = 15 cm, R = 5.0 mm

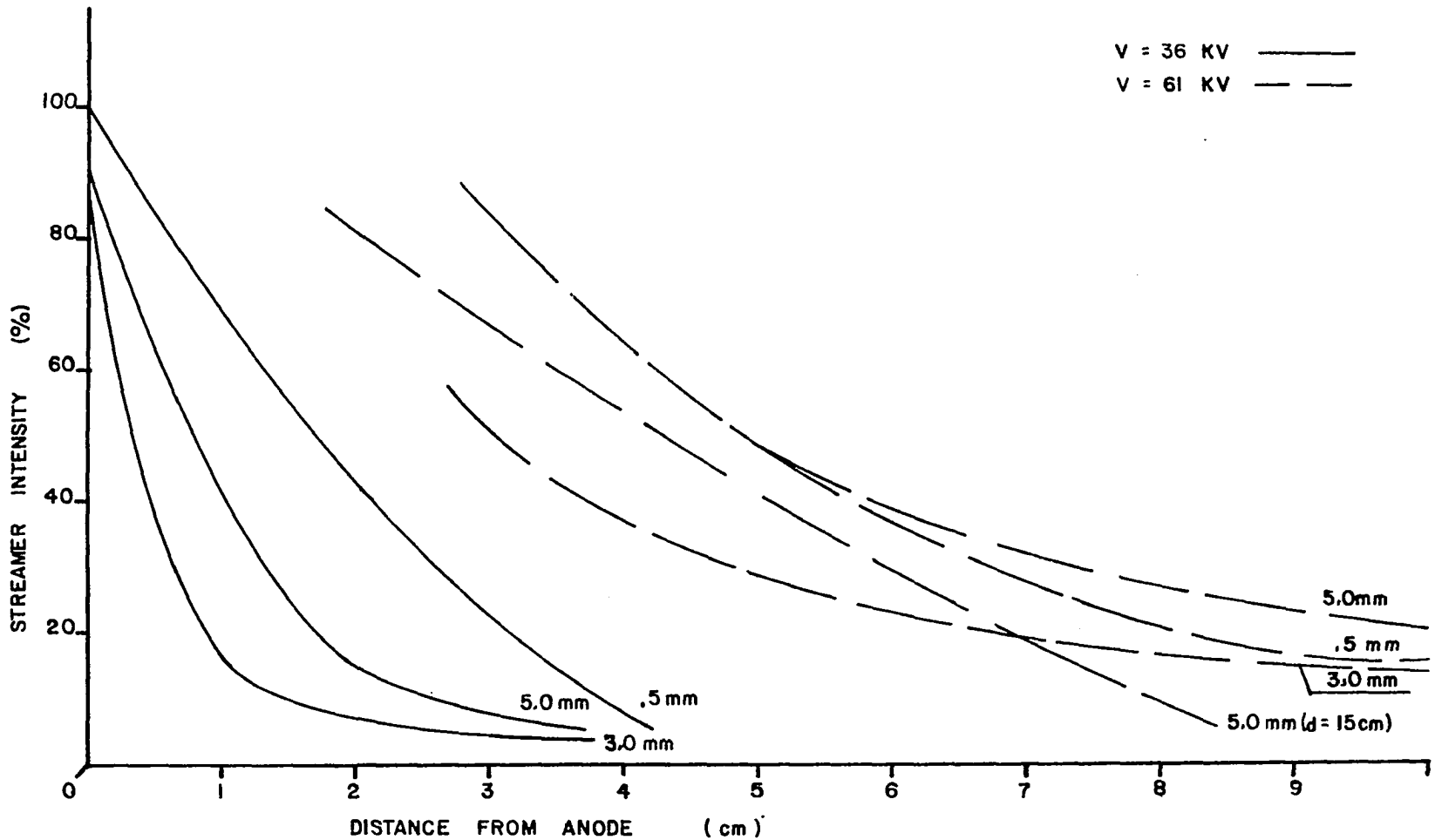

Figure 33. Comparison of streamer light intensities of various point radii at 44 KV and 61 KV.

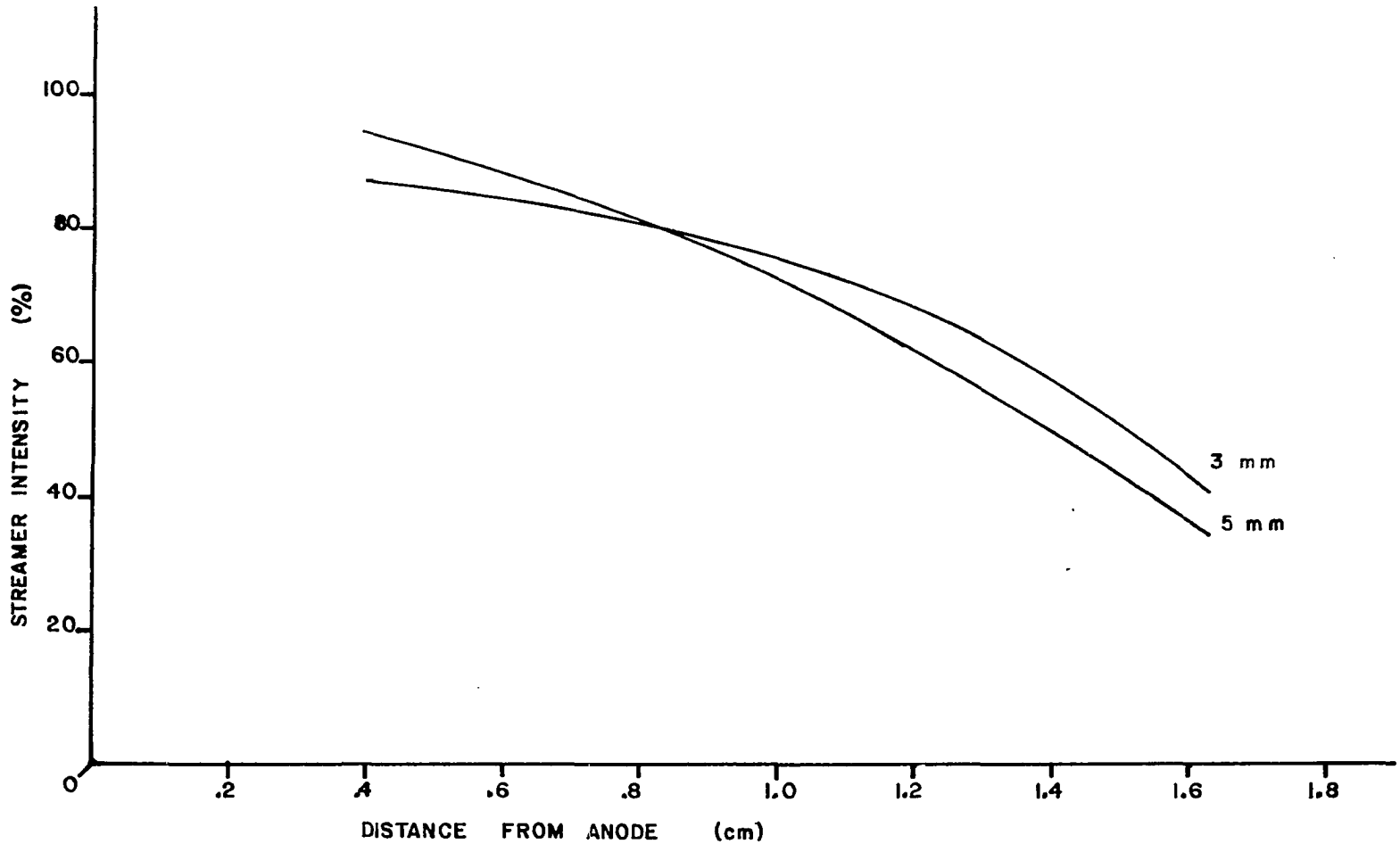

Figure 34. Streamer intensity in the anode region.

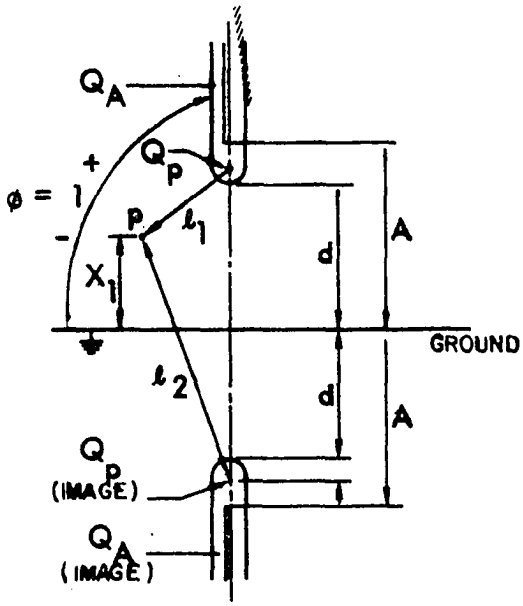

Figure 35. Image charges simulating a point-to-plane gap.

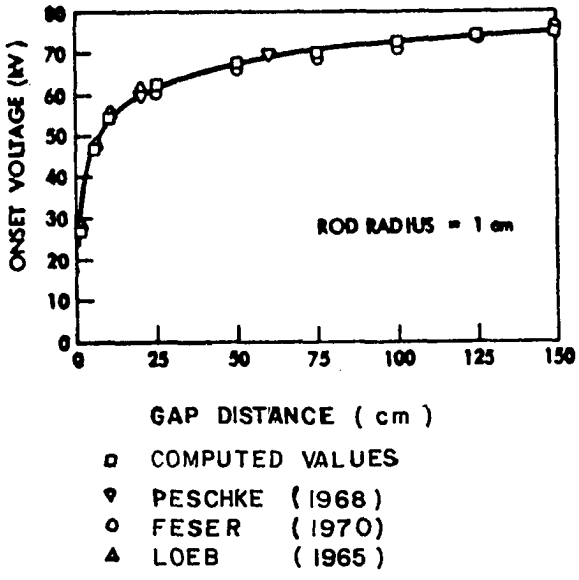

Figure 36. Comparison of computed and measured streamer onset potential.

R = 1 cm

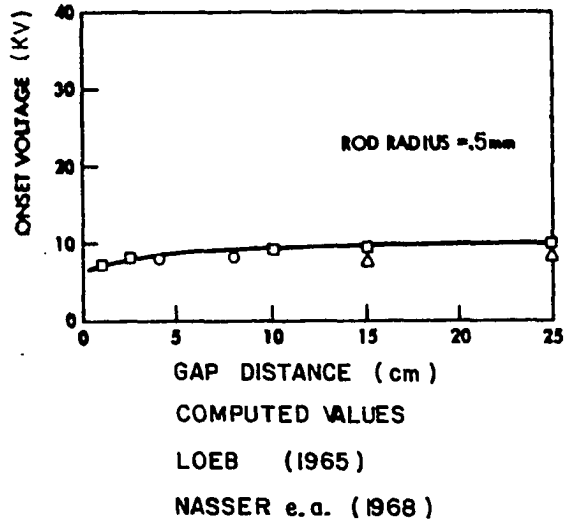

Figure 37. Comparison of computed and measured streamer onset potential.

R = .5 mm

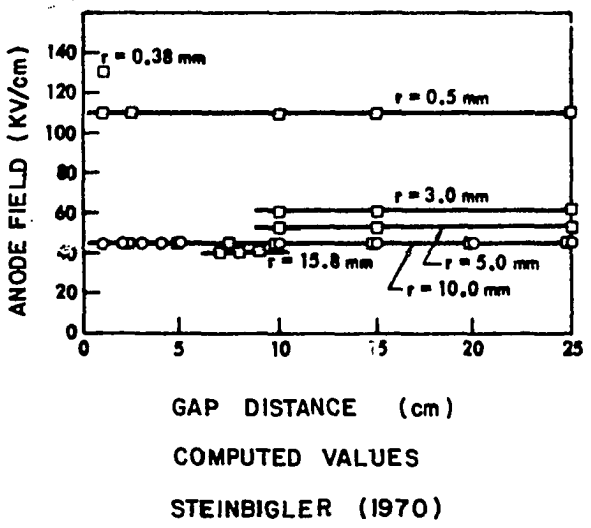

Figure 38. Comparison of computed and measured anode field intensity at streamer onset.

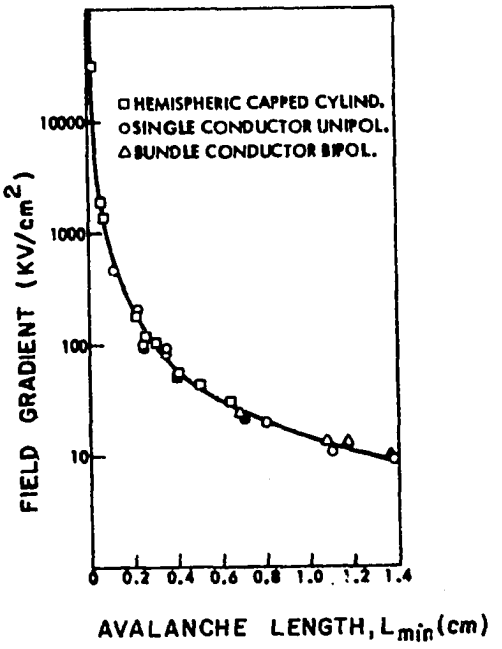

Figure 39. Relationship between optimum avalanche length L_{min} and average field gradient at streamer onset.

Figure 40a. Field distribution in the vicinity of the anode for various point radii.

d = 10 cm

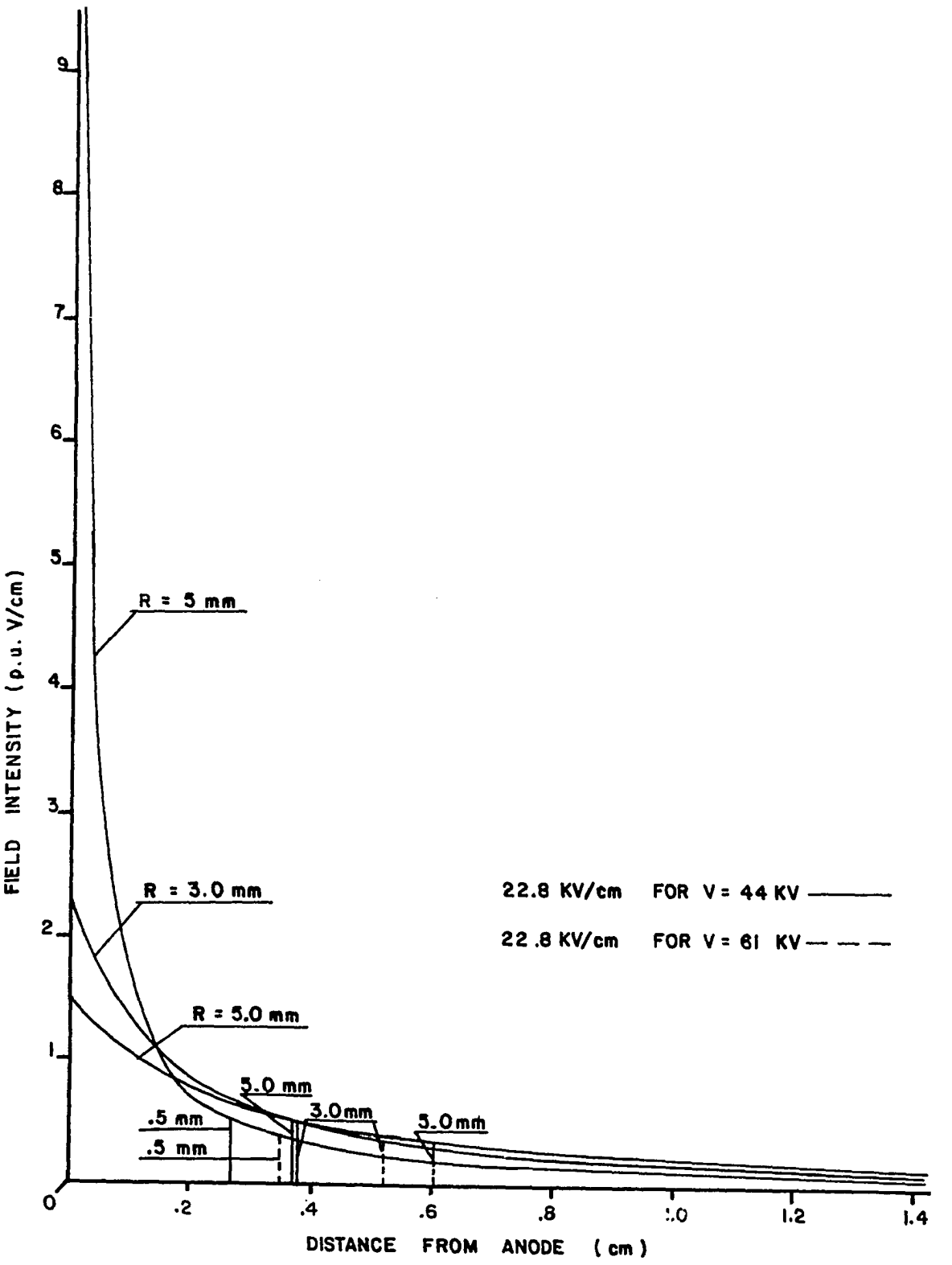
FIELD INTENSITY (p.u. V/cm)
9
8
7
6
5
4
3
2
1
0
R = 5 mm
R = 3.0 mm
R = 5.0 mm
22.8 KV/cm FOR V = 44 KV
22.8 KV/cm FOR V = 61 KV
5.0 mm
3.0mm
5.0mm
.5 mm
.5 mm
.2
.4
.6
.8
1.0
1.2
1.4
DISTANCE FROM ANODE (cm)

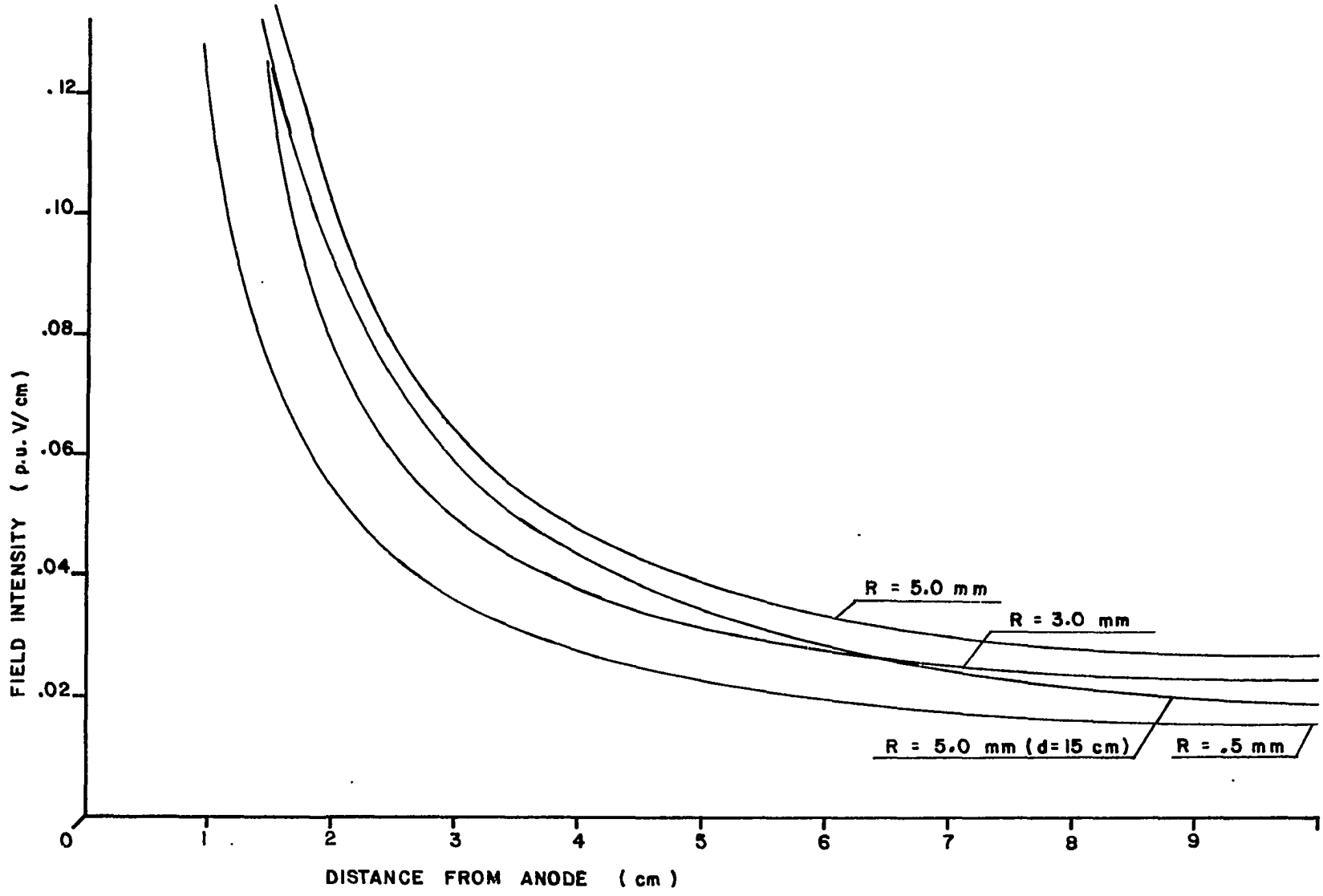

Figure 40b. Field distribution in the low field region for various point radii.

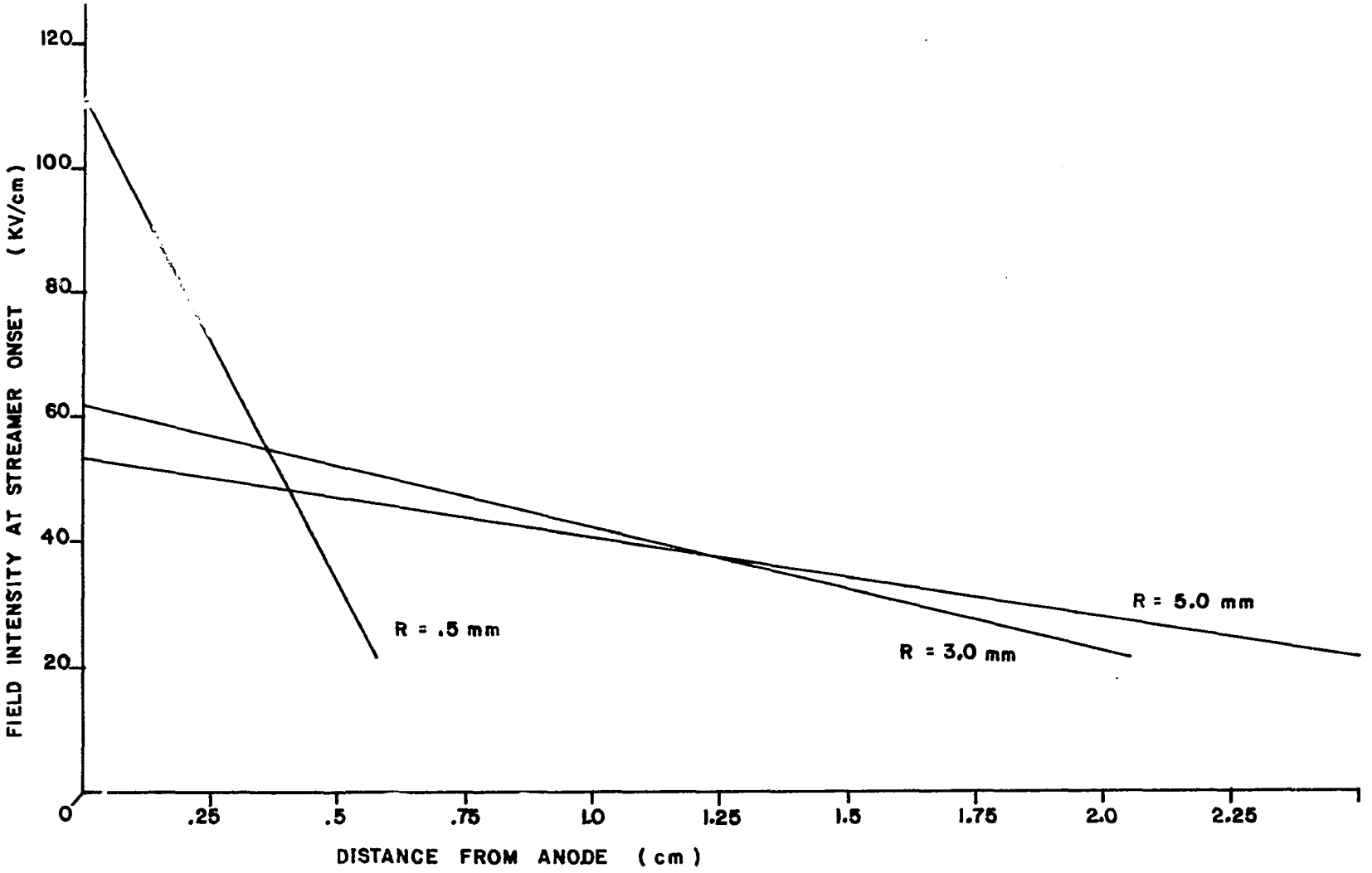

Figure 41. Field intensity and initial avalanche length for d = 10 cm and various point radii of streamer onset.

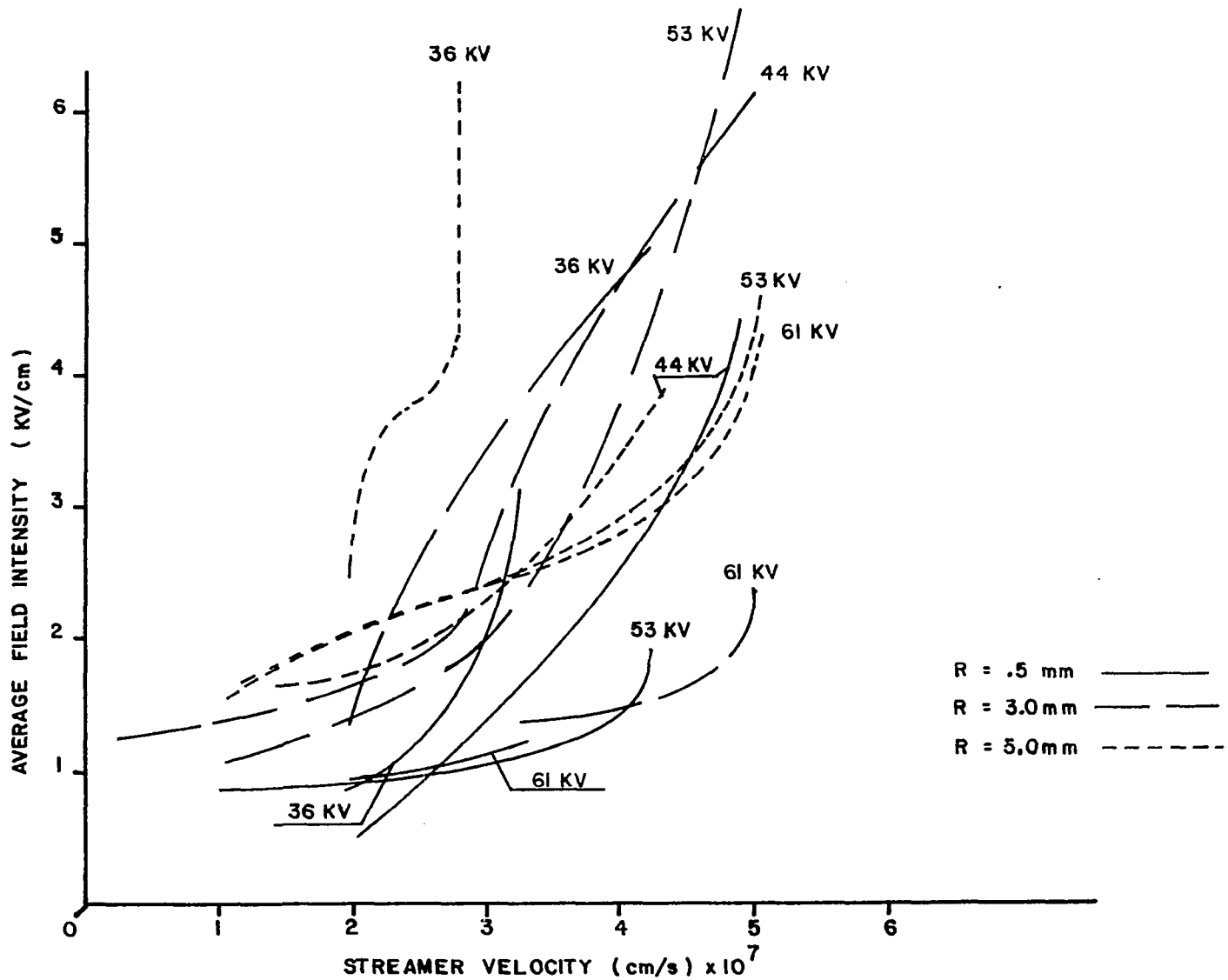

Figure 42. Field intensity streamer velocity for various point radii and potentials.

Figure 43. Field intensity versus decrease of streamer intensity for various point radii and potentials.

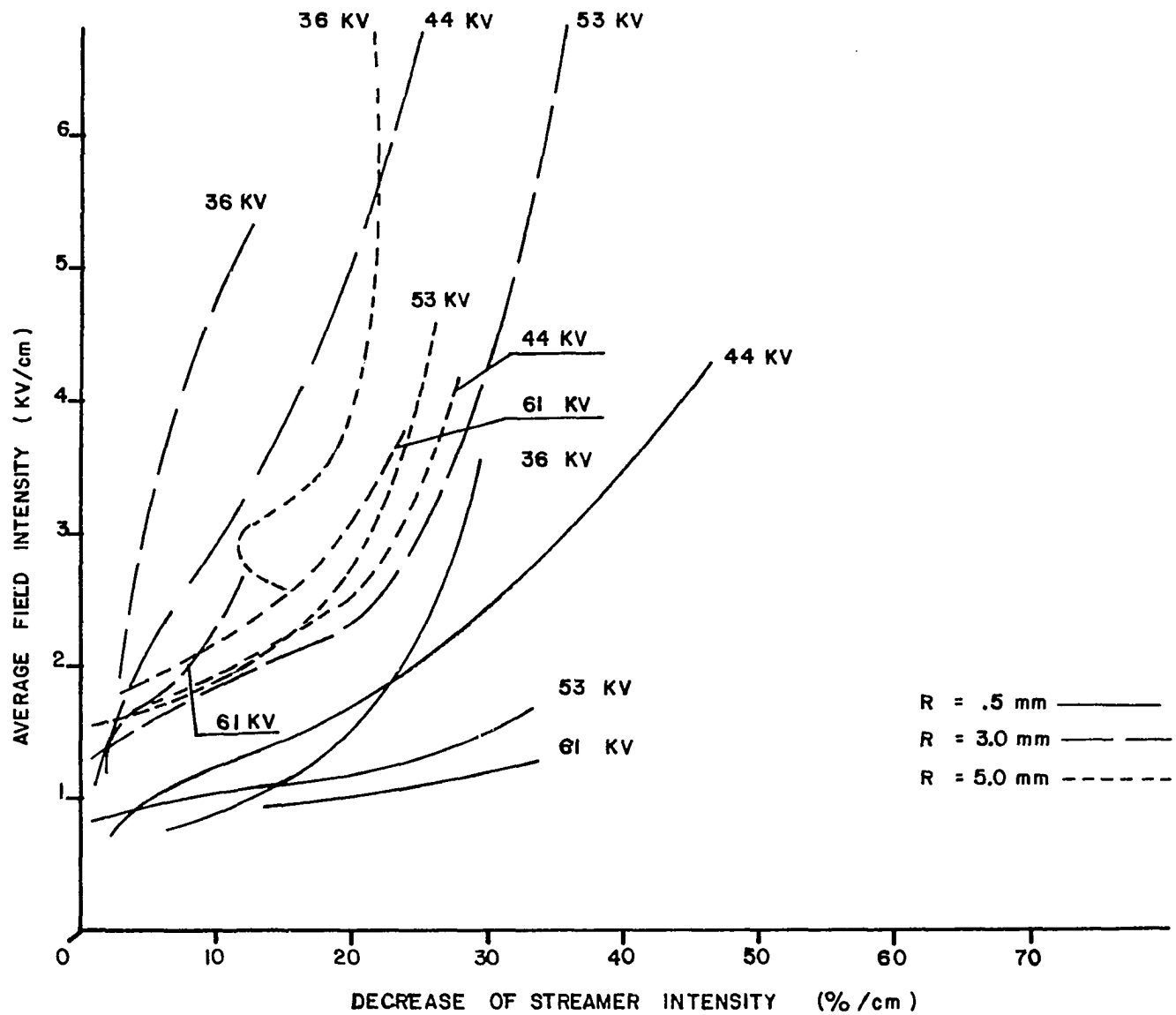
36 KV
44 KV
53 KV
36 KV
53 KV
44 KV
61 KV
36 KV
44 KV
53 KV
61 KV
61 KV
R = .5 mm
R = 3.0 mm
R = 5.0 mm
AVERAGE FIELD INTENSITY (KV/cm)
DECREASE OF STREAMER INTENSITY (% /cm)
0
10
20
30
40
50
60
70
1
2
3
4
5
6

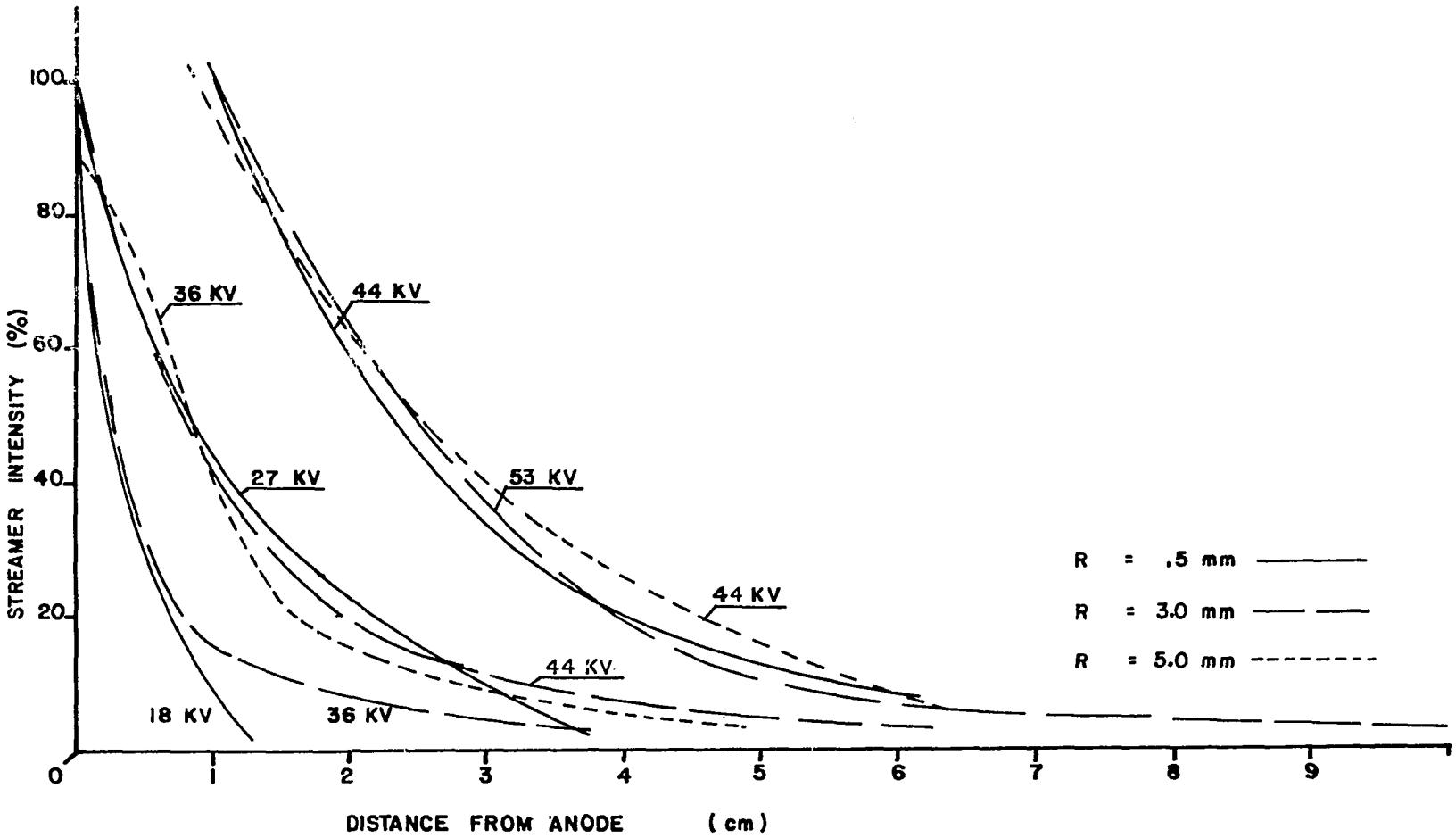

Figure 44. Comparison of streamer intensity decrease of various point radii and potentials.

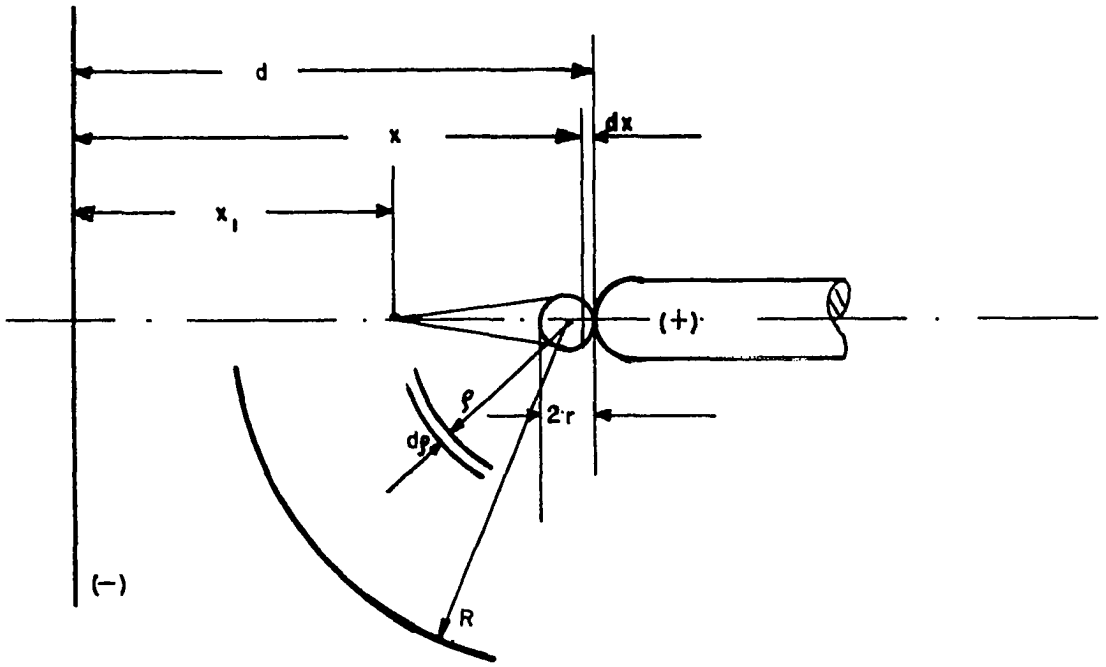

Figure 45. Critical avalanche of streamer onset.

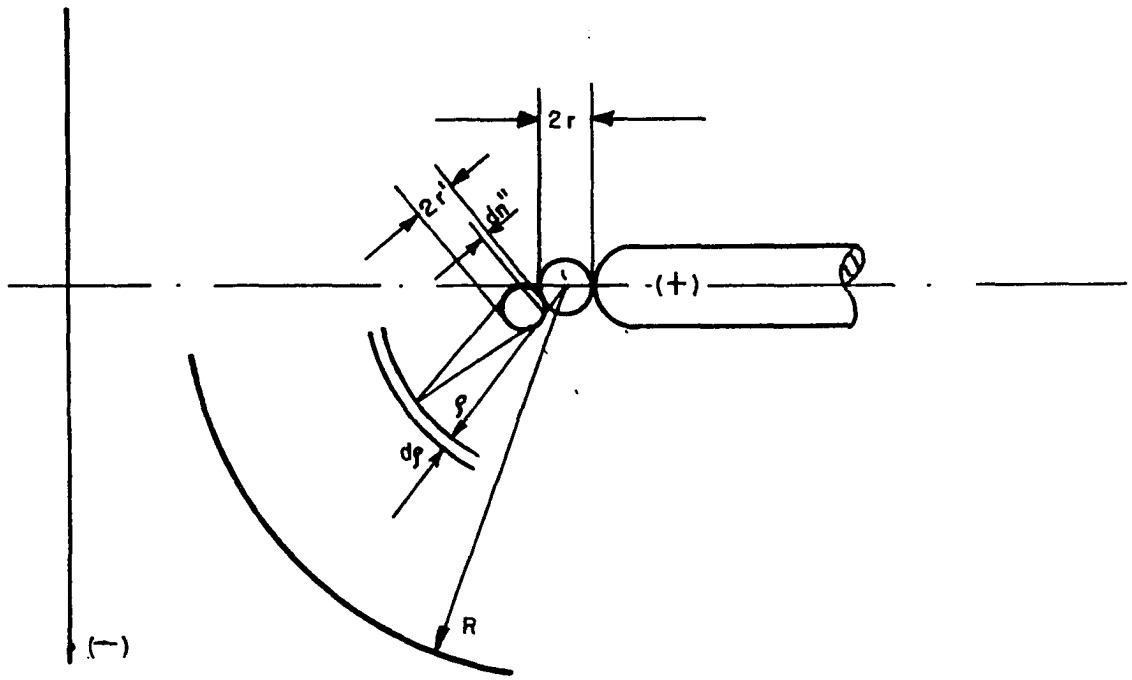

Figure 46. Photoelectron avalanches of streamer onset.

Figure 47. Hemispherically capped cylinder rods.

Figure 48. Ground plate (aluminum, polished surface).

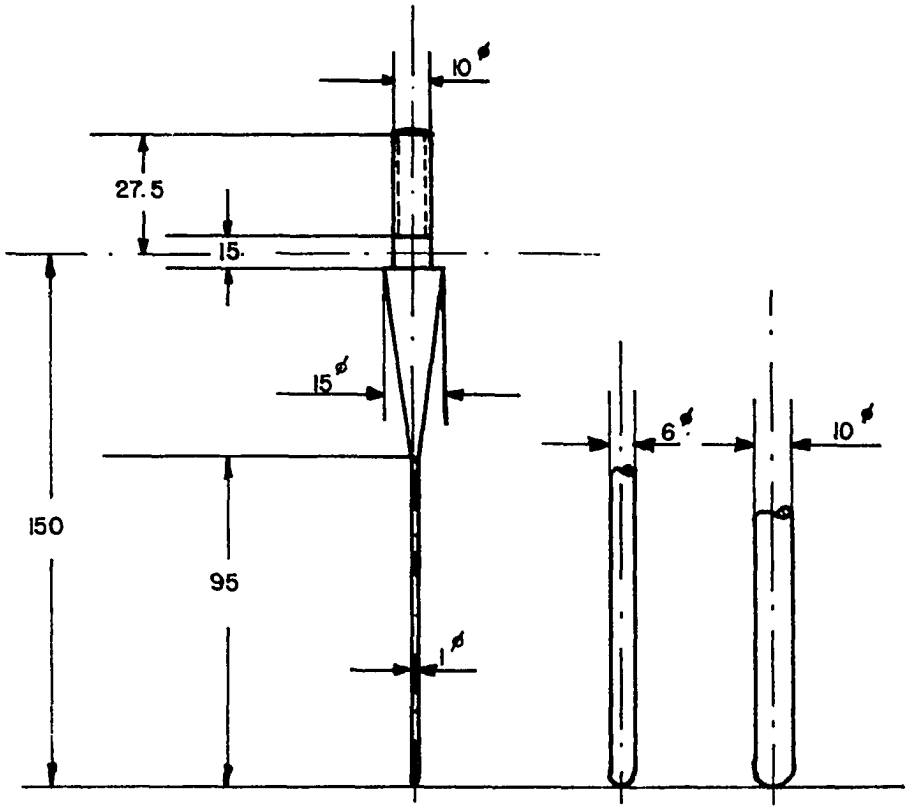
10 ø
27.5
15
15 ø
150
95
1 ø
6 ø
10 ø

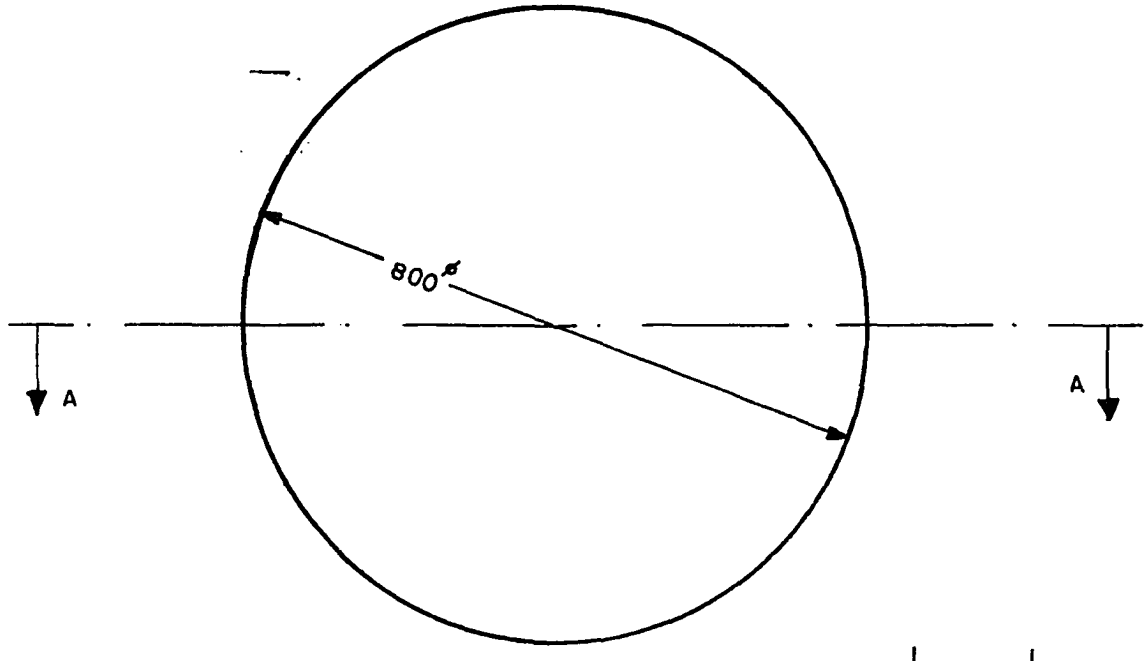
800 ø
A
A

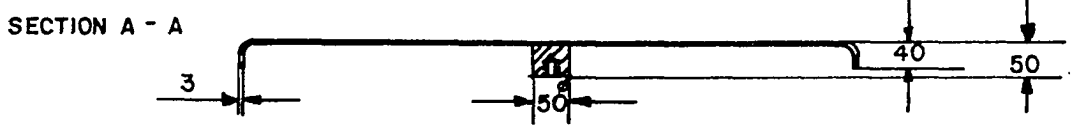
SECTION A - A
3
50
40
50

Figure 49. Side and top view of the gap frame.

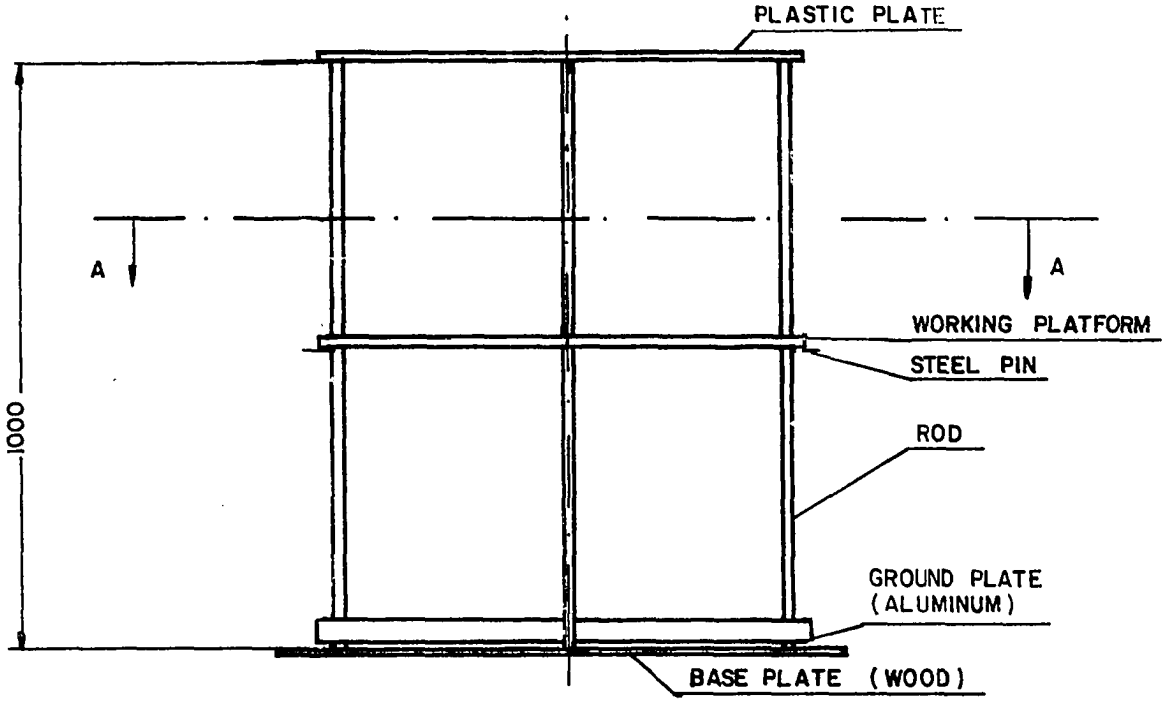
PLASTIC PLATE
A
A
WORKING PLATFORM
STEEL PIN
1000
ROD
GROUND PLATE
(ALUMINUM)
BASE PLATE (WOOD)

SECTION A - A

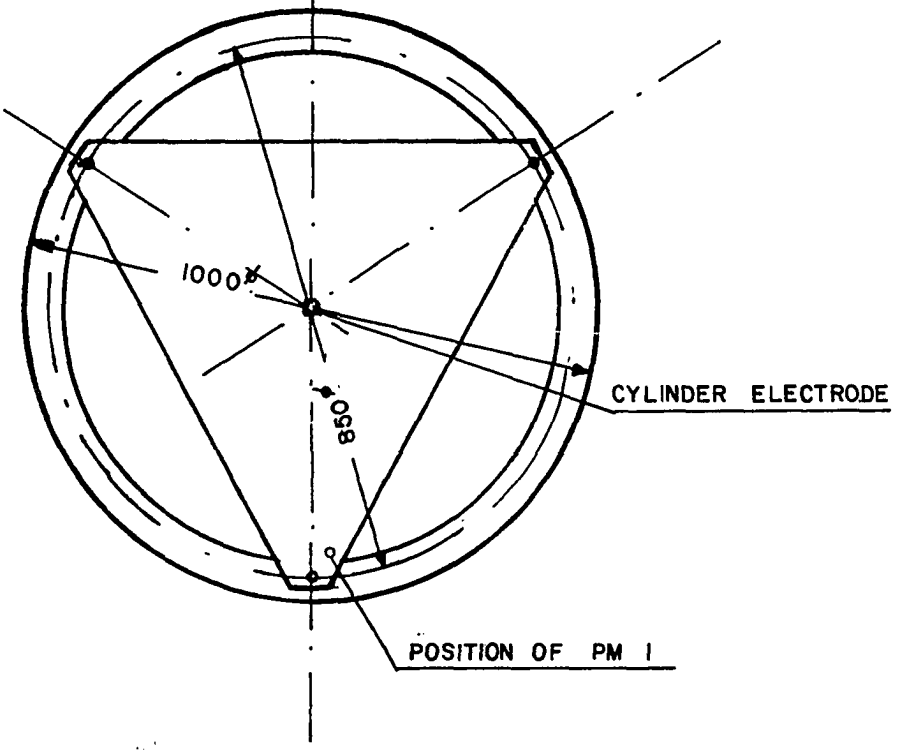
1000
CYLINDER ELECTRODE
850
POSITION OF PM I

Figure 50. Point to plane gap.

Figure 51. View of impulse generator.

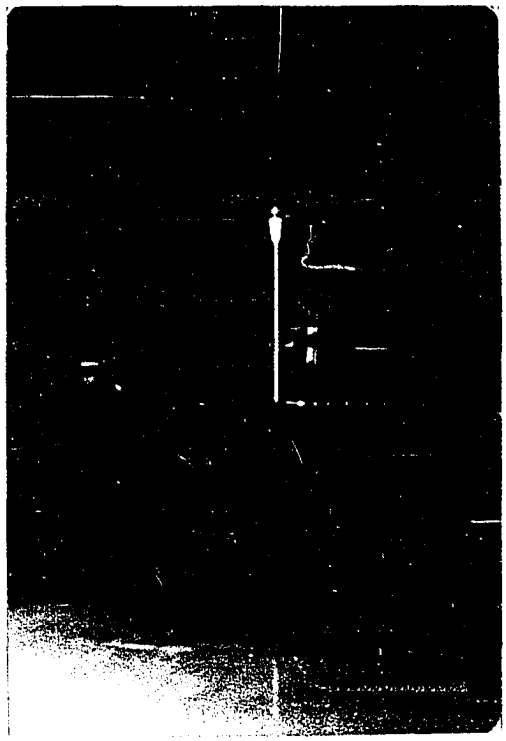

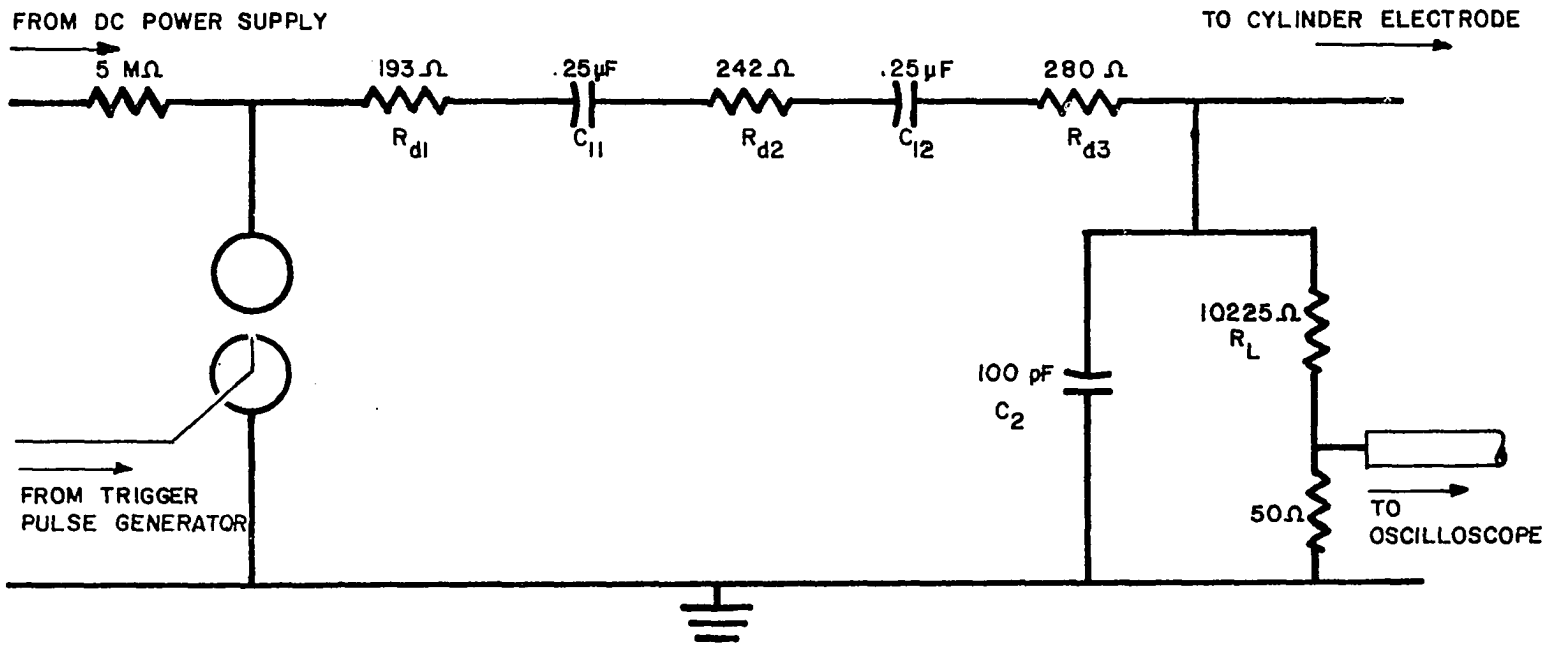

Figure 52. Impulse generator circuit.

Figure 53. Voltage pulse 60 KV.

horizontal: 50 ns/cm

vertical: 100 V/cm

Figure 54. Voltage pulse 60 KV.

horizontal: 100 μs/cm

vertical: 100 V/cm

Figure 55. Response of the pulse measuring circuit to a 60 ns, 4 V pulse.

horizontal: .05 μs/cm

vertical: 5.0 V/cm

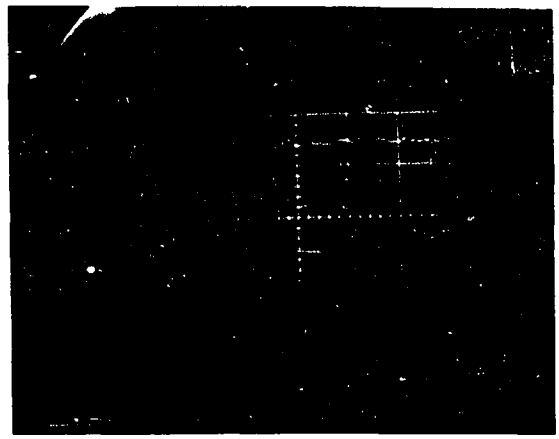

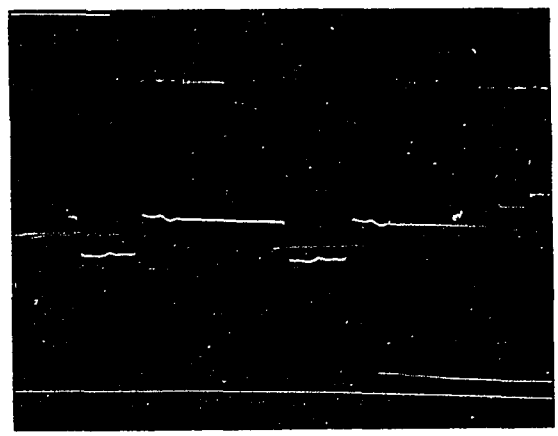

Figure 56. Determination of pulse generator efficiency factor.

a. Divider output: .2 V/cm, .2 msec/cm

b. Pulse generator output: 50 V/cm, .2 msec/cm

c. Pulse generator input: 50 V/cm, .2 msec/cm

Figure 57. Test pulse at the voltage divider no measurements taken at the point electrode.

horizontal: .1 msec/cm

vertical: .1 V/cm

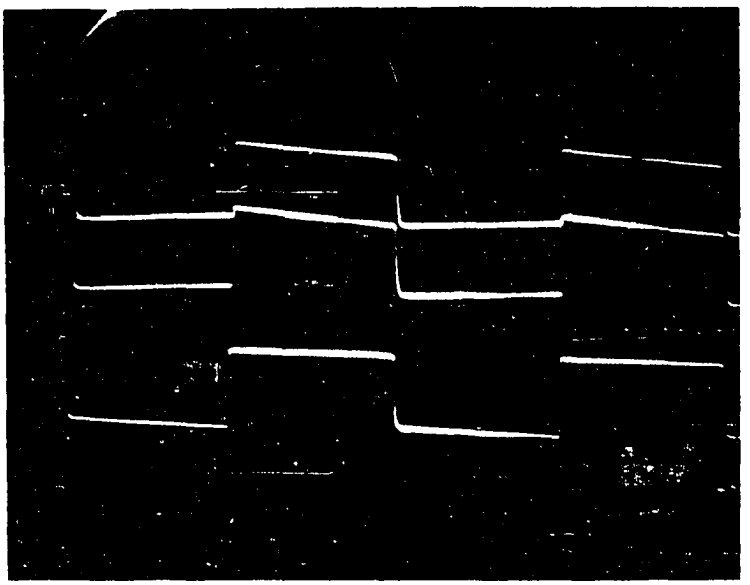

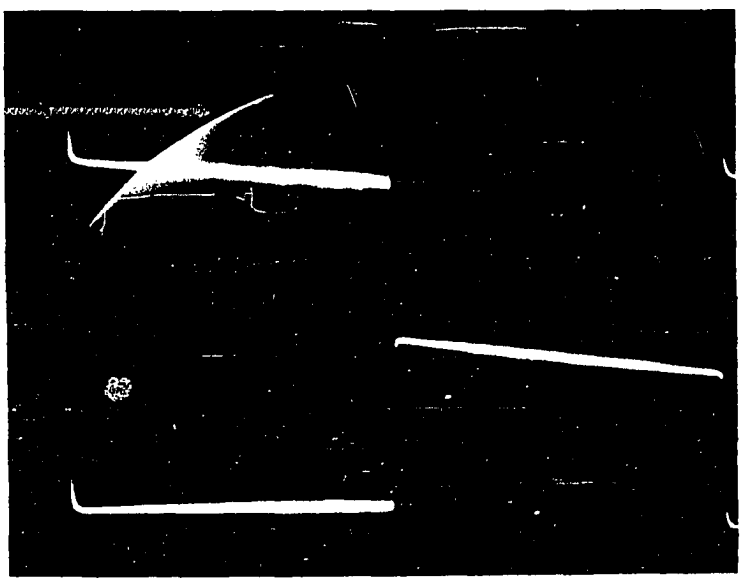

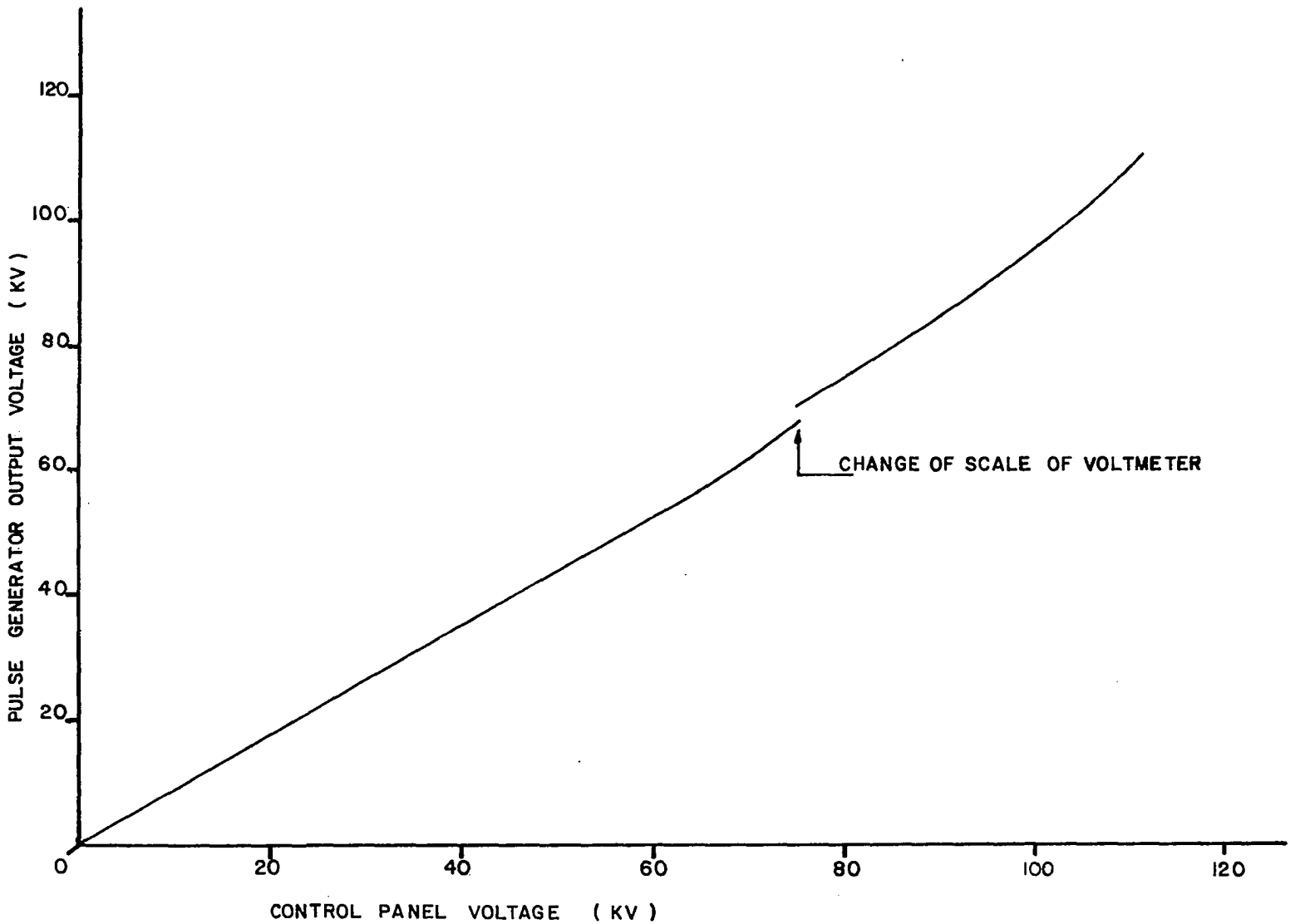

Figure 58. Calibration of the impulse generator.

Figure 59. Lichtenberg figure technique.

a. Axial mode.

b. Coplanar mode.

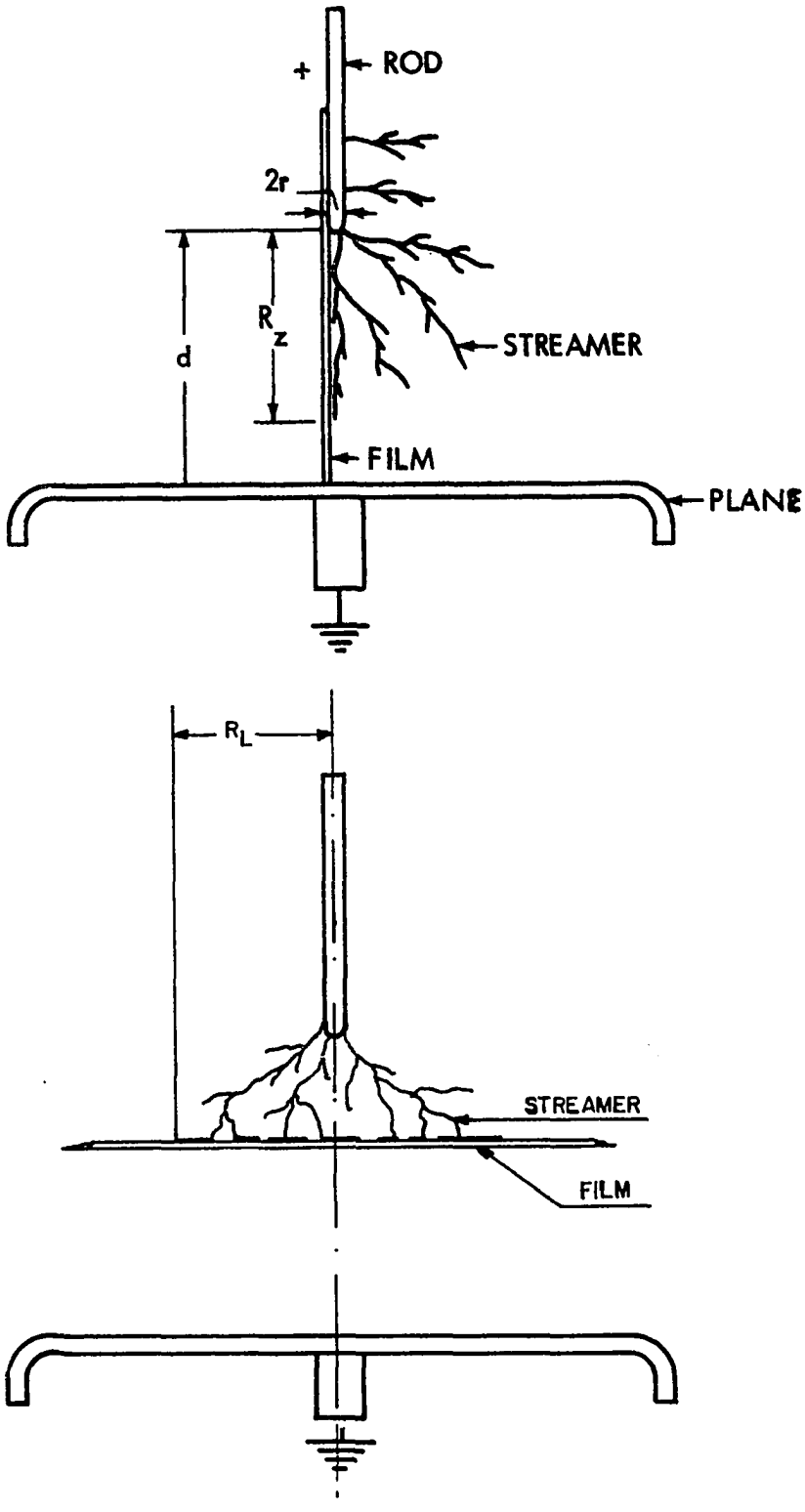
+
ROD
2r
d
R_z
STREAMER
FILM
PLANE
R_L
STREAMER
FILM

Figure 60. Lichtenberg figure - axial mode, anode on top, and cathode on bottom.

d = 15 cm, R = 5 mm, V = 26.6 KV

Figure 61. Lichtenberg figure - coplanar mode.

d = 2.5 cm, R = 5 mm, V = 26.2 KV, S = 1 cm

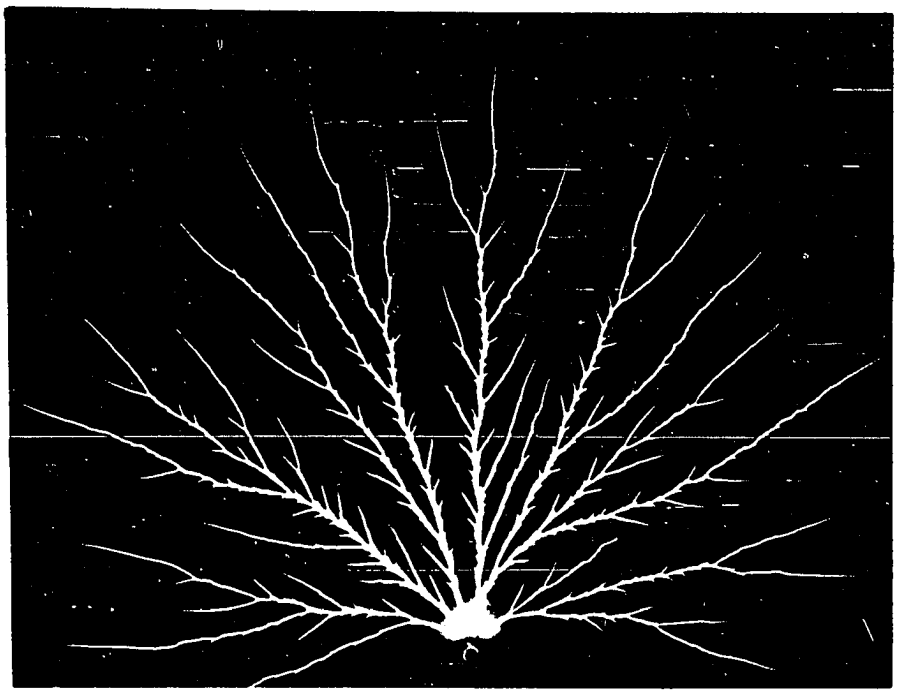

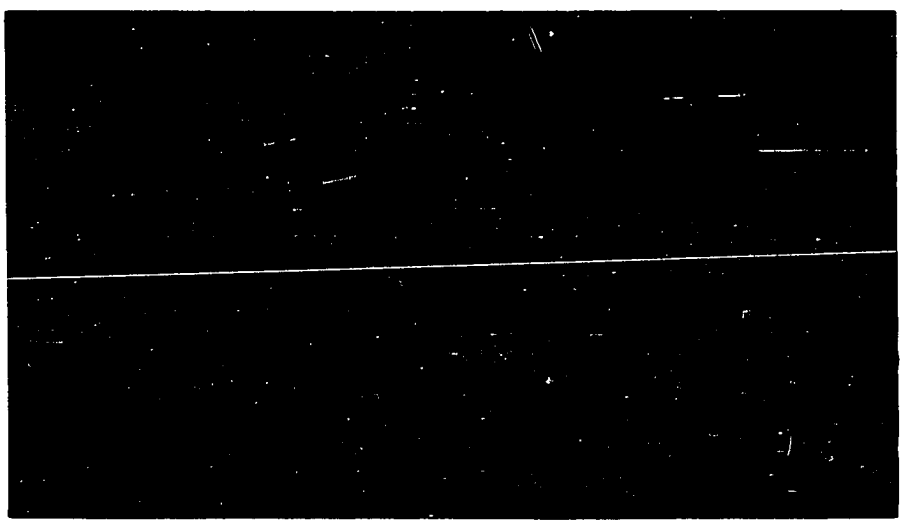

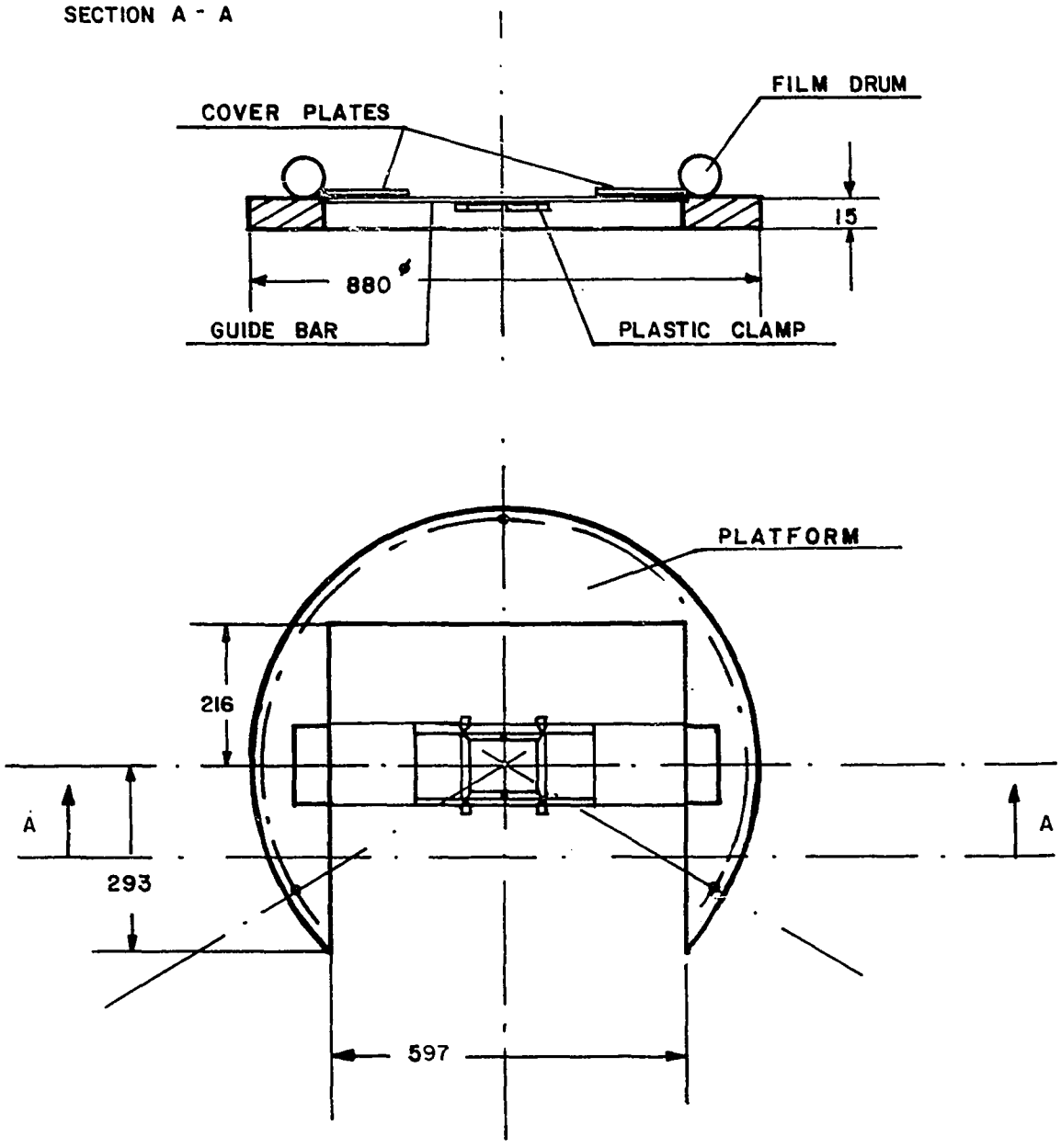

Figure 62. Platform holding film for Lichtenberg figure technique.

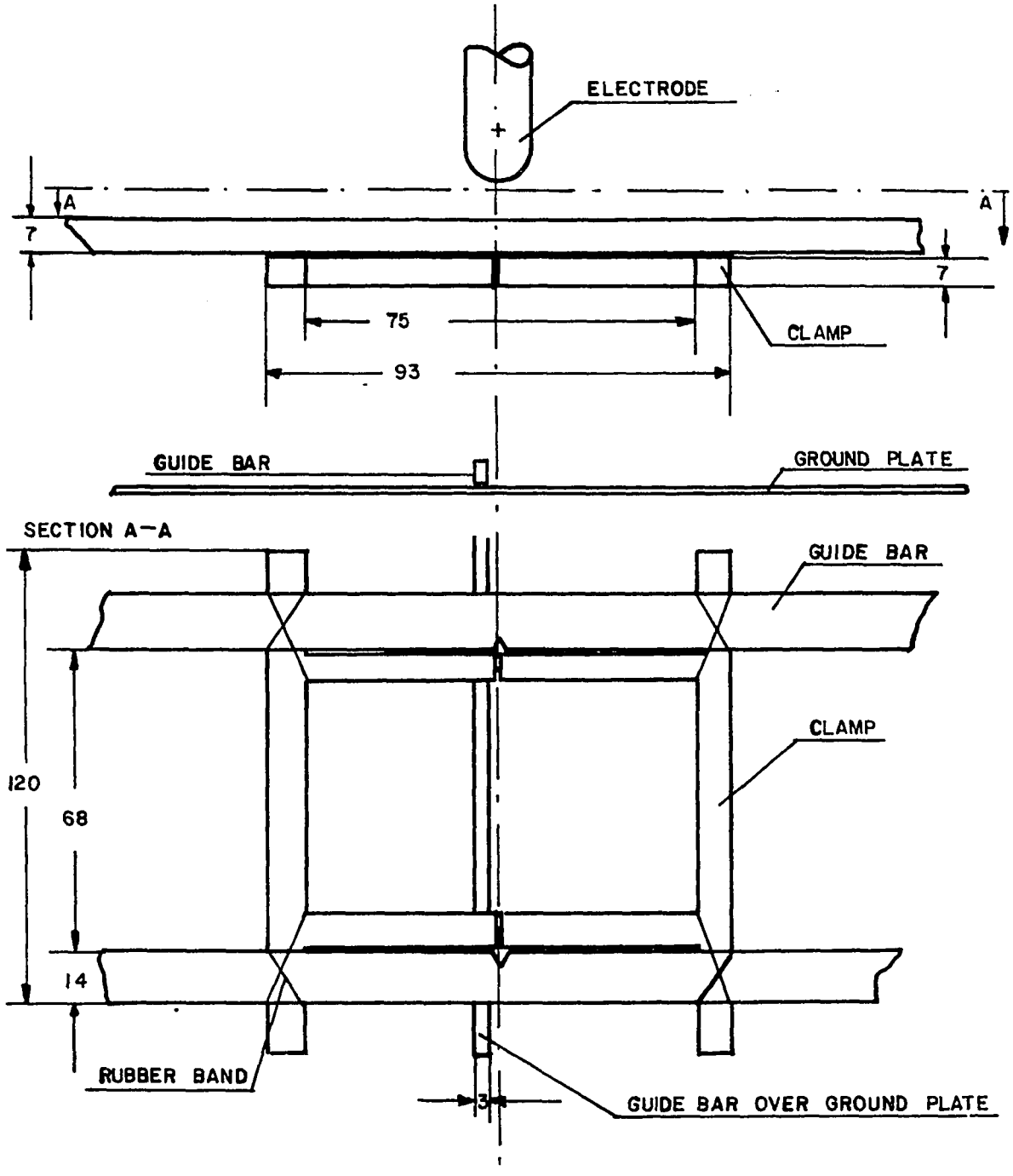

Figure 63. Detail of film suspension near anode.

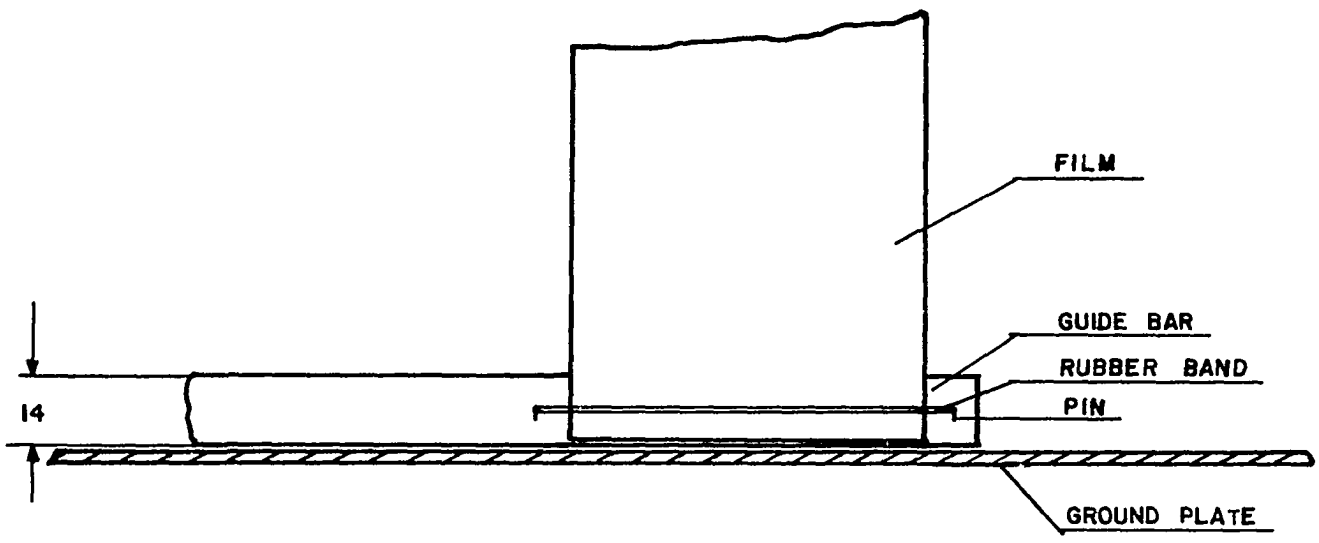

Figure 64. Detail of film suspension near cathode.

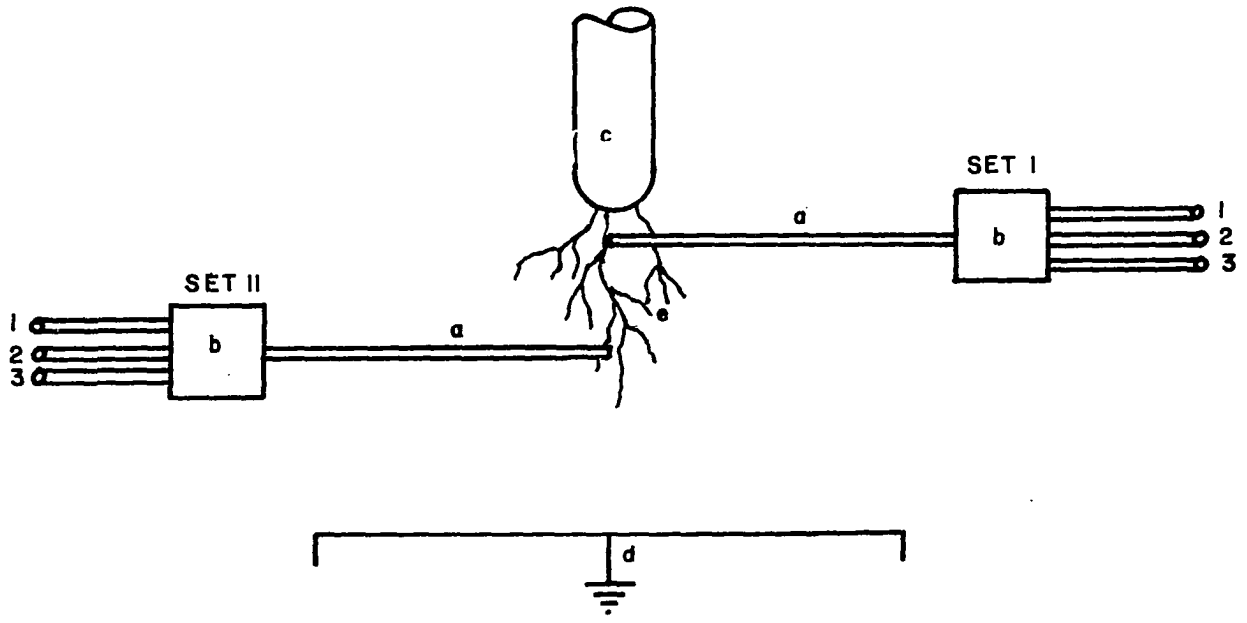

1 TO OSCILLOSCOPE
2 FROM POWER SUPPLY -1 KV DC
3 FROM POWER SUPPLY 11 V DC

a LIGHT PIPE
b PHOTOMULTIPLIER
c ANODE (120 KV MAX.)
d CATHODE
e STREAMER

Figure 65. Basic setup of photomultipliers with light pipes.

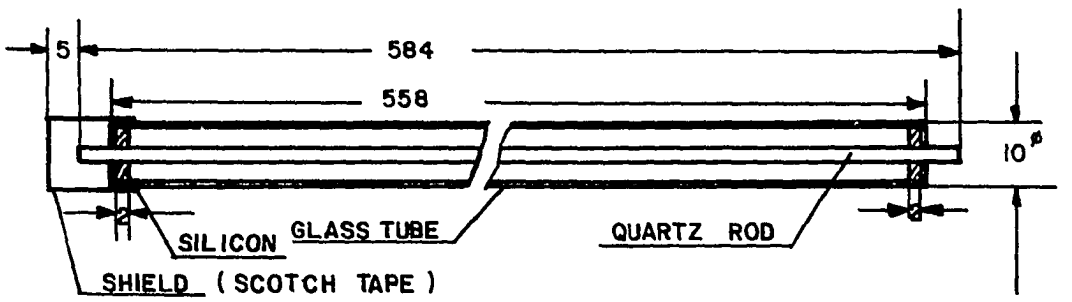

Figure 66. Light pipe assembly.

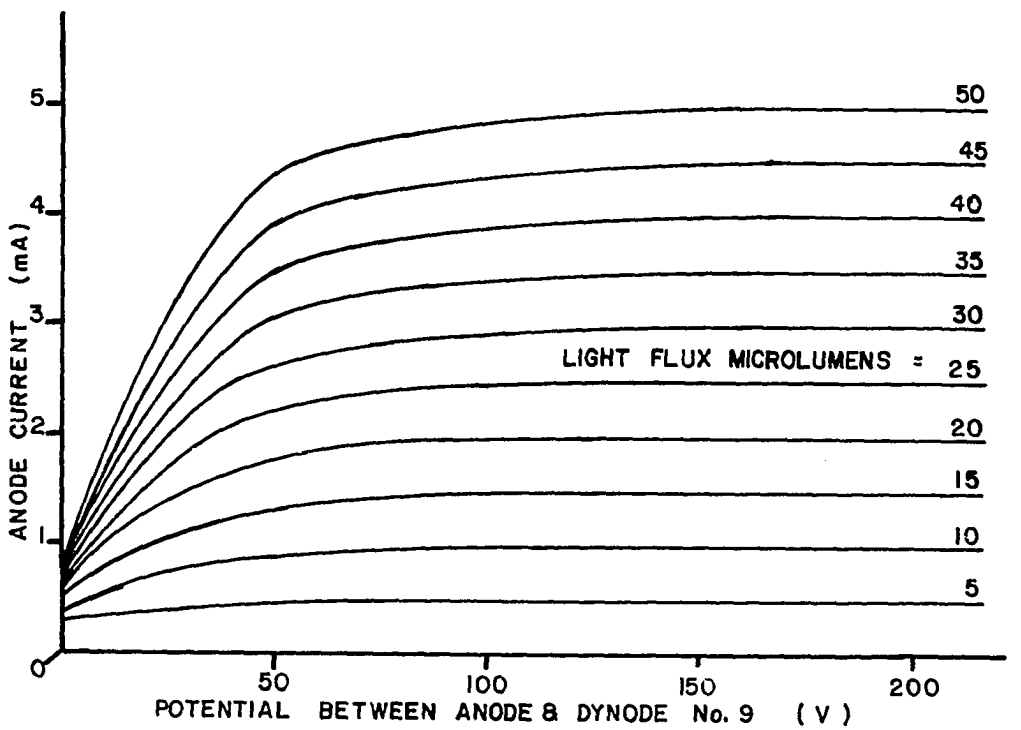

Figure 67. Photomultiplier anode characteristics.

Figure 68. 1 KV power supply and photomultiplier circuitry.

Figure 69. Field effect transistor circuit.

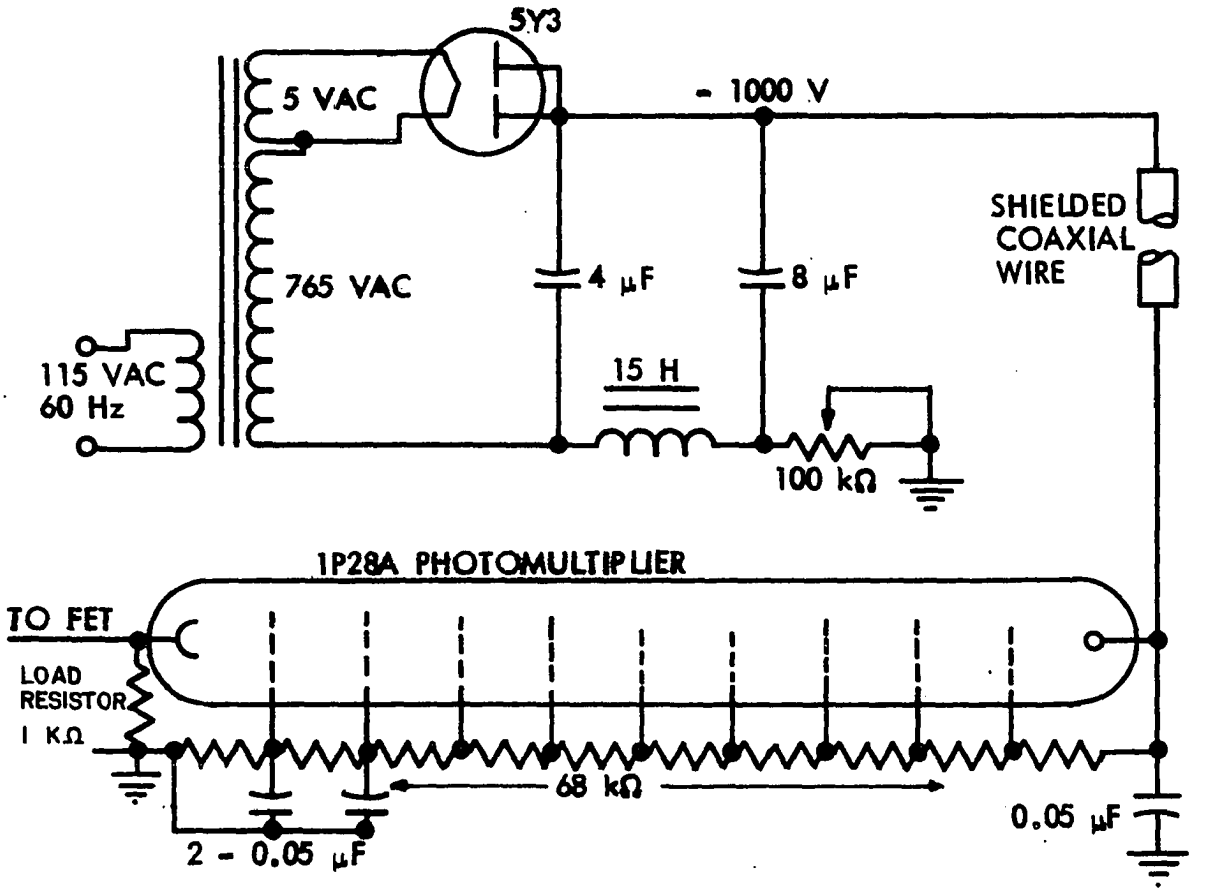
5Y3
5 VAC
- 1000 V
SHIELDED
COAXIAL
WIRE
765 VAC
4 μF
8 μF
115 VAC
60 Hz
15 H
100 kΩ
1P28A PHOTOMULTIPLIER
TO FET
LOAD
RESISTOR
1 KΩ
68 kΩ
0.05 μF
2 - 0.05 μF

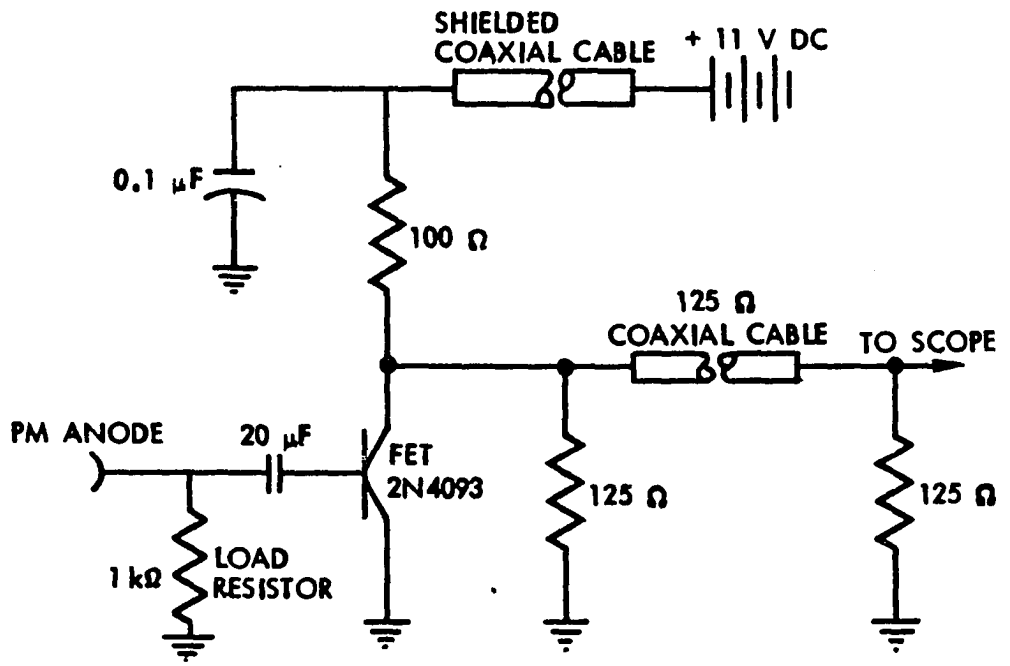
SHIELDED
COAXIAL CABLE
+ 11 V DC
0.1 μF
100 Ω
125 Ω
COAXIAL CABLE
TO SCOPE
PM ANODE
20 μF
FET
2N4093
125 Ω
125 Ω
1 kΩ
LOAD
RESISTOR

Figure 70. Transmission characteristics of coaxial cables.

horizontal: .05 μs/cm

vertical: a) 50 Ω coax .5 V/cm
b) 75 Ω coax .5 V/cm
c) 125 Ω coax .5 V/cm

Figure 71a. Transmission characteristics of FET circuit with 75 Ω coax.

horizontal: .05 μs/cm

vertical: a) FET circuit 1.0 V/cm
b) 75 Ω coax .5 V/cm

Figure 71b. Transmission characteristics of FET circuit with 125 Ω coax.

horizontal: .05 μs/cm

vertical: a) FET circuit .5 V/cm
b) 125 Ω coax .5 V/cm

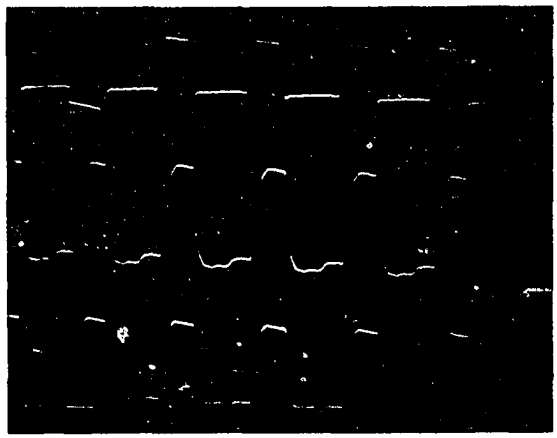

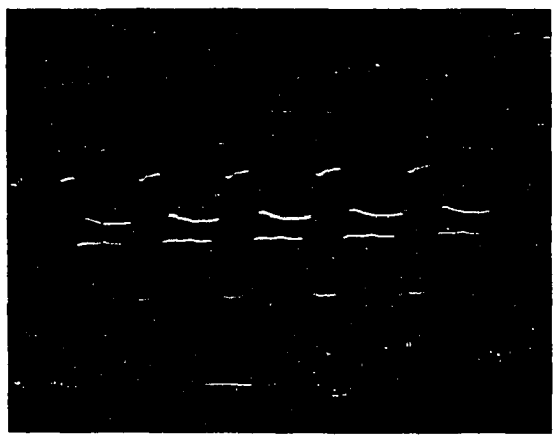

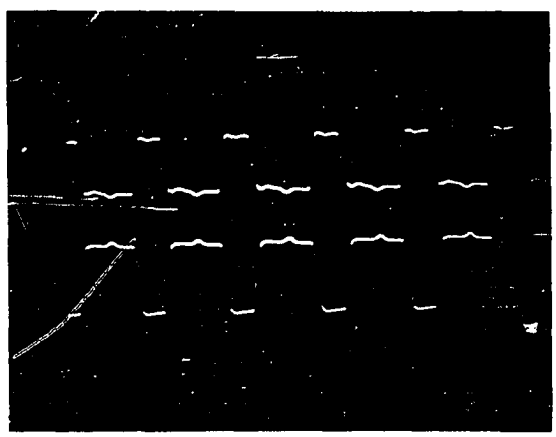

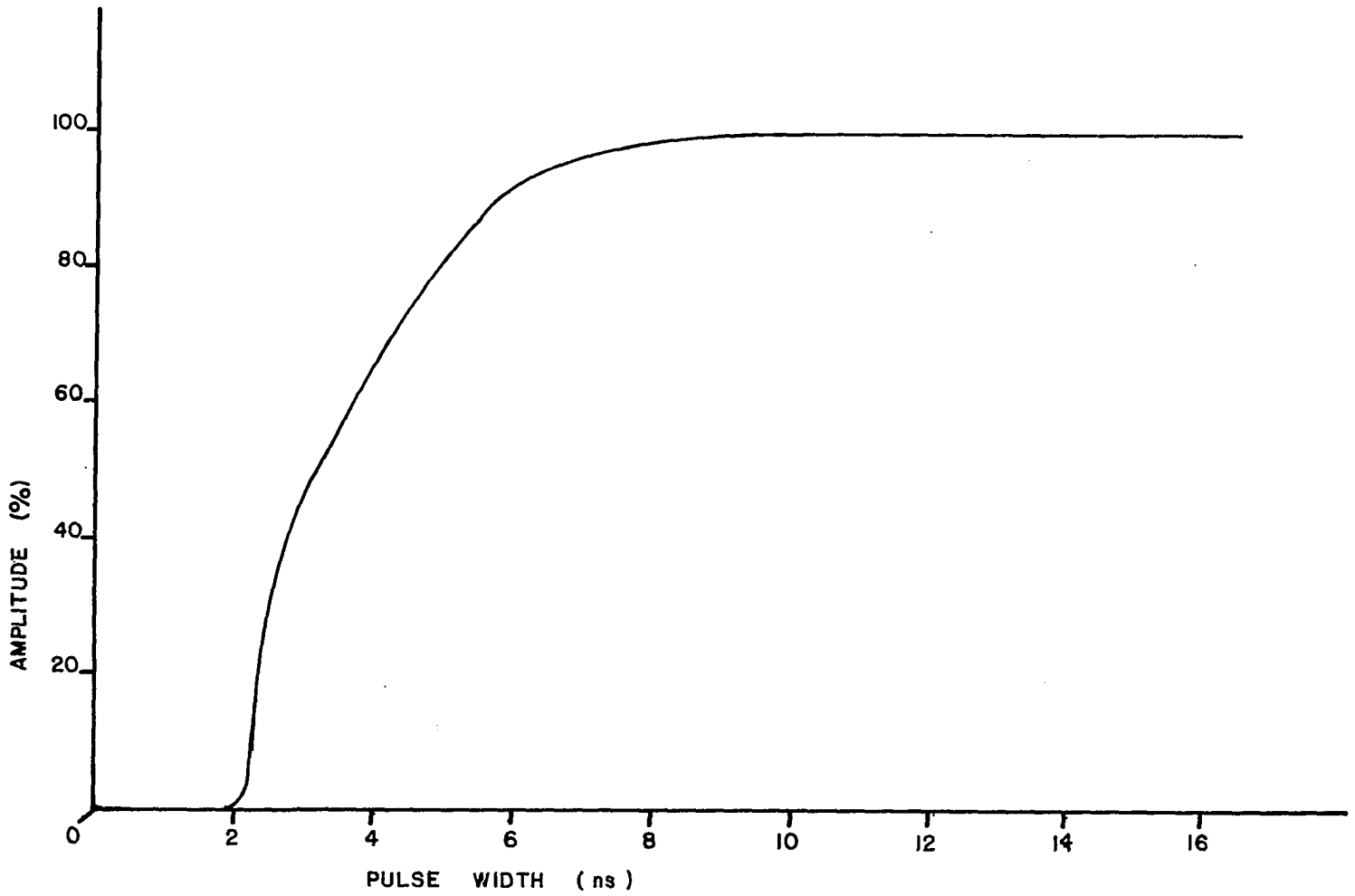

Figure 72. Response of measuring circuit to nanosecond pulses.

Figure 73. Response of the measuring circuit to nsec pulses of varying width.

horizontal: .05 μsec/cm, vertical: .5 V/cm

pulse width (from top to bottom):

a) 3 ns
b) 4 ns
c) 6 ns
d) 10 ns
e) 50 ns

Figure 74a. Voltage calibration of the measuring circuit (from top to bottom).

horizontal: .05 μs/cm

vertical (from top to bottom):

a)	FET circuit	1.0 V/cm	} same input voltage
a')	probe at anode	5.0 V/cm	
b)	probe at anode	5.0 V/cm	} same input voltage
b')	FET circuit	2.0 V/cm	

Figure 74b. Voltage calibration of the measuring circuit (from top to bottom).

horizontal: .05 μ

vertical (from top to bottom):

a')	probe at anode	1 V/cm	} same input voltage
a)	FET circuit	.5 V/cm	
b')	probe at anode	2 V/cm	} same input voltage
b)	FET circuit	1.0 V/cm	

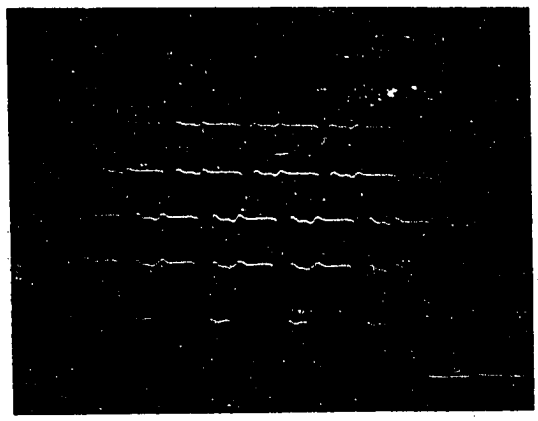

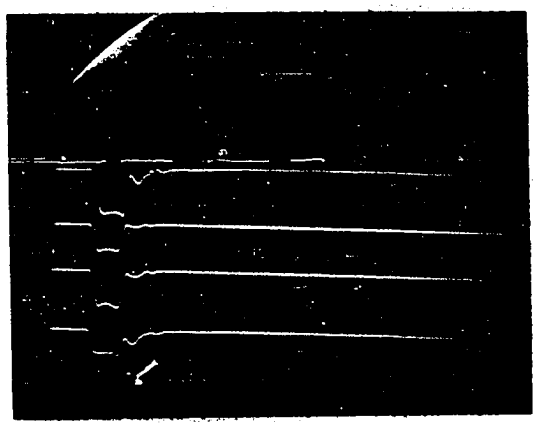

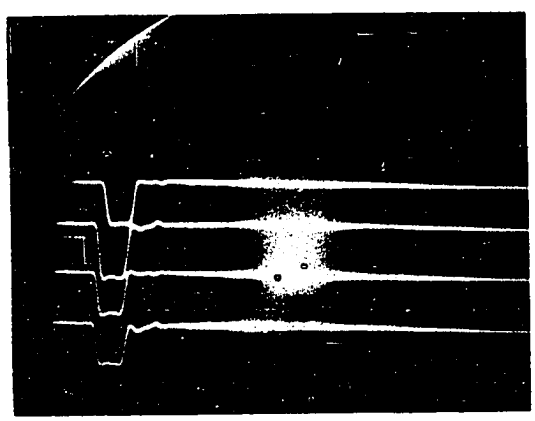

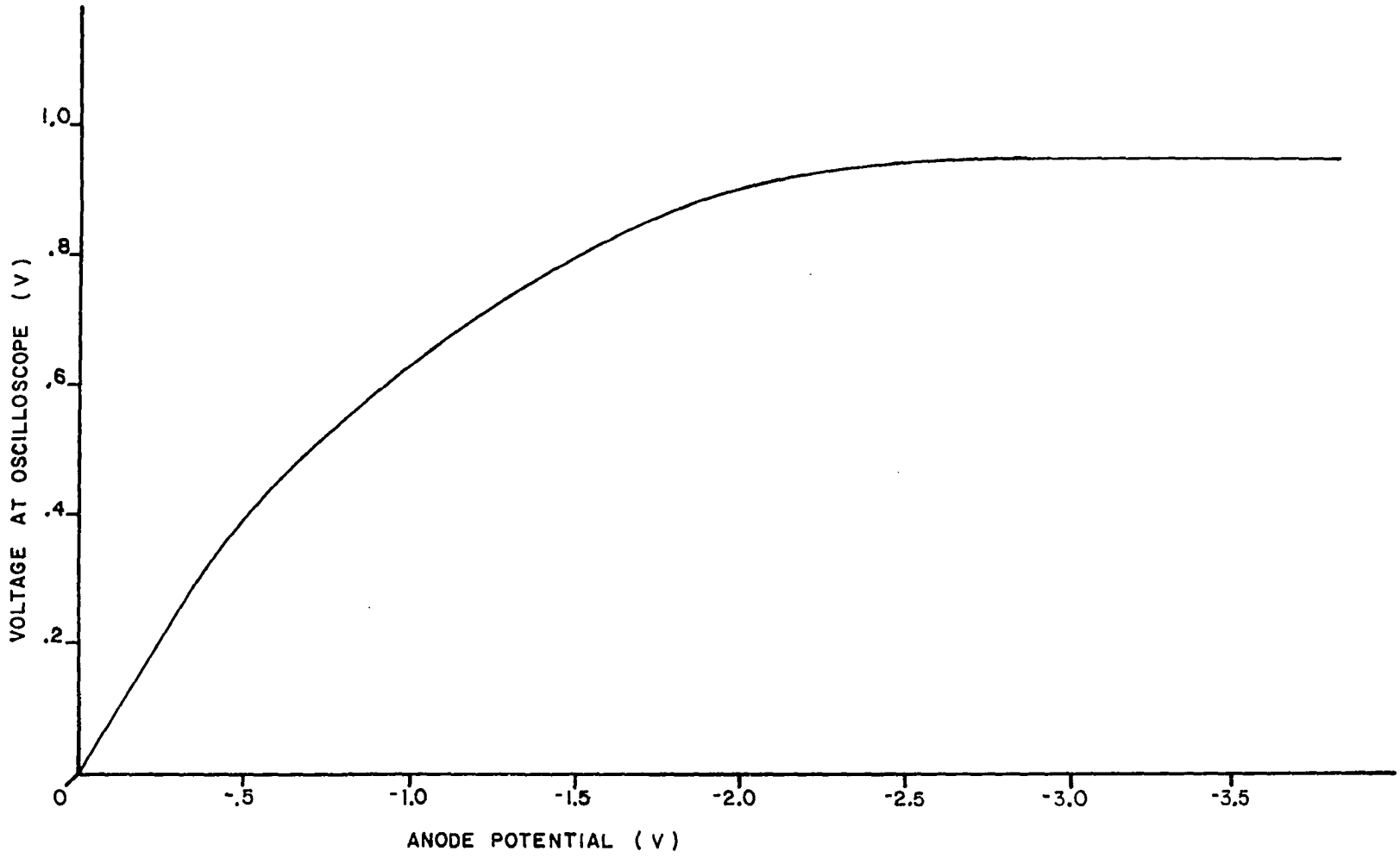

Figure 75. Calibration of the measuring circuit.

Figure 76. Comparison of FET circuit gain to regular 75 Ω coax cable measuring change of intensity of ambient room light.

horizontal: 2 msec/cm

vertical:

a.	FET circuit	.1 V/cm
b.	75 Ω coax	.01 V/cm

Figure 77: Effect of transistor follower stage on frequency response.

horizontal: .05 μs/cm

vertical:

a.	FET with trans. foll. st.	1.0 V/cm
b.	75 Ω coax	1.0 V/cm

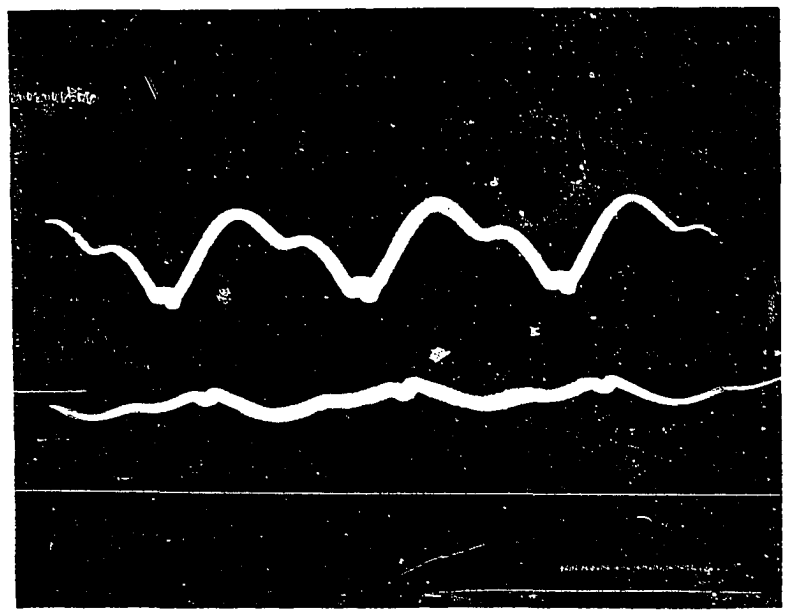

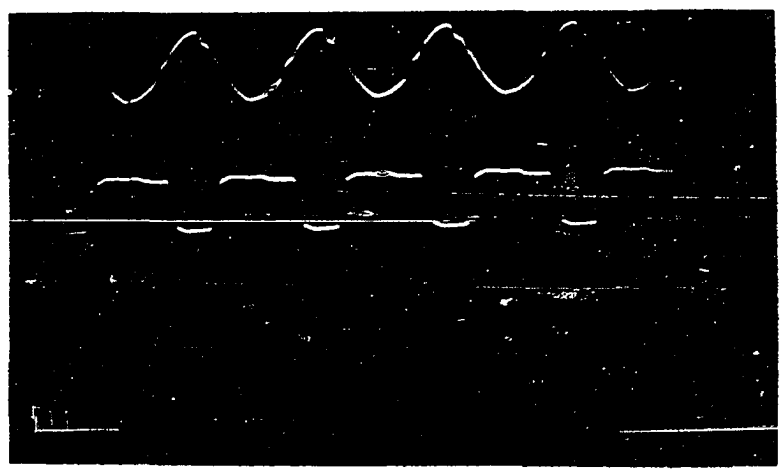

Figure 78. Dark current pulses of the photomultiplier.

horizontal: .05 μs/cm

vertical: .05 V/cm

½ second exposure

Figure 79. Comparison of dark current signal and streamer signal (saturated FET) at maximum sensitivity of the measuring circuit.

horizontal: .1 μs/cm

vertical: .5 V/cm